AD_____

Award Number: DAMD17-02-2-0006

TITLE: Center for Innovative Minimally Invasive Therapy (CIMIT)

PRINCIPAL INVESTIGATOR: John A. Parrish, M.D.

CONTRACTING ORGANIZATION: The General Hospital Corporation
Boston, MA 02114

REPORT DATE: October 2004

TYPE OF REPORT: Annual

PREPARED FOR: U.S. Army Medical Research and Materiel Command
Fort Detrick, Maryland 21702-5012

DISTRIBUTION STATEMENT: Approved for Public Release;
Distribution Unlimited

REPORT DOCUMENTATION PAGE

Form Approved
OMB No. 074-0188

1. AGENCY USE ONLY (Leave blank)	2. REPORT DATE	3. REPORT TYPE AND DATES COVERED
	October 2004	Annual (1 Oct 2003 - 1 Oct 2004)

4. TITLE AND SUBTITLE
Center for Innovative Minimally Invasive Therapy (CIMIT)

5. FUNDING NUMBERS
DAMD17-02-2-0006

6. AUTHOR(S)

John A. Parrish, M.D.

7. PERFORMING ORGANIZATION NAME(S) AND ADDRESS(ES)

The General Hospital Corporation
Boston, MA 02114

E-Mail: japarrish@partners.org

8. PERFORMING ORGANIZATION REPORT NUMBER

9. SPONSORING / MONITORING AGENCY NAME(S) AND ADDRESS(ES)
U.S. Army Medical Research and Materiel Command
Fort Detrick, Maryland 21702-5012

10. SPONSORING / MONITORING AGENCY REPORT NUMBER

11. SUPPLEMENTARY NOTES

Original contains color plates: ALL DTIC reproductions will be in black and white

12a. DISTRIBUTION / AVAILABILITY STATEMENT
Approved for Public Release; Distribution Unlimited

12b. DISTRIBUTION CODE

13. ABSTRACT (Maximum 200 Words)

The Center for Integration of Medicine and Innovative Technology (CIMIT), is a consortium of nonprofit Massachusetts-based institutions led by Massachusetts General Hospital and includes Brigham and Women's Hospital, Massachusetts Institute of Technology and Draper Laboratory. CIMIT develops technologies to advance the diagnosis and treatment of patients using minimally invasive and less costly approaches. CIMIT coordinates and implements research programs in cardiovascular disease, cancer, trauma, and critical care, supported by basic science and engineering development in biomaterials, endoscopic tools, energy delivery, medical imaging, and other novel technologies. This unique military/civilian partnership allows DoD the transfer to the military of successful minimally invasive approaches developed at CIMIT. The overall goal of CIMIT is to create a national program that combines clinical and technological excellence and educational components to generate, develop, and reduce-to-practice innovative and high-impact concepts in minimally invasive therapy.

14. SUBJECT TERMS
Not Provided

15. NUMBER OF PAGES
134

16. PRICE CODE

17. SECURITY CLASSIFICATION OF REPORT	18. SECURITY CLASSIFICATION OF THIS PAGE	19. SECURITY CLASSIFICATION OF ABSTRACT	20. LIMITATION OF ABSTRACT
Unclassified	Unclassified	Unclassified	Unlimited

FOREWORD

Opinions, interpretations, conclusions and recommendations are those of the author and are not necessarily endorsed by the U.S. Army.

X	Where copyrighted material is quoted, permission has been obtained to use such material.
X	Where material from documents designated for limited distribution is quoted, permission has been obtained to use the material.
X	Citations of commercial organizations and trade names in this report do not constitute an official Department of the Army endorsement or approval of the products or services of these organizations.
X	In conducting research using animals, the investigator(s) adhered to the "Guide for the Care and Use of Laboratory Animals," prepared by the Committee on Care and Use of Laboratory Animals of the Institute of Laboratory Animal Resources, National Research Council (NIH Publication No. 86-23, Revised 1985).
	For the protection of human subjects, the investigator(s) have adhered to policies of applicable Federal law 45 CFR 46.
	In conducting research utilizing recombinant DNA, the investigator(s) adhered to NIH Guidelines for Research Involving Recombinant DNA Molecules.
	In the conduct of research involving hazardous organisms, the investigator(s) adhered to the CDC-NIH Guide for Biosafety in Microbiological and Biomedical Laboratories.

K.G. Vosburgh 10/28/04

SIGNATURE DATE

CONTENTS

PROGRAM

PROGRAM

PROGRAM

TRAUMA/CASUALTY CARE

VULNERABLE PLAQUE

*Project not funded by DoD

Characterization of Pyrolysis-FAIMS for the Detection of *Bacillus* Spores

Cristina E. Davis, Ph.D. Principal Investigator

Overall Objectives and Approach

The goal of this project is to develop and characterize a High Field Asymmetric Ion Mobility Spectrometer (pyrolysis-FAIMS) to detect organic compounds released from bacterial spores through pyrolysis or AP-MALDI ionization, with special attention to creating an inexpensive hand-held analyzer either for constant, automated air monitoring or for single point analysis. The presence and/or change in bacterial spore count in the sampled air can be sensed and used for "first-alarm" purposes and as a trigger for a more specific biological agent detector. Specific detection of *B. anthracis* could be achieved by monitoring samples for fingerprint patterns of unique biomarkers present in spore cell walls.

Progress on Specific Aims

Specific Aim 1 Evaluate and implement AP-MALDI as an alternate sample introduction technique

Progress

Evaluation and optimization of the AP-MALDI-FAIMS interface is in progress. The commercial AP-MALDI unit (Agilent Technologies) has been mounted to the custom-designed and built interface. We have installed a new laser controller so that sample plate translation and laser operation is reliably controlled via a remote computer. The aim of the system evaluation is to test the ability to desorb, ionize, and detect test samples. For these early experiments α-cyano-2-hydroxycinnamic acid, 2,5-dihydroxybenzoic acid (two common AP-MALDI matrices) and Desmosine / α-cyano-2-hydroxycinnamic acid are being used.

The plot in Figure 1 was generated by ablation of a small area of 2 μg crystallized α-cyano-2-hydroxycinnamic acid spotted on the AP-MALDI target plate. The ions produced in this operation were introduced into the carrier gas flow through the FAIMS via the high-voltage capillary inlet.

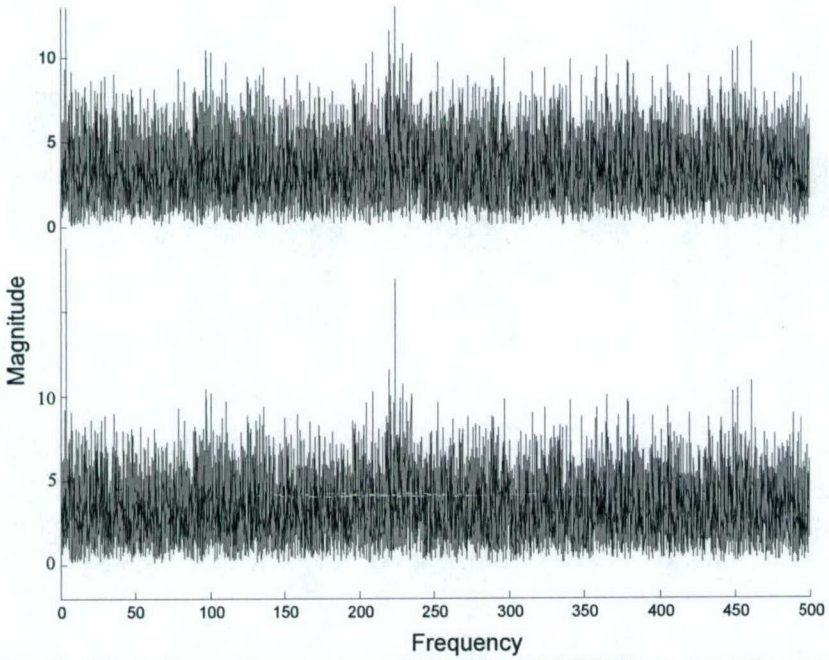

Figure 1. Fourier-Transform of concatenated AP-MALDI-DMS spectra of α -cyano-2-hydroxycinnamic acid.

The data generated in a FAIMS spectrum is the abundance of ions as a function of the compensation voltage. The red and green traces in Figure 1 are a representation of the Fourier Transform of the FAIMS spectral data collected during AP-MALDI operation. The green trace represents the magnitude of the transform of data taken when the AP-MALDI matrix was ablated. The red trace represents the magnitude of the transform of data taken when a blank area was ablated. The data from the compensation voltage scans generated by the FAIMS was chronologically concatenated in a vector, to which the Fast Fourier Transform algorithm was applied to calculate the Discrete Fourier Transform. The graph shows the magnitude of the first 500 hundred frequency values produced by the operation. Two overlays of these transforms are shown on the same plot for comparison purposes. The upper overlay shows the sample transform on top of the background transform, and the lower overlay shows the same background transform on top of the sample transform. From these overlays, we can see that the amplitude of the sample transform is higher than the amplitude of the blank/background transform, indicating that there is more power/information in the data collected when matrix is ablated. In addition the sample trace is seen to have an upward shift as compared to the background trace.

Although more sophisticated data analysis should further elucidate successful AP-MALDI-FAIMS operation, these experiments indicate that ionized sample is passing through the FAIMS. Current efforts in interface evaluation will lead to optimization of the ion transport process. Together with hardware modifications, methodology optimization and data analysis we expect to employ the AP-MALDI-FAIMS system to identify agent-specific features in the data from desorbed and ionized spore samples.

Plan

Further development of the AP-MALDI-FAIMS system will occur. Once successful operation of the system is proven, we will test spores in the instrument. Data from the AP-MALDI-TOF mass

spectrometer will continue to be collected for comparison with data from the AP-MALDI-FAIMS unit.

Specific Aim 2 Generate *B. subtilis* training set and evaluate its predictive power compared to *B. thuringiensis* and *B. cereus*

The pyrolysis-FAIMS setup has been optimized. This consists of a pyrolysis unit from CDS Analytical with a control that programs the interface temperature, the ramping rate, and the temperature and time of pyrolysis. The sample is loaded onto a quartz capillary tube which is then placed into a platinum coil on the pyrolysis probe and inserted into the pyrolysis unit where the sample undergoes pyrolysis. It then travels through a guard column in a GC oven to the FAIMS detector. Pyrolysis-FAIMS experiments were performed for *Bacillus subtilis*, *Bacillus cereus*, and *Bacillus thuringiensis*. These data sets did not look different from each other with simple visual inspection. The data was converted to be consistent with Correlogic System's pattern recognition algorithms and analyzed with their software, ProteomeQuest™. This software uses a pattern recognition algorithm, which analyzes complex data sets that can be manipulated through a computer-driven analog of natural selection process. It also uses self-organizing adaptive pattern recognition systems that group data together based on similarity, recognize novel events, and track rare instances of biomarkers. With this bioinformatic analysis method, we were able to distinguish between all three bacillus species. Even with extremely small data sets (n=100) we were able to distinguish between these species with high probability. At a concentration of 80,000 spores / experiment, Correlogic algorithms distinguished *B. subtilis* from *B. cereus* with 99% accuracy, *B. subtilis* from *B. thuringiensis* with 99% accuracy, and *B. cereus* from *B. thuringiensis* with 83% accuracy. As *B. cereus* and *B. thuringiensis* are almost identical genetically, this result is not surprising. At lower concentrations, the spores can still be distinguished. At 10k levels, *B. subtilis* and *B. cereus* are 98% correctly classified, *B. subtilis* and *B. thuringiensis* 95%, and *B. cereus* and *B. thuringiensis* 52%. At 5k levels, *B. subtilis* and *B. cereus* 98%, *B. subtilis* and *B. thuringiensis* 95%, and *B. cereus* and *B. thuringiensis* 52%.

We are also currently setting up an experiment that will allow us to determine if we can distinguish live spores from dead spores using this method.

Specific Aim 3 Optimize biomarker selection to reduce false positives/negatives.

We have been examining spores at varying concentration levels in an effort to find a set of biomarkers that remains consistent at all concentrations. We believe that this set will provide us with the lowest false positive and false negative rates.

Although we desire to find an overall fingerprint pattern for the spores using FAIMS, we believe that our results would be strengthened by the addition of analytical chemistry data. Adapting AP-MALDI to the FAIMS detector does have some special considerations. Any MALDI experiment requires identification of an appropriate matrix in which the sample is crystallized. The identification and optimization process is usually an empirical one. An important task will be to identify and exclude the effects of the appropriate matrix (or matrices) for our spore samples.

Specific Aim 4 Determine the effect of spore production method

We have compiled a list of growth media for each of the three spore species as found in literature. *B. subtilis* and *B. cereus* will be grown in two different media each (the two that are the most dissimilar in composition) and examined using the same pyrolysis-FAIMS conditions. We will then determine if Correlogic algorithms can make any distinction between the same species grown in different media, and if so, work to modify the biomarkers selected so that they remain constant despite the growth media used.

Publications and Presentations

Krebs MD, Zapata AM, Nazarov EG, Miller RA, Costa IS, Sonenshein AL, Davis CE. Detection of biological and chemical agents using differential mobility spectrometry (DMS). (*in review, IEEE Sensors Special Edition on Anti-Terrorism*) *Note: this is still in review.

External Proposal Activity

The Draper and MGH investigators have been awarded a contract from the Combating Terrorism Technology Support Office Technology Support Working Group (TSWG) of the Department of Homeland Security (DHS). The proposal "Facility Airborne Biological Toxin Alarm System (FABTAS)" is a combined effort over 18 months to use the FAIMS to detect biological toxins in building ventilation systems. The requested funding is $2.1M for the program. Participating institutes will be Draper, MGH (prime), New Hampshire Department of Health and Human Services and United Technologies Research Center. The proposed research is closely related to the current project in many important ways.

An additional opportunity to respond to a call for proposals to the Department of Homeland Security for an instantaneous biological aerosol detector system (IBADS) is in process. A team of Draper, CIMIT and other investigators is being assembled to write a white paper for additional funding.

Acknowledgements

Sarah J. Cohen, B. S.	Pyrolysis-FAIMS experiments
Joung-Mo Kang, M.S.	Pyrolysis-FAIMS experiments
Melissa D. Krebs, M.S.	Pyrolysis-FAIMS experiment planning
Ernie Kim, M.S.	AP-MALDI-FAIMS design and development
Priya Agrawal, B.S.	AP-MALDI-FAIMS design and development
Angela M. Zapata, Ph.D.	AP-MALDI-FAIMS design and development

Non-invasive Breath Analysis Using FAIMS and Bioinformatics Pattern Recognition

Cristina E. Davis, Ph.D. Principal Investigator

Overall Objectives and Approach

Early diagnosis of victims of aerosolized bioweapons is necessary for public health response efforts and for the effective use of limited vaccines and treatments. Diagnosis should take place at the point-of-care to maximize the efficacy of therapeutic intervention. There are dozens of volatile organic compounds in exhaled human breath that show promise for diagnosis and management of diseases. Some disease conditions produce specific volatile gases that can often be detected by the physician examining the patient's breath. The goal of this project is to utilize the high field asymmetric ion mobility spectrometer (FAIMS) technology to measure the volatile compounds in human breath. The correlation of disease states with the pattern of volatiles from patient breath will be examined, especially with regard to illness resulting from aerosolized bioweapons. Progress to date has yielded as many as 150 different compounds that vary according to bacteria species in culture. We are currently producing large data sets using the FAIMS technology that will be analyzed using bioinformatics approaches.

Progress on Specific Aims

Specific Aim 1. Set up FAIMS unit for bacterial headspace measurements.

The 7694 automated headspace sampler from Agilent is connected to an HP 5890 gas chromatograph (GC), which is in turn connected to a FAIMS unit.

Specific Aim 2. Biomarker studies.

Progress: Headspace-GC-FAIMS experiments were conducted on three vegetative bacteria species: *B. subtilis*, *E. coli*, and *M. smegmatis*. The bacteria were inoculated into LB media in the headspace vials and allowed to grow for varying amounts of time (from 12 to 24 hours) so any biomarkers found would be independent of the stage of growth. 3-ml of the headspace was then sampled directly without concentration using the headspace sampler. The headspace sample then traveled through a 5-m VOC GC column and into the FAIMS detector.

A spectral trace was recorded from 150 cultures of each species. The spectral plots were then aligned according to event start and point-by-point signal averaged for each of the three species. Small amplitude peaks that vary from trace to trace will average out, whereas small but consistent biomarkers remain in the final signal averaged trace. **Figure 1A** shows the *B. subtilis* and *M. smegmatis* average spectral plots (left). One of the average spectral plots was subtracted from the other, and the resulting average spectral difference is shown on the right. Several points appear to distinguish these two bacteria species, and also many smaller amplitude ones are scattered across the spectral field. **Figure 1B** shows the remaining 2 species average difference spectral plots.

These data sets were sent to Correlogic Systems, Inc. for pattern recognition after 2D alignment (they were aligned in both the Vc and the time dimensions). Prior to alignment, classification was only ~60% accurate. After alignment, this went up to 91%. Additionally, we have since modified our experimental protocol to enrich the headspace signal, and so we believe that the ability to classify different species will now increase dramatically.

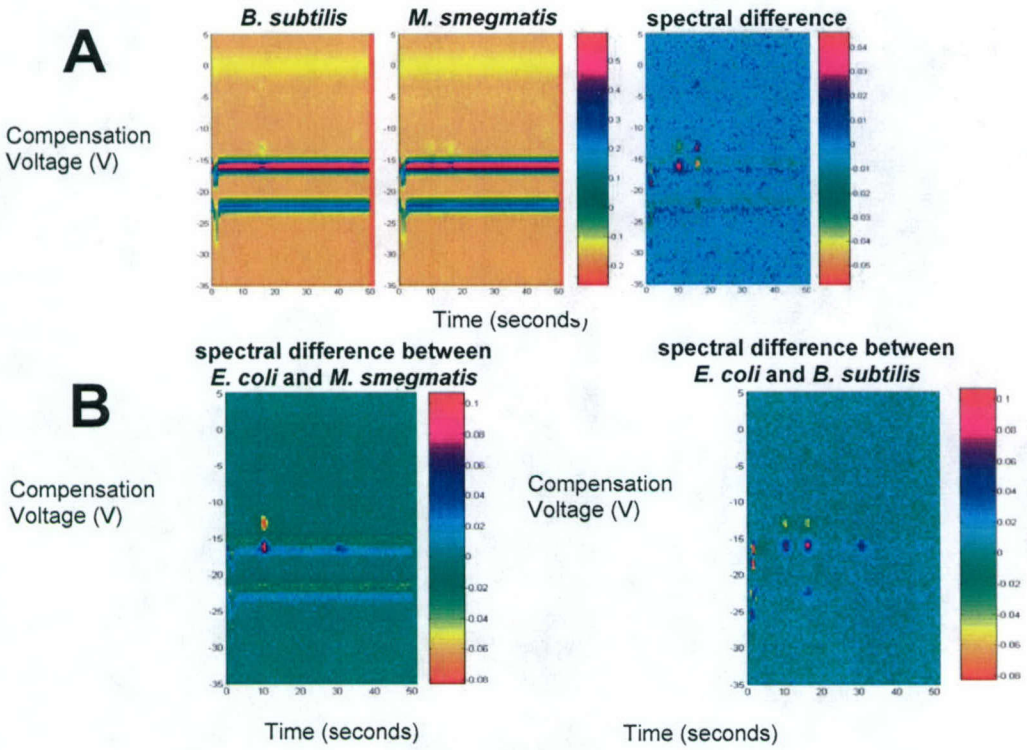

Figure 1: (A) GC-FAIMS analysis of ambient headspace above vegative bacteria cultures. Spectral plots represent a 3-dimentional signal average of n=150 data files. A modified GC column length (1m) and run time produces each data file in less than 1 minute, with no concentration of the culture headspace necessary. The signal average emphasizes biomarkers that are present in the majority of data files, and the spectral difference highlights sets of biomarkers that may distinguish *B. subtilis* from *M. smegmatis*. (B) Spectral difference plots are shown distinguishing between *E. coli* and *M. smegmatis* (n=150, each) and *E. coli* and *B. subtilis* (n=150, each).

We have also been examining individual chemicals using this setup, chosen based on their presence in the GC-MS chromatograms as identified by the NIST database. One example is shown in Figure 2. Headspace from an *E. coli* culture is shown on the left. One of the strongest signals found in the *E. coli* headspace during GC-MS runs was indole. The FAIMS spectra for indole is shown on the right. Indole appears around a compensation voltage of -5 V. There is also a large signal at -5 V in the *E. coli* headspace, very likely from indole.

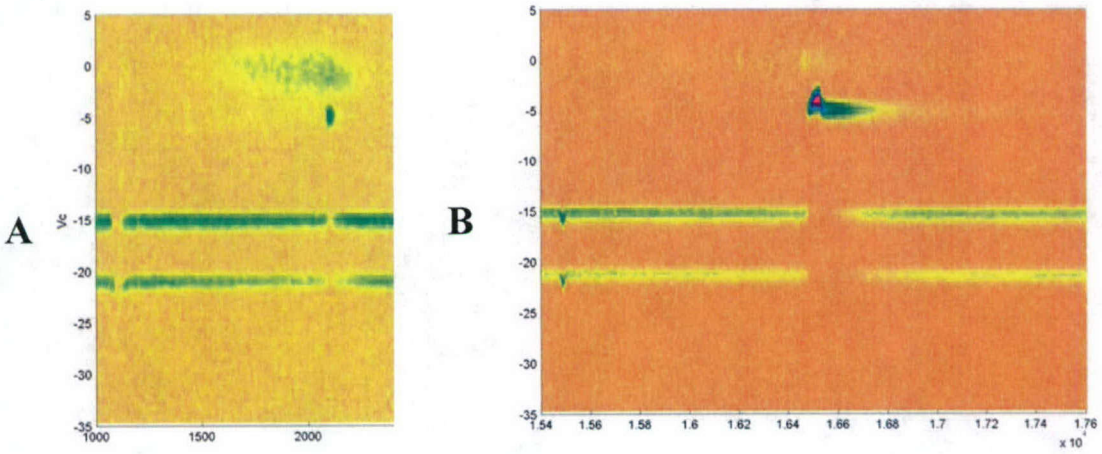

FIGURE 2. (A) *E. coli* headspace (B) Indole (solid) headspace

Specific Aim 3. Increased sampling frequency.
SPME-GC-MS analysis of bacteria headspace was performed as described above for cultures at varying ages. We have found that some volatiles change depending on which phase of the growth cycle the bacteria are in. The bacterial cultures used in the headspace-GC-FAIMS analysis were sampled anywhere between 12-24 hours. We believe that sampling such a wide variety of growth times will help determine which biomarkers are consistently present, regardless of the stage of growth.

Specific Aim 4. Establish expected biomarker spectra for clinical samples.
We are still awaiting IRB approval for the clinical trials.

Publications and Presentations

Krebs MD, Tingley RD, Zeskind JE, Kang, JM, Holmboe ME, Davis CE. Novel bioinformatics approaches to signal processing and data classification for chemical and biological detection systems. New England Regional Center for Excellence fall symposium on Biodefense.

Krebs MD, Shnayderman M, Kang JM, Holmboe ME, Callahan MV, Stair TO, Ryan ET, Dorkin HL, Gill CJ, Gelfand JA, Davis CE. Non-invasive breath analysis using field asymmetric ion mobility spectrometry and bioinformatics pattern recognition. New England Regional Center for Excellence fall symposium on Biodefense.

Davis CE, Callahan MV, Gelfand JA, Borenstein JT. CIMIT's rise to FAIMS. Center for the Integration of Medicine and Innovative Technology. Grand Rounds - Annual Stakeholder Meeting. October 2003.

Patents
Miller RA, Nazarov EG, Kyrlov EV, Eiceman GA, Zapata AM, Davis CE. High Field Ion Mobility Method and Apparatus for Detection of Biomarkers. (Sionex Corporation, 10/31/2002) #10/697,708

Davis CE, Borenstein JT, Zapata AM, Gelfand JA, Callahan MV, Stair TO, Miller RA. Non-invasive breath analysis using field asymmetric ion mobility spectrometry. (Draper Laboratory, 04/01/2002) #60/459,424 and PCT/US04/010288

External Proposal Activity

Our team submitted a full application to the Bill and Melinda Gates Foundation to request funding. Out of 1,500 submitted letters of intent, we were selected to respond with a full proposal (out of an estimated 400 full solicitations). The proposal "Non-invasive diagnosis of pulmonary tuberculosis from human breath using a novel biosensor" will cover 4 years of work at multiple institutions with a total budget request of $3.8M. Participating institutes will be The Charles Stark Draper Laboratory (prime), Massachusetts General Hospital, Boston University School of Public Health, Lemuel Shattuck Hospital, Brigham and Women's Hospital, and the Tropical Disease Research Center (Ndola, Zambia). Our team will directly leverage progress from this project to apply to tuberculosis diagnostics using breath samples.

Acknowledgements

Marianna Shnayderman, B.S.	Bacteria HS-FAIMS experiments.
Melissa D. Krebs, M.S.	Bacteria HS-FAIMS assistance.
Julie E. Zeskind, M.S.	HS-FAIMS experimental setup assistance.
T. John Kauppinen, B.S.	SPME-GC-MS assistance.
Gregg L. Tolliver, M.D.	Microbiology consulting.
Angela M. Zapata, Ph.D.	FAIMS consulting and instrumentation assistance.

Electrostrictive Polymer Artificial Muscles for Magnetic Resonance Imaging

Professor Steven Dubowsky Principal Investigator

Overall Objectives and Approach

The purpose of this study is to investigate the application of Electrostrictive Polimer Artificial Muscle (EPAM) in the MRI machines as actuators that can be remotely controllable. The EPAM actuators are constructed entirely in plastic materials and are actuated with static electric field so that they have essentially no interactions with the high magnetic field experienced within the MRI device.

Progress on Specific Aims

Quarter 1

Development of the reconfigurable imaging coil has been concluded at MIT. Testing and concept validation has been achieved at the MRI facilities at Brigham and Women's Hospital. The concept and initial experimental device (shown in Figure 1) proved feasible. The EPAM devices functioned in the MRI system without affecting image quality. A resizable image coil was able to effectively change the imaging characteristics of the MRI machine by remote control. The results of this work are summarized in a paper submitted to the 2004 IEEE International Conference on Robotics and Automation (cited below). Additional testing has since been done at BWH to further characterize the imaging capabilities of the device. An example of the results from this is shown in Figure1.

First quarter work focused on the development of manipulation systems for MRI environments. A concept for discrete linear positioning device has been developed. Fabrication of a simple prototype has shown feasibility, and concepts for integrating such a device into a 2-D positioning system have been proposed. The development of 3-D manipulator systems for assisting minimally invasive procedures within the MRI was then started based on earlier EPAM manipulators developed at MIT. Improvement of actuator performance during the last fiscal year lead to the development of more sophisticated concepts. In particular we investigated ways of increasing potential workspace of the manipulator by integrating bi-stable devices activated by EPAM actuators.

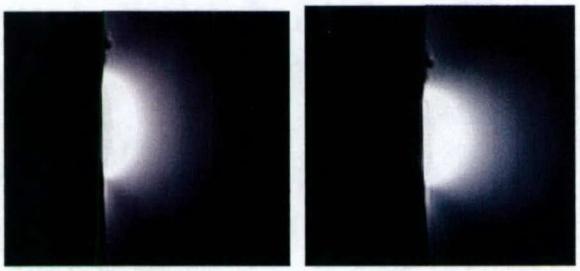

a) b)

Figure 1. Imaging results for conventional imaging coil alone (a) and imaging coil with actuated EPAM actuator directly beside it (b).

Quarter 2

The goal of this quarter remained the investigation of EPAMS fundamental behavior of this technology in MRI environments and the development of practical applications. While continuing developing binary EPAM manipulators, we addressed several important characteristics of EPAM actuators that have made these actuators unreliable in the past. Fundamental actuator failure modes were identified, and methods of increasing reliability were studied. One conclusion was that these actuators have limited life expectancies when large actuation strains are held for a long time. The device will prematurely fail if it is held in a static position for several seconds under power. By

integrating bi-stable elements into EPAM actuators structure, the actuators can be turned off between motions, thus preventing pre-mature failure. Such bi-stable designs can also increase the static stiffness of the device. This means that while a device only requires a certain actuation force to be manipulated, it would be able to reject much larger external disturbance forces. This could be very useful if a device, such as a needle or imaging apparatus, needs to be held in a stable configuration in the presence of a moving patient.

An early prototype of such a bi-stable module is shown in Figure 2. Several of these bi-stable modules can be integrated into a full manipulator design to achieve the desired manipulator workspace.

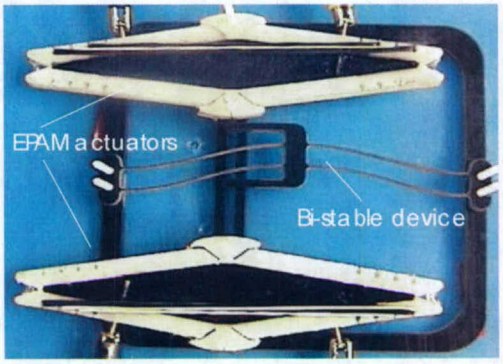

Figure 2. Early prototype of bi-stable device with EPAM actuators

Quarter 3

In the third quarter a manipulation device activated by EPAM binary actuators was optimized. This manipulator was based on a previous one developed within the contest of this project. It requires 6 binary EPAM actuators that allow 8 stable configurations. Each configuration is bi-stable and is actuated by binary actuators can be turned off between motions preventing even small interferences with the machine magnetic field that might arise. The potential applications for this manipulator are for minimally invasive procedures within the MRI machine such as breast biopsy or for other generic actuations such as palpation of breast by remote control. A sequence of all the possible configurations for the prototype manipulator developed at MIT is shown in Figure 3.

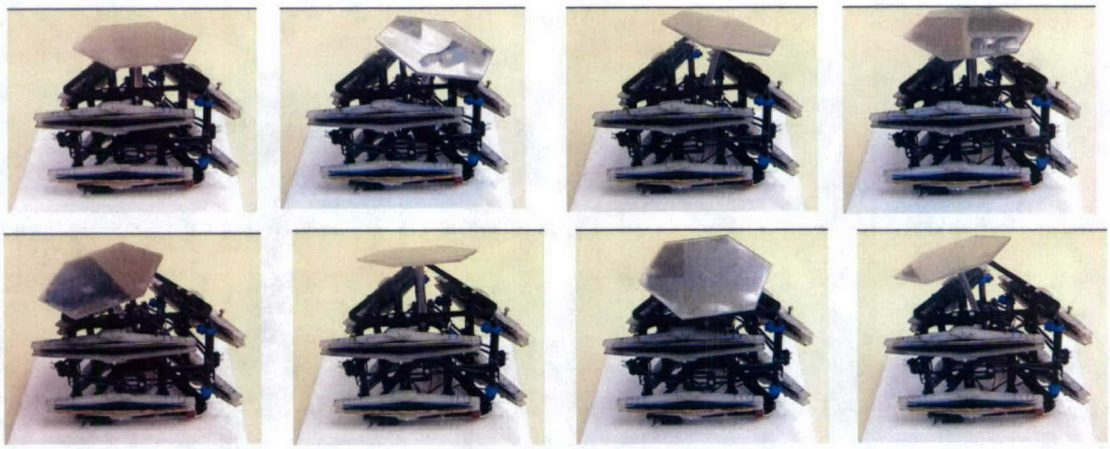
Figure 3. Prototype for an MRI manipulator. Sequence of all the 8 stable configurations.

Quarter 4

Even though bi-stable mechanisms avoid long time actuator activation and therefore eliminate some possible failure modes, other actuator failures have been making these actuators unreliable. During this quarter important aspects of the EPAM actuators manufacture were studied to increase their reliability. Both mechanical and electrical failure modes were intensively studied. The mechanical failures were determined essentially by stress concentration of the actuator polymer and were reduced considerably by improving our actuator design. The electrical failure modes were caused by the electrical field concentration on the edge actuator electrodes and were eliminated by modifying the

deposition procedure. These improvements increased actuators life-cycle by two orders of magnitude (from less than 50 cycles to more than 10000 life-cycles). These remarkable improvements makes our actuators reliable and robust and, combined with the proven compatibility with MRI technology, encourage further development in this field.

Publications and Presentations

The following technical papers documenting the results of this program have been accepted:

1)Vogan, J., Wingert, A., Hafez, M., Plante, J.S., Dubowsky, S., Kacher, D., and Jolesz, F. "Manipulation in MRI Devices using Electrostrictive Polymer Actuators: With an Application to Reconfigurable Imaging Coils,." Proceeings of the 2004 IEEE International Conference on Robotics and Automation (ICRA 2004), April 29, 2004, New Orleans, LA.

2) DF Kacher, J Vogan, A Wingert, M Hafez, J-S Plante, S Dubowsky, FA Jolesz. "Development of a Reconfigurable MRI Coil using Electrostrictive Polymer Artificial Muscle Actuators," Proceedings of the International Society of Magnetic Resonance in Medicine (2004) p3394, 12th Scientific Meeting, (May 15-21, 2004) Kyoto, Japan.

3) April 2004, Digital Mechatronics and Polymer Muscle Actuators for Robotic Systems and Medical Devices," The First Long Wen Tsai Memorial Lecture, Broad Area Colloquium For AI-Geometry-Graphics-Robotics-Vision, Department of Computer Science, Stanford University, Sanford California.

4) Liberatore, S., Plante, J-S. and S. Dubowsky, "On the Failure Modes of Dielectric Elastomer," manuscript in preparation.

External Proposal Activity

None

An Operational Near-infrared Fluorescence Imaging System Prototype for Large Animal Surgery

John V. Frangioni, M.D. Principal Investigator

Overall Objectives and Approach

By providing sensitive, specific, and real-time intraoperative visualization of normal and disease processes, intraoperative near-infrared (NIR) fluorescence imaging has the potential to revolutionize human surgery. With the assistance of a CIMIT Proof of Principle Award, we have formed a network of CIMIT investigators focused on the use of an intraoperative NIR fluorescence imaging system that permits the surgeon to "see" surgical anatomy and NIR fluorescence simultaneously, non-invasively, with high spatial resolution, in real-time, and without moving parts.

Progress on Specific Aims

We are pleased to report that our specific aims have been completed. Under CIMIT support, we designed, engineered, constructed, and evaluated two new intraoperative NIR fluorescence imaging systems, and have delivered them to the following:

1. Dr. Mihaljevic's CIMIT laboratory at the Brigham and Women's Hospital in February, 2004
2. Dr. Hajjar's CIMIT laboratory at the Massachusetts General Hospital in September, 2004.

Hence, combined with our own system at the BIDMC, we have now created a CIMIT-based network of laboratories applying NIR fluorescence technology to important surgical applications.

Even during this short time, the CIMIT NIR Network has been extremely productive (see below). We have systematically studied the application of this novel imaging technology to two important clinical problems, namely sentinel lymph node (SLN) mapping and cardioplegia delivery during coronary artery bypass grafting (CABG).

We believe that our results in SLN mapping will change this technique forever. Using our custom intraoperative imaging system, invisible NIR fluorescent light, and novel lymph tracers synthesized by our laboratory, we have developed methods for performing SLN mapping under complete image guidance. This includes visualization of lymphatic flow in real-time, rapid (seconds to minutes) identification of the SLN node, image-guided resection of the SLN, high sensitivity inspection of the surgical field to assess completeness of resection, and image-guided pathologic assessment of resected tissue. These important concepts are outlined in a series of papers that are either in press or in review. To date, using animal model systems approaching the size of human, we have optimized techniques for SLN mapping of the skin, esophagus, stomach, small intestine, colon, lung, and pleural space. These data suggest that the radioactive tracers and chromophoric dyes now used for SLN mapping can be replaced with a more safe, sensitive, and rapid technique.

A second clinical problem of major importance is the assessment of cardioplegia delivery during CABG surgery. Cardioplegia is a clear, colorless salt solution that stops the heart from beating and protects it from damage. At the present time, cardioplegia is infused "blindly" into the heart, without any assessment of how well the heart is being perfused (and hence protected). Using our intraoperative NIR fluorescence imaging system, and a NIR fluorophore already FDA-approved for another human use, we have demonstrated that cardioplegia can now be delivered under image-guidance, with quantitative assessment of heart protection. We anticipate that this advance could reduce the number of complications from CABG surgery since it ensures that all areas of the heart are protected during the procedure.

In summary, CIMIT funding has permitted us to develop a fully-functioning intraoperative NIR fluorescence imaging system for large animal surgery, deploy the technology to three CIMIT laboratories, and most importantly, to utilize the technology to improve human surgery.

Publications and Presentations

Manuscripts In Press

1) Parungo, C.P. ... Frangioni, J.V. "*In vivo* optical imaging of pleural space drainage to lymph nodes of prognostic significance". Annals of Surgical Oncology, *In Press*.
2) Parungo, C.P. ... Frangioni, J.V. "Intraoperative identification of esophageal sentinel lymph nodes using NIR fluorescence imaging". J. Cardiovasc. Thoracic Surg. *In Press*.
3) Soltesz, E.G. ... Frangioni, J.V. and Mihaljevic, T. "Real-time optical mapping of the sentinel lymph nodes of lung and application to lung cancer resection and prognosis". Annals of Thoracic Surgery, *In Press*.
4) Frangioni, J.V. and Hajjar, R.J. "*In vivo* tracking of stem cells for clinical trials in cardiovascular disease". Circulation, *In Press*.

Manuscripts Submitted for Publication

1) Soltesz, E.G. ... Frangioni, J.V. "Sentinel Lymph Node Mapping of the Gastrointestinal System with Near-Infrared Fluorescent Quantum Dots". Submitted 8/04 to Ann. Surg.
2) Parungo, C.P. ... Frangioni, J.V. "Sentinel lymph node mapping of the pleural space". Submitted 8/04 to Chest.

Manuscripts in Preparation

1) Soltesz, E.G. ... Frangioni, J.V. "Image-guided quantitation of cardioplegia delivery during coronary artery bypass grafting".

Proposals Submitted

1) Frangioni, John V. (Principal Investigator) Title: Optical Imaging of Lymphatic Repair in Surgical Intervention Type: R01 sent 2/1/04 to the National Cancer Institute, NIH
2) Hajjar, Roger J. ((Principal Investigator) Title: Optical & MRI Imaging of Stem Cells in Diseased Hearts Type: R01 sent 2/1/04 to the National Heart, Lung, and Blood Institute, NIH
3) Frangioni, John V. (Principal Investigator) Title: Laser-Based Light Source for NIR Fluorescence Imaging Type: STTR Sent 4/1/04 to the National Cancer Institute, NIH
4) Frangioni, John V. (Principal Investigator) Title: Sentinel Lymph Node Resection by Optical/Nuclear Imaging Type: R01 Sent 6/1/04 to the National Cancer Institute, NIH
5) Frangioni, John V. (Principal Investigator) Title: NIH Director's Pioneer Award Type: Semi-Finalist, Invited Award Application Sent 6/21/04 to the NIH
6) Frangioni, John V. (Principal Investigator) Title: Intraoperative Near-Infrared Fluorescence Imaging Type: BRP (R01) Sent 8/20/04 to the National Cancer Institute, NIH

Talks

1) Massachusetts General Hospital, Boston, MA. Center for Molecular Imaging Research, talk titled "Intraoperative near-infrared fluorescence imaging". 5/24/04 Massachusetts General Hospital, Boston, MA.
2) Breast Cancer Grand Rounds, talk titled "Preclinical development of near-infrared fluorescence imaging for breast cancer diagnosis and treatment".
3) 6/15/04 Gordon Conference titled "Metals in Medicine", Colby College, Waterville, ME. Talk titled "Small molecules and metals in cancer detection and treatment". 6/17/04.
4) 9/7/04 Wellman Center for Photomedicine, MGH, Boston, MA. Talk titled "Near-Infrared Fluorescent Contrast Agents and Imaging Systems for Intraoperative Use".

Microcoils for Electrode-free Tumor Ablation and Imaging

Daniel K. Sodickson, MD, PhD Principal Investigator
Aaron K. Grant, PhD Co-investigator
Benjamin M. Schwartz, Research Assistant

Overall Objectives and Approach

The overall aim of this project is to investigate the feasibility of using microfabricated injectable or ingestible resonant coils for localized therapeutic heating of tissues. Suitably designed microcoils might be expected to allow local focusing of an externally applied electromagnetic field, thereby combining a capability for deep tissue penetration (if fields with sufficiently low frequency and long wavelength are used as external stimuli) with a high degree of therapeutic localization (commensurate with the size of the microcoils used). In this New Concept project, we are investigating the theoretical and technological prerequisites for microfabricated resonant structures suitable for noninvasive tissue ablation and follow-up imaging.

Progress on Specific Aims

Our specific aims are as follows:

1. determine the scaling of resonant frequency with resonator size and structure
2. select materials for micro- or nano-fabrication
3. construct a simple generalized transmitter and sample microcoils
4. test the behavior of this prototype apparatus in phantoms

To address Aims 1 and 2, we have modeled local heat delivery as a function of resonator size, material properties, and applied field strength and frequency. The resulting scaling properties were found to be unexpectedly unfavorable, presenting various practical challenges for effective tissue heating with micro- or nano-scale structures. Therefore, in lieu of our original Aims 3 and 4, we sought to explore in more depth the mechanisms of energy delivery at small scales. In the course of these investigations, we have devised a new mechanism for local energy focusing that is scale invariant, and that might therefore help to overcome the practical limitations of microcoil heating. With the knowledge gained during this funding period, we will go on to test this hypothetical mechanism and its potential applications not only for local tissue heating but also for fine molecular control.

Model of Heat Delivery

Since our original goal in this work was to deliver heat selectively *in vivo*, a crucial consideration is the balance between heat delivered by a candidate microstructure and heat delivered directly to tissue by the applied RF field. Heating of tissue other than the specific ablation target must be maintained within safe limits. Thus, the quantity of interest is not the absolute power delivered by the microstructure, but rather the local amplification, expressed quantitatively as a power ratio. This concept is familiar from the field of tumor hyperthermia with thermal seeds (1-4), with which we have become familiar during this project.

In order to evaluate the denominator of this ratio – the RF power density P_t delivered directly to tissue in the absence of a microcoil – we have used a model of tissue heating from the hyperthermia literature (2):

$$P_t = \omega^2 \mu_t^2 r^2 \sigma_t B_0^2 / 8 \times 10^{-6} \text{ W/cm}^3 \quad [1]$$

Here ω is the frequency (in radians/sec) of the applied RF field; B_0 is its amplitude; μ_t is the magnetic permeability of tissue, which is typically nearly equal to the permeability of free space μ_0; r is the radial distance of the tissue region being considered from the center axis of the body; and σ_t is the conductivity of tissue.

At small spatial scales, the power P_c dissipated in a solenoidal microcoil of radius b consisting of N windings of "wire" with radius c and conductivity σ_c, is

$$P_c = \pi^2 \omega^2 \mu_0^2 \sigma_c N b^3 c^2 B_0^2 / 2 \quad [2]$$

One noteworthy observation from our early modeling is that at small spatial scales electrical resonance per se is not a significant determinant of power absorption. (This is contrary to the experience with macroscopic MRI coils which originally motivated this project.) Instead, the partitioning of power from the RF field is dictated primarily by the relative resistivity (or, alternatively, the relative conductivity) of the microstructure as compared with the surrounding tissue, as is apparent from the power ratio

$$\frac{P_c}{P_t} \propto \frac{\sigma_c}{\sigma_t} \frac{N b^3 c^2}{r^2} \quad [3]$$

Another noteworthy feature of Eq. [3] is the scaling with the fifth power of a characteristic microcoil dimension (b and c), which results in a rapid decrease in the power ratio as coil size decreases.

One approach to this scaling problem would be to increase the frequency of the applied field to the point that skin depth considerations become important. In this case, some of the powers of coil dimension would be replaced by powers of the skin depth $\delta = \left(2/\omega\mu\sigma\right)^{1/2}$. In attempting to treat the fuller electromagnetic problem, we have found that our microcoil model effectively reduces (with some minor geometrical adjustments) to the known problem of inductive heating of a conductive object by an oscillating applied magnetic field. The analytic expression for the power P_s dissipated (via eddy currents subject to ohmic energy losses) in a sphere of radius a subject to an externally applied field may be shown to have to the following asymptotic behavior (2, 5, 6):

$$P_s \xrightarrow[a \gg \delta]{} 3\pi a^2 \left(\omega \mu_s / \sigma_s\right)^{1/2} B_0^2 / 2^{1/2}$$

$$P_s \xrightarrow[a \ll \delta]{} \frac{\pi a^5 \omega^2 \mu_s^2 \sigma_s B_0^2}{\frac{5}{3}\left(\mu_s - \mu_0\right)^2 + 10\left(\mu_s - \mu_0\right) + 15} \quad [4]$$

The use of millimeter- to centimeter-sized implants at moderate (e.g. 100kHz to 1MHz) frequencies has been shown to allow appreciable power ratios P_s/P_t and consequent selective heating for tumor hyperthermia (2). For this range of parameters, $a \gg \delta$, and the P_s takes the form at the top of Eq. [4]. However, if we would like to design injectible structures that can be targeted chemically, we are interested in smaller spatial scales that (in the absence of very high frequencies) place us in the opposite limit $a \ll \delta$, and we are "stuck" with the fifth-power spatial dependence we would like to avoid. As was also recognized in the hyperthermia field, the use of

ferromagnetic materials with large permeability μ_s can provide increased power amplifications by intensifying the magnetic field (and hence the power-dissipating eddy currents) inside a thermal seed. However, this enhancement may not be sufficient to provide efficient power delivery at the spatial scales of interest to us. Figures 1 and 2 show surface plots of the power ratio P_s / P_t for a broad range of frequencies and object sizes a. Recognizing that significant local heating may be accomplished immediately adjacent to a microsphere, in Figure 2 we have also plotted ratios of the power density in W/cm^3 at the surface of the sphere itself, which has a more modest a^2 dependence for $a \square \delta$. Appreciable power density ratios are attained at small spatial scales using a ferromagnetic material (iron, for purposes of demonstration). However, a high density of microstructures would be required to achieve this kind of heating over a macroscopic tumor, and of course the use of ferromagnetic implants would limit subsequent use of MRI for follow-up evaluation.

A Proposed New Mechanism for Scale-Invariant Energy Delivery: The "Lightning-Rod Effect"

Clearly, our original concept of resonant local energy delivery does not extend easily to our target spatial scales. However, a more encouraging example of nano-scale heating was recently published by a group at MIT, who used 1GHz RF irradiation to selectively denature DNA that had been bound to gold nanocrystals (7). Although the title and introduction of the article describing this work indicate inductive heating of the gold nanocrystals as the presumptive mechanism of heat delivery, scaling calculations such as those shown in Figures 1 and 2 here call this hypothesis into question. Indeed, the authors speculate that other mechanisms, such as induced dipole torque, may be responsible for the observed effects. We have explored various models that introduce mechanical energy deposition into the problem, but have discovered no favorable scaling relations that might explain the nanocrystal results.

When we turned our attention to the immediate surroundings of nanocrystals or other conductive structures, however, we discovered an effect which could account for the observed MIT results. It is a well-known property of conductive structures that they draw electric field lines to their surface. The resulting bunching of field lines helps, for example, to draw electric discharges to the points of lightning rods, and it may also allow for highly localized energy deposition for our purposes. Although no energy is deposited inside a perfectly conducting sphere (due to exclusion of field from the interior of the sphere) the distortion of field lines at the surface of the sphere may be shown to result in a ninefold increase in power deposition in the more modestly conducting surrounding medium, as compared to the baseline energy deposition in the medium. In other words, in the immediate neighborhood of a perfectly conducting sphere, the power ratio as defined in the previous section automatically takes the highly favorable value of $P_s/P_t = 9$. For realistic conductivities, field focusing still occurs and the power ratio continues to be favorable. Figure 3a shows the results of a simulation verifying this theoretically expected effect.

This field focusing effect is essentially independent of the frequency of applied irradiation and the size of the focusing object. Thus, we can in principle choose any frequency that is convenient, and can count upon a degree of enhanced energy deposition even at the micro- or nano-scales, without concerning ourselves with attenuations by large powers of the object size. Some remaining scaling issues may remain when thermal diffusion is taken into account: in particular, when local energy deposition is translated into temperature increases using simple diffusion models, a second power of object size enters into the problem again. A numerical simulation of relative temperatures around a conductive sphere is shown in Fig. 3b. The correlation of temperature fields with structural damage at nanoscales, however, is unclear. Another practical issue of scaling may be appreciated from both plots in Fig. 3: both power deposition and temperature increase fall off rapidly with distance from the focusing object, such that the effect is

negligible beyond one or two object radii. This high degree of localization may be a disadvantage for bulk tissue ablation, and this may explain why the lightning rod effect does not appear to have been exploited in tumor hyperthermia research. Nevertheless, this same spatial selectivity may represent an advantage for applications in molecular control such as those envisioned by the MIT group.

If the lightning rod hypothesis can be verified, it will help to guide the design of improved focusing structures. For example, pointed objects may be expected to yield far more favorable power ratios than spheres (ratios on the order of 100, rather than 9 for the sphere, have been seen in simulations). Practical issues involving fabrication of the requisite sharp features at nanoscales, as well as alignment of these features with the applied field, remain to be explored.

Future work

Much work clearly remains to be done in testing and exploring the consequences of the lightning rod hypothesis. We plan to study the size- and frequency-dependence of the effect in actual conductive particles (both macroscopic, microscopic, and nanoscale). We also aim to learn more about the physics of the nanoenvironment (e.g. the hydration shell around very small objects) which could play an important role in practical energy delivery. As discussed above, we are also adjusting our conceptions of target applications. Although this New Concept project began as a practical feasibility study of one particular mechanism of localized energy delivery, it has led us, happily if unexpectedly, into a deeper study of basic mechanisms and new applications. We hope to continue this study in collaboration with groups at MIT and elsewhere who have expertise in nanotechnology and molecular targeting.

Publications and Presentations

Given the early stage of development of this work and our evolving understanding of the basic mechanisms behind micro- and nano-scale energy deposition, we have deferred public presentations at this stage.

External Proposal Activity

We will continue to gather preliminary data prior to submitting external applications for additional funding.

References

1. Stauffer PR, Cetas TC, Fletcher AM, DeYoung DW, Dewhirst MW, Oleson JR, Roemer RB. Observations on the use of ferromagnetic implants for inducing hyperthermia. IEEE Trans Biomed Eng 1984;31(1):76-90.
2. Stauffer PR, Cetas TC, Jones RC. Magnetic induction heating of ferromagnetic implants for inducing localized hyperthermia in deep-seated tumors. IEEE Trans Biomed Eng 1984;31(2):235-51.
3. Jordan A, Wust P, Fahling H, John W, Hinz A, Felix R. Inductive heating of ferrimagnetic particles and magnetic fluids: physical evaluation of their potential for hyperthermia. Int J Hyperthermia 1993;9(1):51-68.
4. Hergt R, Andra W, d'Ambly CG, Hilger I, Kaiser WA, Richter U, Schmidt H-G. Physical Limits of Hyperthermia Using Magnetite Fine Particles. IEEE Trans Magn 1998;34(5):3745-3754.
5. Smythe WR. Static and Dynamic Electricity. New York: McGraw-Hll, 1950.

6. Landau LD, Lifshitz EM, Pitaevskii LP. Electrodynamics of Continuous Media. (2nd ed.) New York: Pergamon Press, 1984.
7. Hamad-Schifferli K, Schwartz JJ, Santos AT, Zhang S, Jacobson JM. Remote electronic control of DNA hybridization through inductive coupling to an attached metal nanocrystal antenna. Nature 2002;415(6868):152-5.

Illustrations

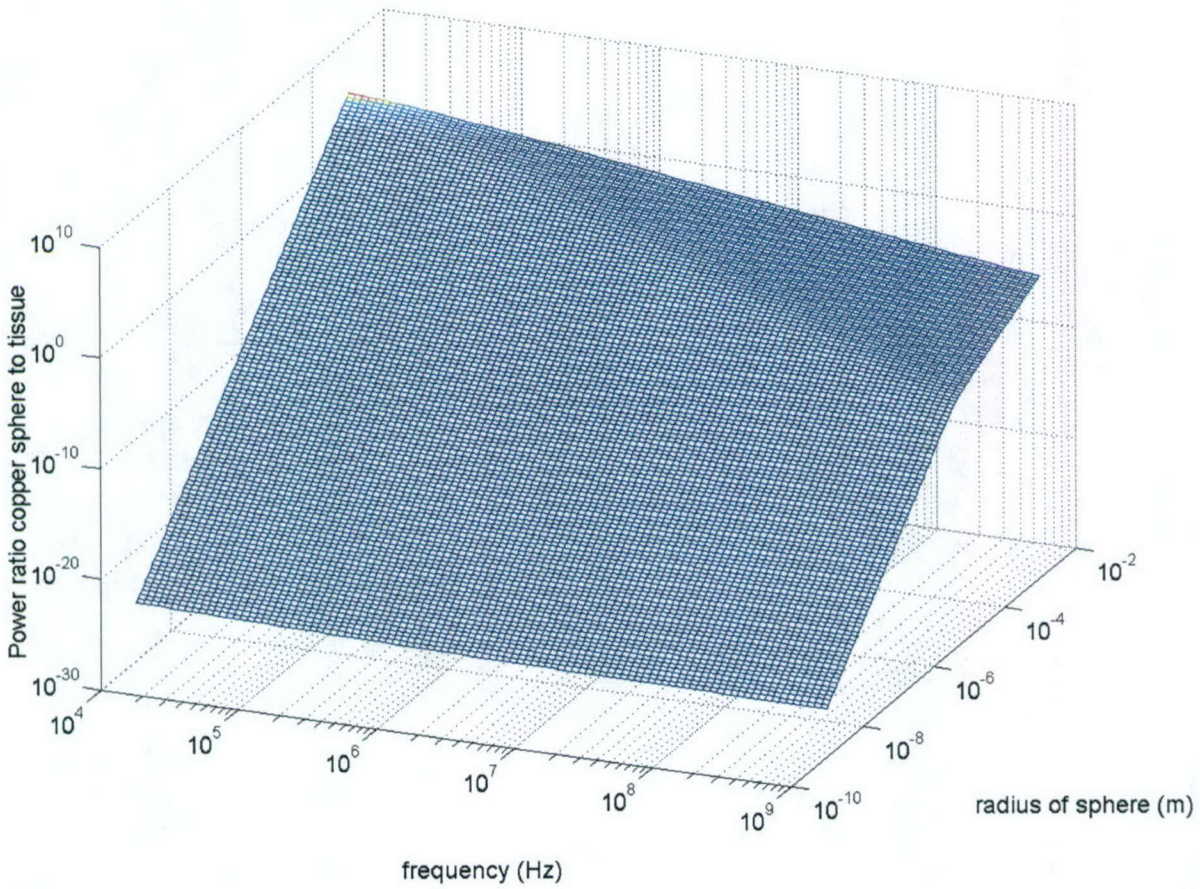

Figure 1: Power ratio P_s / P_t for a copper sphere embedded in tissue over a range of orders of magnitude in frequency and radius (see text for definitions). For the purposes of this calculation, tissue was assigned frequency-dependent conductivity values equal to the published conductivity of small intestine, and a control tissue region 15 cm from the center axis of the body was considered.

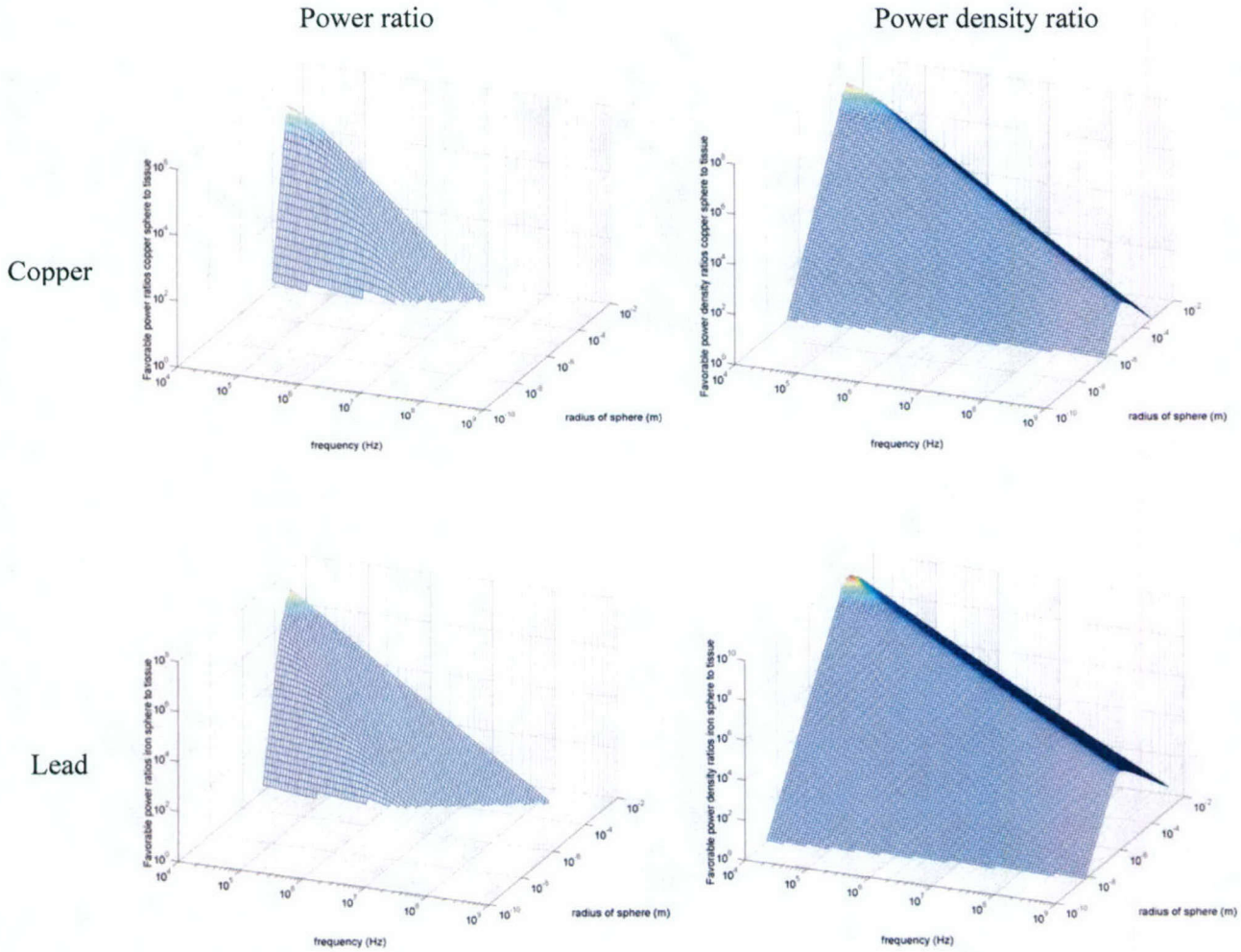

Figure 2: Range of favorable power ratios (left) and power density ratios (right) for copper (top) and lead (bottom) spheres embedded in tissue. Ratios greater than one are defined as favorable, since they entail effective local amplification of power deposition by microspheres over the baseline heating produced directly in tissue by the RF field.

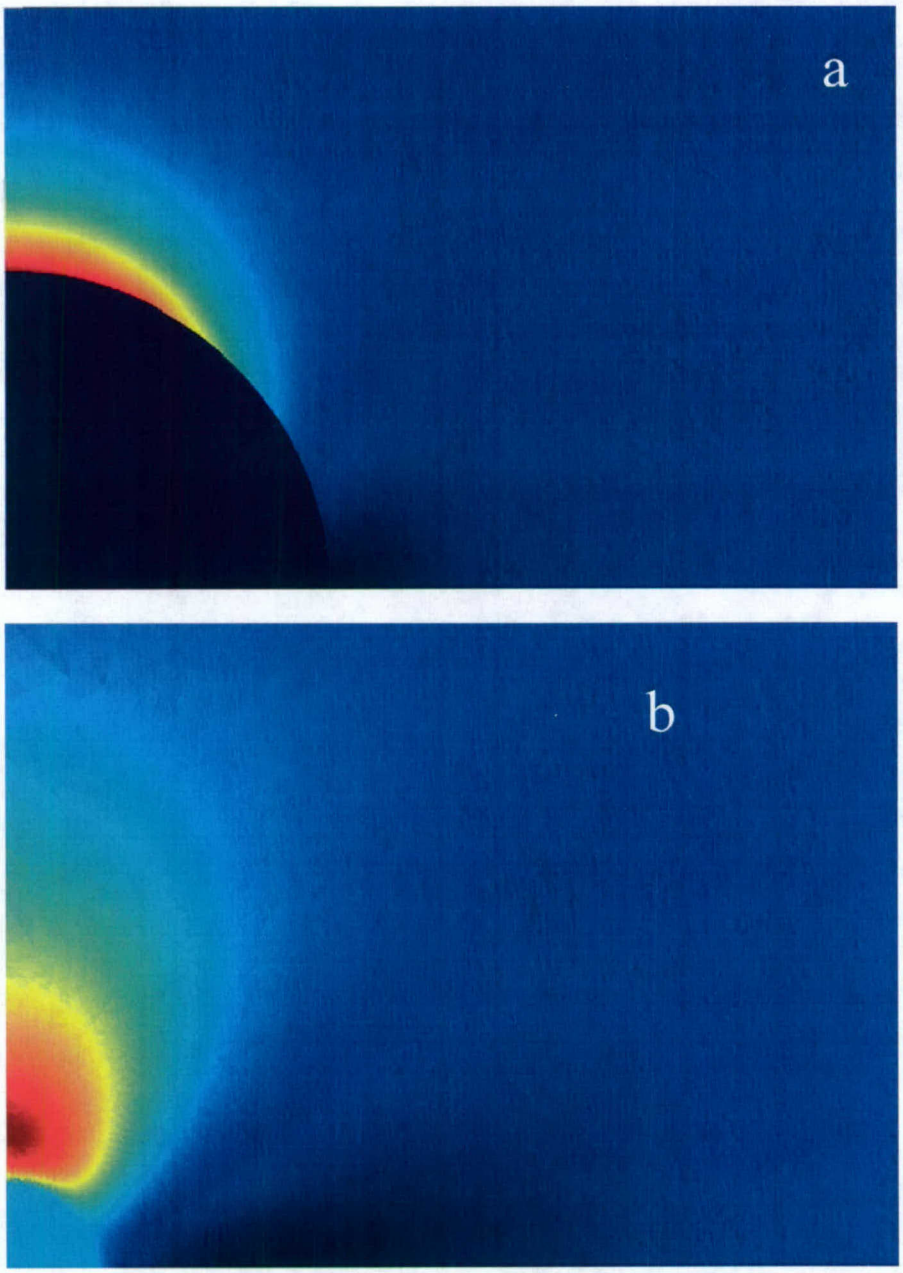

Figure 3: Numerical simulations of the field focusing (or "lightning-rod") effect in the vicinity of a conducting sphere. a) Power deposition field. b) Temperature distribution (red = hotter, blue = cooler).

Advanced Ultrasound Visualization of Vasculature for Surgical Guidance

KG Vosburgh, PhD Principal Investigator (CIMIT/MGH)

Nicholas Stylopoulos, MD (MGH), Sonia Pujol, PhD (BWH), Ashley Vernon, MD (BWH), Raul San Jose Estepar, MSc, PhD candidate (BWH), Karl Krissian, PhD (BWH), Ivan Bricault, MD, PhD (BWH), Matthew Graziano (Boston University)

Summary

We have developed and demonstrated a minimally invasive system for tracking interventional equipment in real time in a living model, with technology suitable for human use. With this system, we have shown that Image-Registered Laparoscopic Ultrasound (IRLUS) has excellent Face Validity and clearly improves the performance of inexperienced users. We will now explore opportunities in human surgery using IRLUS, and seek other applications for the tracker system.

Overall Objectives and Approach

The field of image guided surgery is progressing from static image guidance through the use of real time tracking and registration of instruments, and eventually toward the ability to update and display registered solid organ structure, all with the ultimate goal to improve the efficiency, efficacy, and safety of surgical procedures. The concept of vascular registration is particularly attractive, because vascular structures are seen in many modalities, including x-ray fluoroscopy and ultrasound in real time. Also, vasculature indicates the position of solid organs; if something moves, the blood vessels move with it. Visualization of the vasculature thus may permit the orientation, guidance, and registration of surgical instruments and supporting technical systems. The use of vasculature as a road-mapping system offers the potential to provide real time updated 3D information for a variety of procedures at low cost and transparent complexity.

Our primary goal is to introduce IRLUS-based vascular registration into clinical procedures. To advance toward this goal in FY04, two specific aims were defined:

1. Make the characteristics and performance of the system satisfactory for human use
2. Ensure physician acceptance of the system interface and performance.

A secondary goal is to explore other applications for IRLUS and for the tracking technology in general surgery procedures.

Laparoscopic Ultrasound (LUS) has salient advantages: the ultrasound image quality is superb, and the system is minimally invasive and easily accommodated in the operating room. However, LUS can be difficult to use: Image position and orientation is hard to achieve and maintain, so that Long training and updated experience needed. In FY03, under the leadership of James Ellsmere, MD, this team validated the hypothesis that tracking and display will make LUS easier to use. We assembled core interdisciplinary capabilities demonstrated face validity in animal model (Publications 1,2,3, listed below). Dr. Ellsmere and other collaborators completed a study of pancreatic cancer staging (4), showing that this end application was practical.

Progress on Specific Aims

Specific Aim 1: Make system technically suitable for use in humans

Experiments in FY03 were conducted at the Harvard Medical School Center for Laparoscopic Surgery in a porcine model system with a tracked laparoscopic probe of 18 mm outside diameter. We have moved our animal model studies to the Massachusetts General Hospital (MGH), and thereby obtained proximity to a higher resolution CT,[1] and consolidated activities adjacent to our planned clinical site for tests in humans. Current experimental studies include validation of upgraded hardware and software, rehearsal of "in OR" procedures, including the setting up and operation of the tracked LUS system in the MGH OR, and hands-on collaboration with neurosurgical and Surgical Planning Laboratory investigators. A key thrust is generation of very high quality CT-angio and LUS data sets for studies in registration and fusion with deformed models of the liver (recognizing that the porcine liver does not have good macroscopic correspondence to the human liver, but, if anything, may be a more challenging system). In addition, these porcine model experiments provide subjects for Dr. Mark Ottensmeyer of the CIMIT Simulation Group to gather data on the elastic properties of vascularized tissue, and incidentally acquired cardiovascular data have been shared with investigators in DARPA's Virtual Human Program.

To enable trials in human patients, our team (CIMIT, Ascension Technologies, B-K Medical) has constructed and tested a new tracked LUS probe with diameter of less than 12 mm, which is suitable in size for use in humans. Also, we have modified our software and experimental protocols to use the new CT system with 0.75 mm slice thickness, giving the potential for registration at the level of 1.0 mm. In the porcine model, this system routinely displays secondary and tertiary vascular structures in the liver, offering great potential for registration of these structures with intraoperative ultrasound.

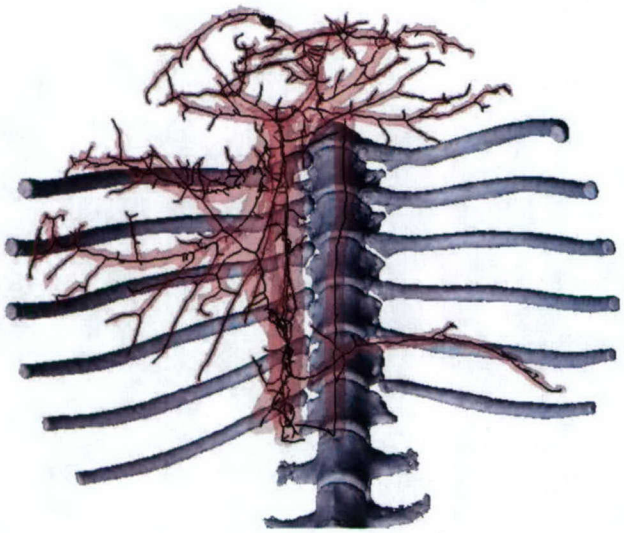

Fig. 1. Extracted display of liver vasculature with vessel centerlines.

This CT system will also be used for studies in humans, thereby simplifying the experimental process. An application has been prepared for the MGH IRB for approval to conduct intraprocedural feasibility tests on up to five patients.

A key feature of this year's work has been the total integration of all hardware and software components on current and stable platforms. In particular, the use of the new Ascension "microbird" transducers has resulted in the elimination of all extra electronics boxes outside the

[1] Somatom "Sensation 16" -- Siemens Medical Systems

computer cabinet. All of the calibration and image registration functions have been incorporated in a single software architecture, with the algorithms in C[+] and the visualization code in TCL. The C++compiler has been upgraded from Version .6 to Version .7. The display system is fully integrated into Slicer 2.

The new software integration permits the real time video acquisition and display of the 2D ultrasound image. With the incorporated position information, segmentation and 3D volume construction inside Slicer will be possible. This system will also serve as a testbed for digital processing of the ultrasound image.

Remaining tasks before OR use approval are 1) Improve the mechanical integrity of the tracker/probe assembly, and 2) ensure that the final unit is easily sterilized.

Specific Aim 2: Ensure physician acceptance of the system interface and performance by demonstrating that image registration improves the efficiency and reduces the stress of using LUS.

We have demonstrated an innovative approach for the localization of hepatic tumors using the IRLUS approach. Intraoperative laparoscopic ultrasonography has been established by others as a valuable tool in localization of liver tumors. However, the physician has limited information about the location of the probe compared to the tumor, and thus mental representation of the ultrasound beam location inside the abdomen remains difficult. IRLUS may assist the physician finding the tumor more easily in laparoscopic ultrasonography, thanks to 3D real-time visualization of the ultrasound plane and its intersection with the tumor.

A synthetic tumor was created by introducing percutaneously 0.7 ml of silicone using a needle in the liver of a pig under general anesthesia, following the method of Restrepo, et al.[2] The needle was placed under transabdominal ultrasound guidance. A two-phase enhanced CT exam was performed with a 2 mm slice thickness. We built models of the tumor, the vessels, and the bones using the 3D Slicer software. The laparoscopic ultrasound probe was equipped with a 6D magnetic sensor, and a paired point registration was computed to align the magnetic tracker reference system and the CT reference system. The abdomen was then insufflated, and two laparoscopic accesses were created for the camera and the

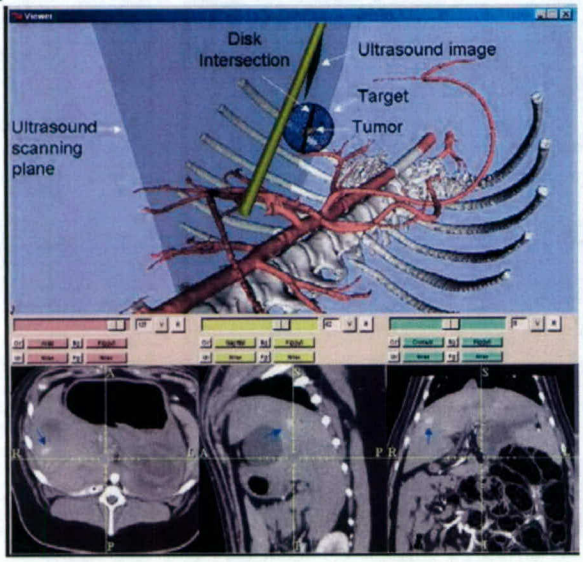

Figure 2.

(Top) The 3D scene shows results of the real-time calculation of the targeted sphere containing the tumor with the magnetically tracked ultrasound plane. *(Bottom)* **The system displays in real-time the re-formatted anatomical CT slices corresponding to the position of the probe. The arrows show the result of the silicone experimental model of tumor.**

[2] Restrepo JI, et al. Laparoscopic ultrasonography: a training model. Dis Colon Rectum. 2001;44(5):632-7

ultrasound probe. The clinical objective for the operator was to find the tumor using laparoscopic ultrasonography. We defined a quantitative criteria Δt to evaluate the assistance provided by the system: Δt equals the localization time separating the positioning of the ultrasound probe inside the abdomen and the successful display of the tumor in the ultrasound image. We built a region of interest in the 3D scene by adding a virtual sphere centered on the tumor. The diameter d of the sphere was calculated regarding both the dimensions of the tumor and the registration errors. In our experiment, the model of tumor resulted in a *15x10x8 mm* ovoid, and the average error on palpation of anatomical landmarks computed after registration was *5.2 mm*. A diameter d = *30mm* provided a realistic targeting area in the visualization. The operator then performed laparoscopic ultrasound imaging of the liver using the indications of the guidance system. When the ultrasound scanning plane intersected the spherical region of interest, the system displayed the resulting disk inter-section in the 3D scene (*Fig.2*). Diameter and position of the disk were updated using magnetic tracking data.

The tumor model system was used to compare LUS and IRLUS in a crossover design. Data were taken for both legs of an experimental protocol and analyzed with criteria developed for evaluating laparoscopic simulation:[3] Kinematic data (elapsed time, instrument orientation, path length, smoothness, and dept perception) were extracted from the positional data streams. As well, the NASA TLX stress evaluation tool,[4] a validated, multi-dimensional rating procedure, was used to characterize the subject workload, with scoring based on a weighted average of ratings on six subscales. The following experimental protocol was used, with subjects being medical interns, residents, and students, who represent therefore an inexperienced user pool.

- In CT suite
    - Implant 2-3 "tumors" (5mm) in liver; check with CT
    - Scans: no contrast, I^+, I^-
    - Reconstruction on scanner
    - Build 3D Model off line
- Surgery with IRLUS and LUS: For each subject,
    - Explain experiment
    - Subject is placed randomly in either in Group A or B
        - A: LUS, then IRLUS
        - B: IRLUS, then LUS
    - Subject seeks tumors, kinematic data are recorded.
    - TLX recorded (off line)
    - Subject repeats with other leg of approach

The kinetic data for n=5 subjects showed no significant difference in the speed of using IRLUS vs. LUS for locating the tumor targets, with the exception of one subject who was unable to find the tumor using LUS. The other kinematic parameters showed significant differences, however, with IRLUS being far superior to LUS:

- Rotation reduced 5.4x
- Path Length reduced 2.7x
- Jerk reduced 2.6x
- Depth Perception improved 7x

In a similar vein, the NASA TLX scores showed that IRLUS was easier to use than LUS, as summarized in Figure 3.

---

[3] Computer-Enhanced Laparoscopic Training System (CELTS) -- Bridging the gap. Stylopoulos, et al. Surg Endosc (2004) 18: 782–789

[4] Hart, S.G., & Staveland, L.E. (1988). Development of NASA-TLX (Task Load Index): Results of empirical and theoretical research. In P.A. Hancock and N. Meshkati (Eds.) Human Mental Workload (pp.139-183). Amsterdam: North-Holland.

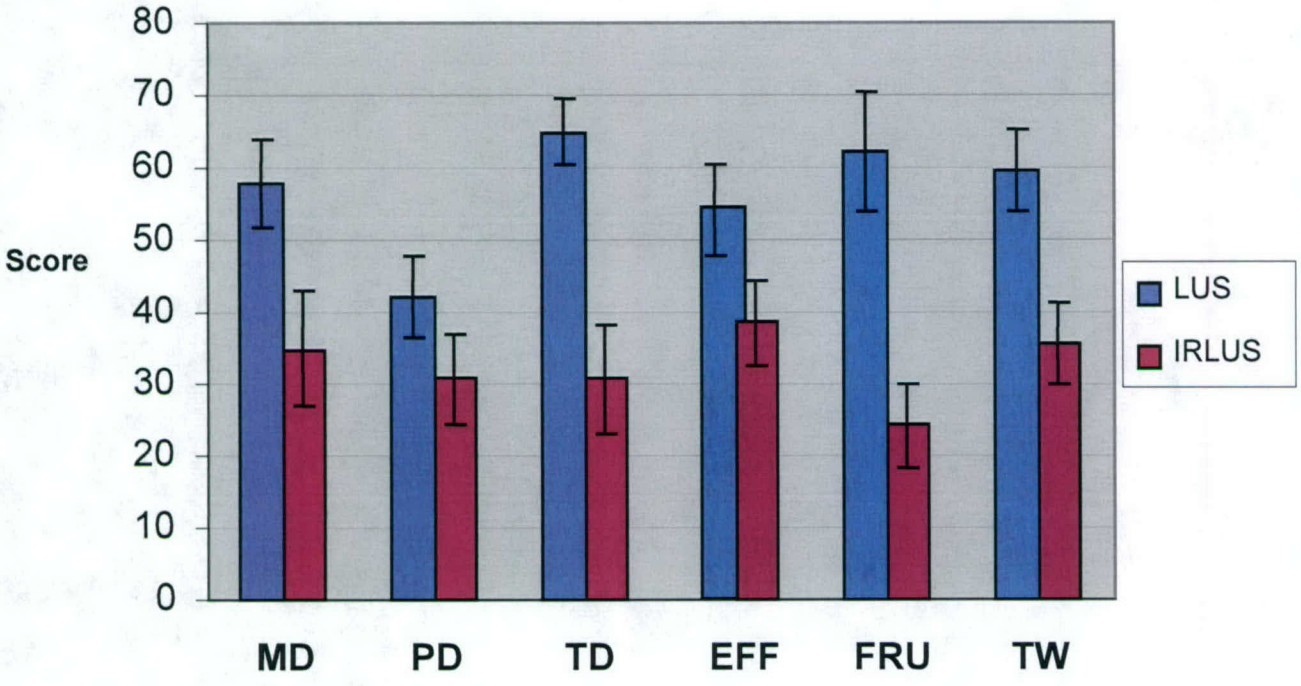

Figure 3
TLX Scores for IRLUS vs LUS for inexperienced users (n=8).

MD: Mental Demands; **PD:** Physical Demands; **TD:** Temporal Demands; **EFF:** Effort;
FRU: Frustration; **TW:** Total Workload

Publications and Presentations

Published/Presented

1) Ellsmere, J., Stoll JA, Rattner DW, Brooks D, Kane, R, Wells WM III, Kikinis R, Vosburgh KG. Integrating preoperative CT data with laparoscopic ultrasound images facilitates interpretation. Soc Amer Gastrointestinal Endoscopic Surgeons. 2003. Los Angeles: Springer Verlag.

2) Ellsmere, J, J. Stoll, D. Rattner, D. Brooks, R. Kane, W. Wells, R. Kikinis, K. Vosburgh, A navigation System of Augmenting Laparoscopic Ultrasound, MICCAI 2003, LNCS 2879:184-191.

3) Ellsmere, J, J. Stoll, W Wells III, R. Kikinis, K Vosburgh, R. Kane, D. Brooks, D. Rattner, A New Visualization Technique for Laparoscopic Ultrasound *Surgery* 2004;136:84-92

4) Ellsmere JC, et al. Does Multidetector-row Computed Tomography Eliminate the Role of Diagnostic Laparoscopy in Assessing Resectability of Pancreatic Head Adenocarcinoma? Surg Endosc. 2004

5) Krissian, K., J. Ellsmere, K. Vosburgh, R. Kikinis, and C. -F. Westin, Multiscale Segmentation of the Aorta in 3D Ultrasound Images, 25th Annual Int. Conf. of the IEEE EMBS (Cancun) 2003: 638-641

Accepted Thesis

6) Ellsmere, JC A Surgical Navigation System for Augmenting Laparoscopic Ultrasound, MS Thesis, Harvard-MIT Division of Health Sciences, June, 2003.

Manuscript Accepted for Presentation

7) Vosburgh, KG, PhD, Stylopoulos, N, MD Pujol, S, PhD San Jose Estepar, R, MS, Krissian, K, PhD, Bricault,I, MD, PhD, Ellsmere, J, MD, MS, Guiding Abdominal Surgery with Image Registered Laparoscopic Ultrasound (IRLUS) -- Radiological Society of North America

Acknowledgements

This work was generously supported through in-kind donations by Ascension Technologies and B-K Medical.

Patient Centric Networking and Applications
Final Report
John Guttag, PhD Principal Investigator

Overall Objectives and Approach

This work explores the potential of patient-centered sensor networks. The work was motivated by the observation that today's sensor electronics and software could be made more capable and integrated more effectively, and that doing so could yield immediate, significant benefits in patient care. The following three activities were pursued in FY03/FY04:

PCN-Robust Patient State Sensing
PCN-Cardiac Auscultation
PCN-Automated Seizure Detection

We developed software infrastructure and new methods and algorithms for screening for mitral valve prolapse (for which a patent application was filed) and detecting the onset of epileptic seizures. This work was tested on de-identified data provided by physicians at MGH and Children's Hospital.

Progress on Specific Aims

Key Results

- Established that our seizure detection algorithm meets the needs of initiating radiopharmaceutical injection for a SPECT imaging protocol.
- Demonstrated that the use of our patient-specific detector would result in the injection of the SPECT radiopharmaceutical, on average, twenty seconds earlier, than current hospital protocols.
- Designed a carotid collar for the identification of carotid stenosis.
- Demonstrated a toolkit for aggregating and analyzing data from hemodynamic sensors
- Built and tested a prototype fall detection system.
- Benchmarked wireless public carrier systems for uni-directional (uplink) information transfer.
- Three students completed masters theses supported by these projects:
  Zeeshan Hassan Syed, Master of Engineering, May 2003
  Jason Gift, Master of Engineering, September 2003
  Ali Shoeb, Master of Engineering, September 2003
- Established cooperative efforts with Emergency Department at BWH.
- Engaged HP Researchers in discussions of joint activity.

1: PCN-Robust Patient State Sensing

Progress

We pursued two directions in this area: building prototypes and investigating deployment opportunities.

Prototypes. We developed a redesign of our patient centric monitoring system.

Figure 1: Patient Centric Network: Streaming Database Architecture in Use

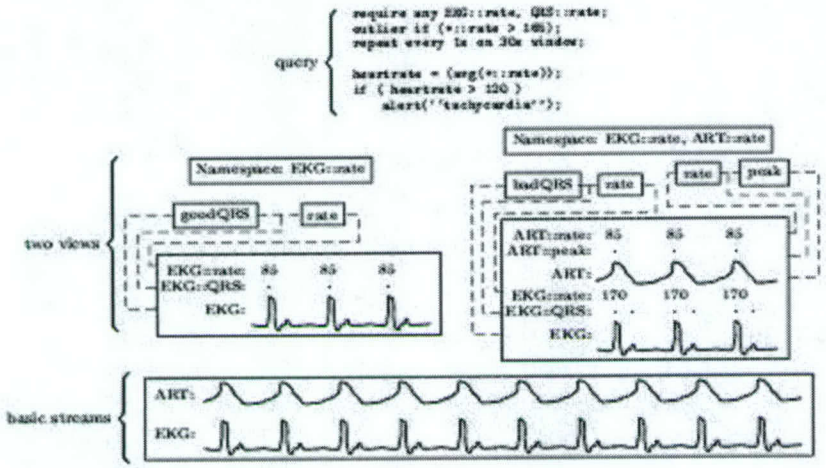

This design is based on a streaming database architecture, as shown in Figure 1. This work includes a user interface that allows the user to select the signals to be monitored and set various medically relevant parameters, synthetic devices to do signal fusion, and an alerting sub-system. These cause queries to be run over the data streams and the results to be displayed to the user. The prototype was demonstrated at the MIT EECS Department's 100th Anniversary in May 2003 and at the Oxygen Partners Meeting in June 2003.

Also, we explored the design of a system that detects when a person has fallen. Through this prototype we are attempting to understand the issues involved in building a **robust mobile** patient monitoring system. The design uses an HP iPaq with a built-in accelerometer.

We continued our work on building a reliable alerting system based on data collected from a potentially unreliable sensor network. The central issue is trading off false alarms against delay in alerting. Our central proposal is to maintain an estimate with an associated confidence interval for each sensor value we read from the network. Missing data decreases the confidence in our estimate. The arrival of data causes the re-estimation of the value and, usually, increases our confidence in this estimate.

To analyze our system's behavior under a variety of data rates, we decided to look at some low data rate sensors. For our experiments, each person will wear up to five sensors. These inexpensive sensors will give us several simple streams of low data-rate data to be integrated.

We continue to work on the problem of providing consistent and correct semantics in the kind of dynamic, noisy, and asynchronous environments typical of real time medical monitoring. We devoted special attention to issues related to the kinds of inconsistencies that arise when incorrect results are reported and then later corrected.

Deployment We visited the Emergency Department at Brigham and Women's Hospital and several Intensive Care Units at Massachusetts General Hospital to understand how a mobile (or untethered) patient monitoring system would improve their operations. We developed an architecture specification and a user interface specification. We are evaluating sensors and

location systems. Working with the Emergency Department at BWH, we have started evaluating inexpensive ECG sensors and are working to understand the quality of signal that is acceptable for monitoring patients in the waiting room.

Follow-on:
Our work with the Emergency Department at BWH has led to a three-year contract with the NLM to continue some aspects of this work.

2: PCN-Cardiac Auscultation

Progress
The main goal of this project is designing, implementing and evaluating an inexpensive to deploy and easy to use automated cardiac screening system that can be used in conjunction with an electronic stethoscope. The system aims to make a recommendation and support its decision with audiovisual diagnostic aids such as the prototypical heart beat and variable-rate playback of heart sounds. The structure of the system is shown in Figure 2. The visual prototypical beat for a normal patient is shown in Figure 3. The visual prototypical beat for a patient suffering from MVP is show in Figure 4.

Figure 2: MIT Automated Auscultation System Block Diagram

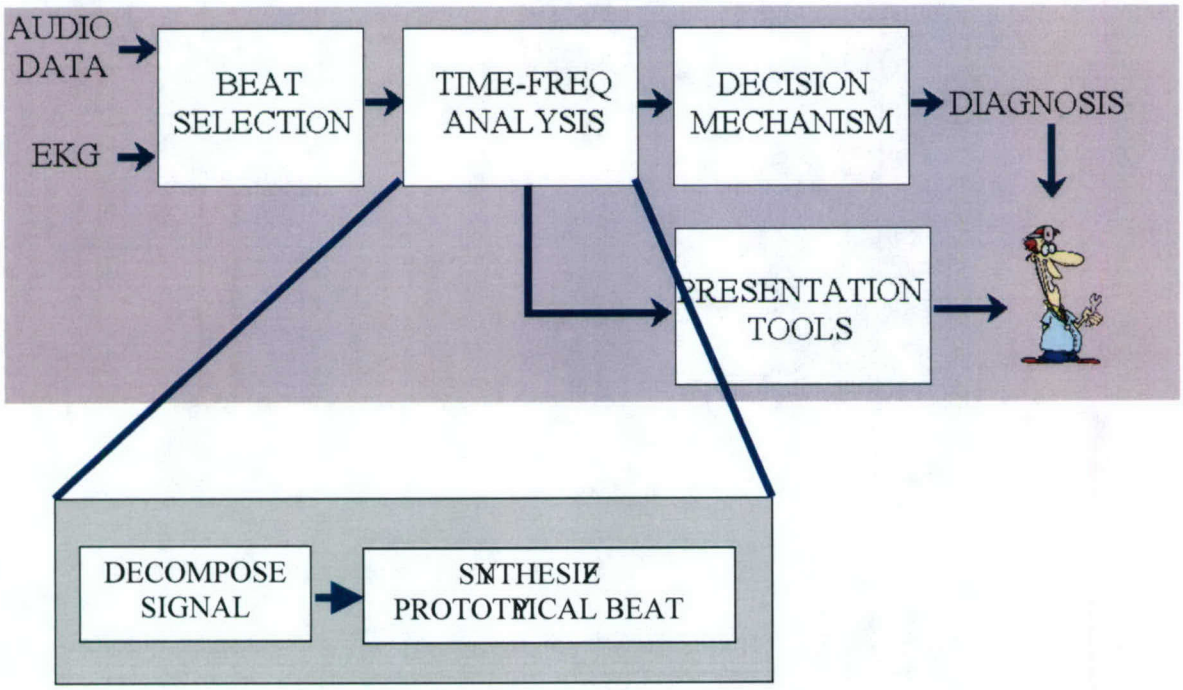

Figure 3: Prototypical Beat for Normal Patient

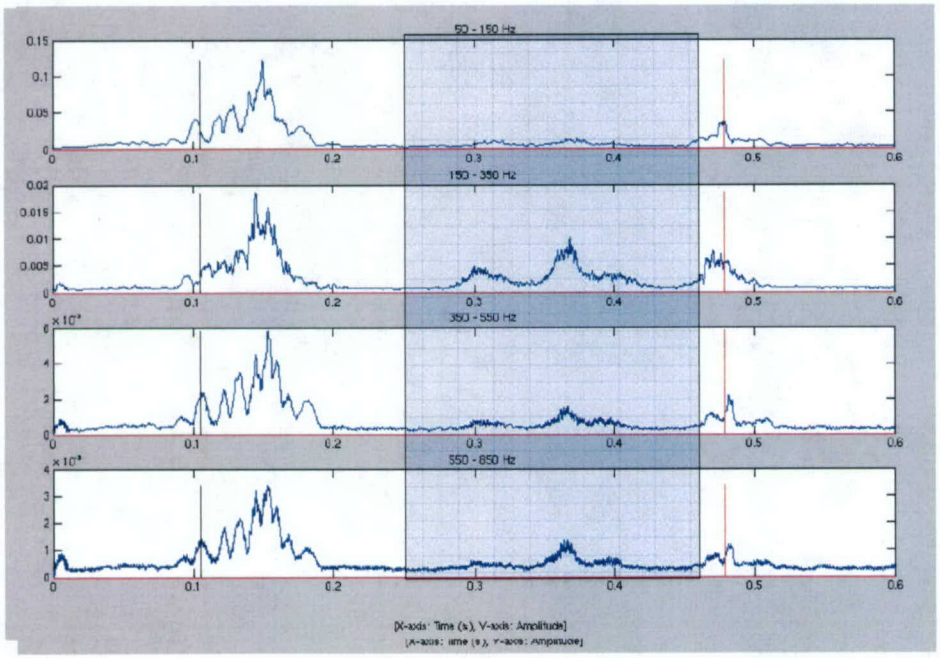

Figure 4: Prototypical Beat for MVP Patient

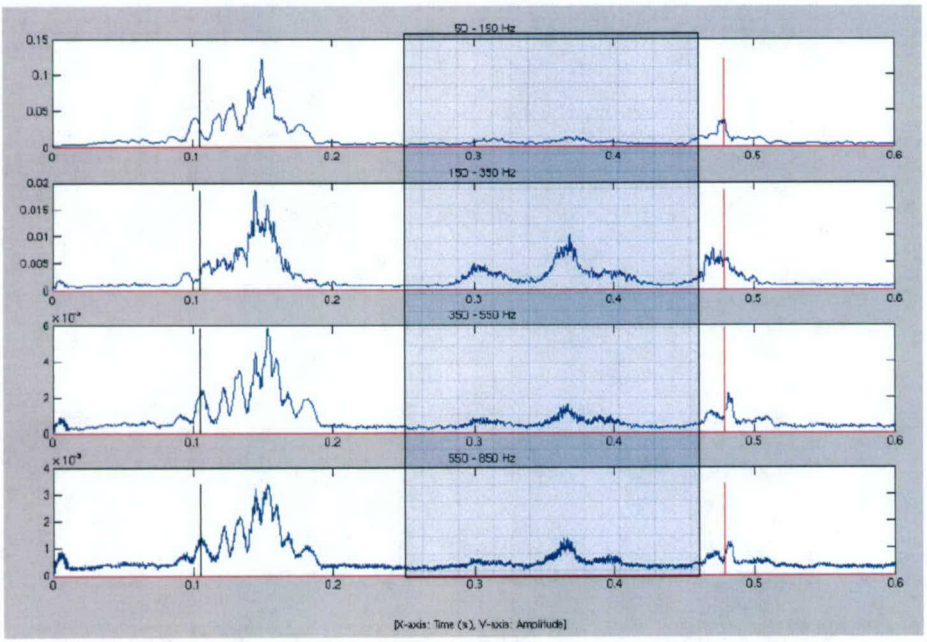

Our current algorithm is focused on separating patients with MVP from normal patients and patients with benign murmurs. Most recently, we have consolidated our results and tuned the parameters of our algorithm. We have tested our detection system on de-identified data from 57 patients, with promising results.

We also looked at applying similar signal processing and audio visual techniques to related medical signals in the area of breathing. We implemented algorithms for counting breaths, crackles and wheezes. We believe this is an important area to pursue, as respiration is a poorly monitored vital sign and it seems that computer automation could help in this area.

In conjunction with physicians at MGH we considered adapting some of our auscultation techniques to the identification and classification of carotid stenosis. We have made progress in this area in designing a system, called the Carotid Collar for capturing data in this area, Figure 5. The system is based on piezo-electric sensors embedded in a cervical collar, Figure 6, to record the sounds from the carotid arteries. It also includes an EKG sensor and another piezo-electric sensor for collecting heart sounds. The software, which runs on a laptop, collects and displays data from these sources, Figure 7

Figure 5 Block Diagram of Carotid Stenosis Sensor System

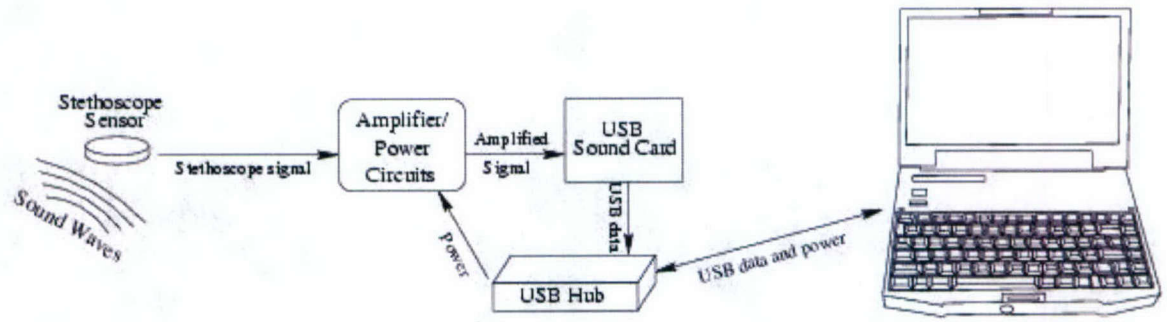

Figure 6 Collar for Recording Carotid Sounds

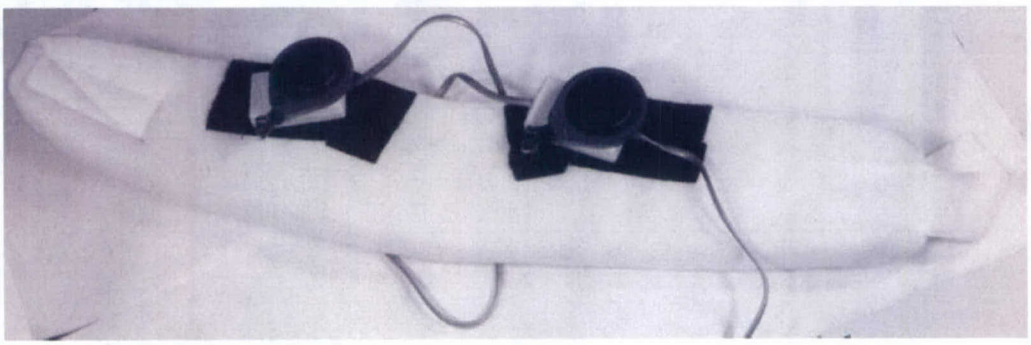

Figure 7 User Interface to Carotid Sensor System

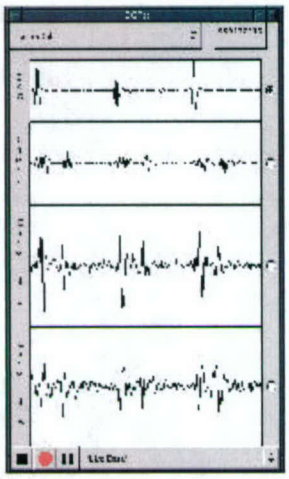

Future work
Again, as a result of the seed money provided by CIMIT we were able to find funding from another source to continue this work. We expect that this will allow us to push this project far enough forward to deploy some test systems. We also expect to publish the results in the medical literature.

3: PCN-Automated Seizure Detection

Progress
The goal of this project is to develop a real-time, patient-specific, epileptic seizure onset detector using scalp EEG. Our collaborators at Children's Hospital are interested in using this system to detect seizure onset more promptly so that the SPECT radio-isotope dye can be injected more promptly so that the SPECT imaging will potentially identify a smaller seizure focus.

Our strategy uses machine learning algorithms and digital signal processing. We use wavelet decomposition to generate the feature set supplied to the learning algorithm. We use a novel approach to reject artifacts, based on a library of EEG artifacts, collected across patients. We explored the utility of two different architectures and two different machine-learning methods for attacking this problem.

The best combination performs extremely well, detecting a seizure with an average delay of 8.0 ± 3.2 seconds (see Figure 8) while correctly declar ing 131 of 139 seizure events (see Figure 9). Furthermore, the detector declared only 11 false detections in 49 hours of randomly selected non-seizure EEG.

Figure 8: Patient Specific Seizure Detector: Latency Results

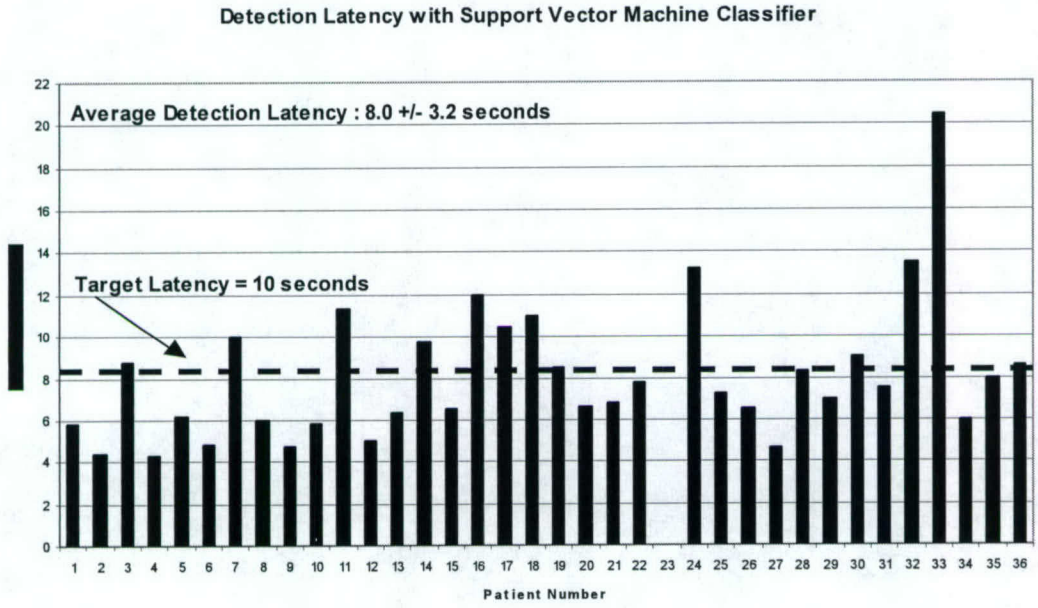

Figure 9: Patient Specific Seizure Detector: Detection Results

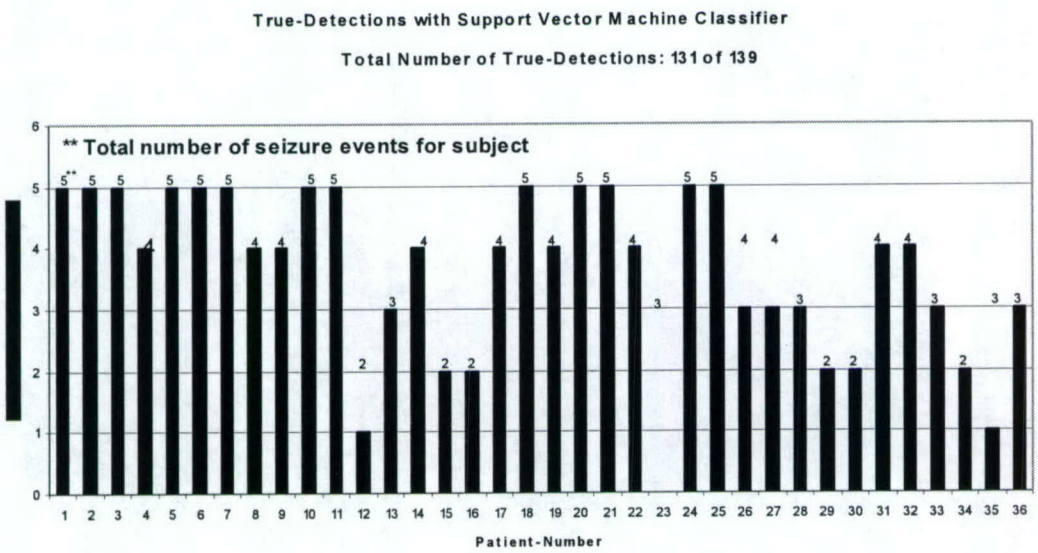

Additionally:
A comparison to non-patient-specific detection suggests strongly that exploiting patient-specificity is highly advantageous.

A study of the impact of number of training seizures indicates that a detector trained on one recording from a test subject is capable, on average, of detecting 91% of that subject's future seizures with a mean latency of 9.5 seconds. When an additional training recording is observed, the detector identifies 96% of the subject's future seizures with a latency of 7.6 seconds. Observing a third recording only slightly improves performance beyond that obtained using two training recordings.

All of this suggests that for most patients initiating an ictal SPECT with our method is favorable given that using the existing protocol the procedure is typically begun 30-45 seconds following seizure onset, which can lead to poor localization of the epileptogenic focus.

We are in the midst of a study comparing the delay incurred by starting injection of the SPECT radiopharmaceutical using existing hospital protocols to the delay that would be incurred provided injections were triggered using our patient-specific seizure onset detector. The study will include seizure recordings from twenty patients, and will provide preliminary results supporting the application of our detector to initiate injection of the SPECT radiopharmaceutical in a clinical setting. Early indications, based on nine patients, are that our detector, on average, would begin injection of the radiopharmaceutical more than twenty seconds before the actual injection.

In related work, we are in the process of developing a tool to analyze hemodynamic signals. Specifically, we are analyzing data collected from premature infants. Our tool should assist researchers in correlating the data with outcomes.

Future Work
Our plans include investigating patent opportunities, and working with researchers at Children's Hospital to design a tool for use in a clinical setting. Specifically, this tool will be used to investigate the effect of the timeliness of the injection of the isotope on the SPECT imaging process for locating the focus of a seizure. The hypothesis is that more prompt injection of the isotope will produce an image with a smaller seizure focus and thus less of the brain will be removed. We anticipate that we will submit an IRB to Children's in the fall of 2004.

We also plan to investigate the potential applicability of our methods to enhance the effectiveness of devices that use nerve stimulation to abort seizures.

Since the termination of this grant, we have submitted a proposal to the Oxygen Partners at MIT to continue work in these areas.

Publications

"Patient-Specific Seizure Onset Detection," manuscript submitted to the journal *Epilepsy and Behavior*. Authors: Ali Shoeb, Herman Edwards, Jack Connolly, Blaise Bourgeois, S. Ted Treves, John Guttag.

"Patient-Specific Seizure Onset Detection," manuscript submitted to the 26th Annual International Conference of the IEEE Engineering in Medicine and Biology Society (EMBS). Authors: Ali Shoeb, Herman Edwards, Jack Connolly, Blaise Bourgeois, Ted Treves, John Guttag.

Abstracts

"Networked Sensor-based Decision Support Systems," John Guttage, Oxygen Partner's Meeting, June, 2003

"ORNet Streaming Database Demonstration," Gregory Harfst, MIT EECS Department 100th Anniversary, May 24, 2003, Oxygen Partners, June 2003.

"Putting Health Care on the Technology Curve," Annual Meeting of American Society for Reproductive Medicine, Plenary presentation, San Antonio, Texas, October 14th, 2004.

"Sensor Based Medical Decision Systems," Distinguished Lecture, Brown University, March 2004.

"Robust Physiological State Sensing and Decision Making," Telemedicine and Advanced Technology Research Center (TATRC), Maryland, March 2004.

"Pervasive Medical Monitoring Using Commodity Hardware," submitted to the First ACM International Workshop on Applications of Mobile Embedded Systems.

Presentations

"Networked Sensor-based Decision Support Systems," John Guttag
CIMIT AIBS Review, May 2003.
Oxygen Partner's Meeting, June 2003.

"ORNet Streaming Database Demonstration," Gregory Harfst,
MIT EECS Department 100th Anniversary, May 24, 2003.
Oxygen Partners, June 2003.

Theses

MIT Automated Auscultation System, Zeeshan Hassan Syed, Master of Engineering Thesis, MIT, May 2003.

Carotid Collar: A Device for Ausultory Detection of Carotid Artery Stenosis, Jason Ayres Gift, Master of Engineering Thesis, MIT, September, 2003.

Patient Specific Seizure Onset Detection, Ali Hossam Shoeb, Master of Engineering Thesis, MIT, September, 2003.

Patents

"MIT Automated Auscultation," Patent Application, Zeeshan Hassan Syed, John Guttag, Robert A. Levine, M.D., Francesca Nesta, M.D., Dorothy Curtis, June 2003.

Portable, Wireless Gait Evaluation and Biofeedback Tool

Donna Moxley Scarborough Principal Investigator

Overall Objectives and Approach

The purpose of this project is to advance development of the wireless, portable gait evaluator and biofeedback tool through progressive reliability testing of the foot position sensors and to initiate a transition into a wearable system. The overall aim of the project is to develop and implement an important medical application of the portable gait evaluation and eventual implementation of the data for gait biofeedback. Funding from CIMIT was allocated to focus on reliability testing of the foot position (kinematic data) sensors and advancing the gait evaluator's portability to create a completely wearable novel clinical tool. The following report is an overview of tasks accomplished over the past year. Currently, we are on a time extension of CIMIT funds and anticipate the depletion of funds and final report to be completed on the first of March 2005.

During the first 2 quarters of this project year, we developed methodology for progression of calibration and reliability testing of kinematic data and initiated analysis of time data for heel/toe and stride and kinematic data. We also began brainstorming on potential hardware for the wearable gait evaluator design, and investigated a possible patent application and grant application(s) for larger external funding. Data collected from the Portable Gait Evaluator on 10 healthy subjects and 6 subjects with Parkinson's disease (PD) during spring and summer 2003 provide the initial database of reliability testing. A total of 19 healthy persons and 7 persons with pathological gait were tested for gait parameter reliability. We focused on planning with collaborators about possible business ventures and initiated letters of intent for possible internal and external funding to facilitate progression and advancement of the project.

Quarters 3 and 4 were spent performing analysis of calibration and reliability testing of kinematic data, time data for heel/toe and strides and kinematic data. Discussions regarding potential hardware for the wearable gait evaluator design were begun. However, we decided to not purchase pocket PC's or PDA's for the hardware design of a wearable system. We determined that focus on improving the software and testing protocol for use of biofeedback to address our current objectives also will improve the opportunity for future funding, as biofeedback is the strongest unique feature of the portable gait evaluator system. In doing this we made use of current equipment, purchased new software for biofeedback testing and created a test protocol. This decision allows us to address both the progression of validation studies simultaneously with the progression of the biofeedback trigger objectives. We received approval from MGH's IRB to add additional subjects for gathering pilot data using the biofeedback sound capability. Subject testing resumed in quarter 4 for continued kinematic reliability testing and progressive testing of the biofeedback tool. We have tested 3 healthy persons using the biofeedback system in the fourth quarter, progressing it's capability. We anticipate continued testing of healthy persons and those with PD in November 2004 using the biofeedback protocol. As the gait evaluator and biofeedback system evolves we have continued to present it at conferences and now refer to the system as the "Smart GaitShoe". We began the initial application process for a patent, and are refining a grant application for larger external funding.

The following are specific updates related to our specific aims:

Specific Aim 1
We propose to test the reliability of the device for obtaining foot and ankle kinematics to support continued development, of the portable gait evaluator. Proposed funding will allow us to validate foot position data. We hypothesize that *a) the portable gait evaluator will provide ankle dorsi/plantar flexion and external/internal foot rotation motion output which will directly correlate to Biomotion Laboratory's data; b) the portable gait evaluator will quantify gait impairments accurately and reflect common gait deviations among subjects with Parkinson's disease (PD).*

The calibration output for the foot/ankle kinematic data was analyzed. A comparison of output from 2 sensors (pitch gyro and a bend sensor) is used to determining ankle dorsi flexion/plantar flexion is underway. The gyroscopic data for foot pitch plot more similar to the data produced by the Biomotion Lab than that from the bend sensor. We are currently working with other types of sensors to determine the best method for measuring ankle pitch.

Our first manuscript describing the validation of initial gait analysis parameters from the wireless portable GaitShoe was submitted to IEEE 6/1/04. We analyzed a total of 270 de-identified gait trials collected from fifteen de-identified subjects. Each trial could have multiple steps per trial of data for possible comparison (dependent on stride length as visible for the Biomotion Lab camera viewing volume size). The data we report in our submitted manuscript include the following data.

The GaitShoe stride length compared to the BML data (GaitShoe-BML data) was 7.4 ± 13.6 cm mean difference Pearson's correlation = .841 (sample of 315 strides).

The mean difference between Gait Shoe maximum foot pitch and BML maximum foot pitch was -0.7 ± 6.6 degrees (sample of 1132 foot positions) and the Pearson's correlation value was = 0.99. The mean difference between the Gait Shoe heel-strike times and the BML heel-strike times was -6.7 ± 22.9 ms (sample of 77 times) and Pearson's correlation = .999.

The mean difference between the GaitShoe and the BML toe off times was -2.9 ± 16.9 ms. (sample of 75 times) and Pearson's correlation = 1.000.

Continued work is being done to compare internal and external foot rotations. These data are more difficult to calibrate and determine from the shoe data.

We are now performing initial analysis on gait variability of gait parameters for the persons with PD and healthy subjects. It is our intention to complete comparisons of step length, stride length, gait speed, foot pitch, foot to floor height, foot roll time, across trials of various tasks including the use of Rhythmic Auditory Stimulation (RAS). Initial comparisons have been completed.

Specific Aim 2
Further develop the current gait evaluator's portable laptop system into a smaller, wearable device. The current laptop-based data collection and analysis program will be ported to a small, wearable PDA. Software will be further developed using a systematic approach for timing automatic data collection and to trigger on and off collection times. The trigger method will be crucial in development of the device, to enable clinicians and patients to know when the wearer is stopping purposefully versus, e.g., an episodic freezing event. We hypothesize that *the wearable gait evaluator will successfully trigger when data is and is not to be collected.*

Progress on development of trigger for data collection and wearable design has progressed with regards to use as biofeedback tool. Software has been developed to know to trigger auditory sound for feedback. The gait evaluation software was developed for the PC and the biofeedback program created was written for Mac Lap top computer. During quarter 4 we purchased software to allow the biofeedback program to be further developed on a PC lap top. We currently are improving upon this new transition of both the gait evaluator and the biofeedback programs merging together on a PC based computer. Currently, we have developed use with FSR sensors for triggering biofeedback auditory sounds. Cost of engineer to develop PDA for wearable system was too great for current budget without stopping basic development. Therefore, we decided to develop the capability and software of the current portable designto include the real time biofeedback function. We believe that continued development of the Smart GaitShoe, a novel portable gait evaluator and biofeedback system, will produce a valuable clinical tool.

Illustrations

Output of the 2 heel FSR sensors of the right shoe and metronome beats targeting right heel strikes. The vertical lines mark the auditory rhythmic sound provided continuously. The subject turned around at the 7th second and quickly returned to target heel strike with the rhythmic sound.

Illustration of a 3 dimensional android model of a 65 y.o. male with PD during a self selected 'free' gait trial and a metronome paced gait trial.

Figure showing plots of PGE pressure sensor data and Biomotion Lab Force plate data from simultaneous data collection from the right foot of one healthy subject. Top plot illustrates output form all FSR's from PGE. Middle plot illustrates the sum of all FSR output data from the PGE. Bottom plot illustrates the ground reaction force output from the Biomotion Lab's force plates. Of note is the similarity of the middle and bottom plots. The data from the PGE is continuous showing 3 steps. Although the data stream from the Biomotion Lab is continuous for 3 seconds, the force plates are a fixed length and therefore data is limited to the one step.

Publications and Presentations

1. Scarborough DM et al. Platform presentation *Introduction to a Portable, Wireless Gait Evaluation and Biofeedback Tool* at the XVth International Congress of the International Society of Electrophysiology and Kinesiology (ISEK), held on June 20, 2004 at Boston University, Boston, Massachusetts.

2. Stacy Morris Bamberg et al. PhD thesis completed and presented (MIT) on initial development of the PGE (co-investigator) May 2004.

3. Stacy Morris Bamberg et al. Submission to IEEE 6/01/04: *Gait Analysis Using a Shoe-Integrated Wireless Sensor System.*

4. Scarborough DM et al. Submitted application (August 2004) to present *Portable, Wireless Gait Evaluation and Auditory Biofeedback* at the 2005 Combined Sections Meetings. American Physical Therapy Association.

External Proposal Activity

1. A Letter of Intent was submitted to MGH's innovative ECOR grant committee May 27th 2004 for request to submit a proposal. *It was denied.*

2. A Letter of Intent is being submitted to The Michael J. Fox Foundation's Fast Track grants June 28th 2004 for request to submit a proposal. *The LOI was not accepted.*

3. A grant application for a NIH RO3 is near completion.

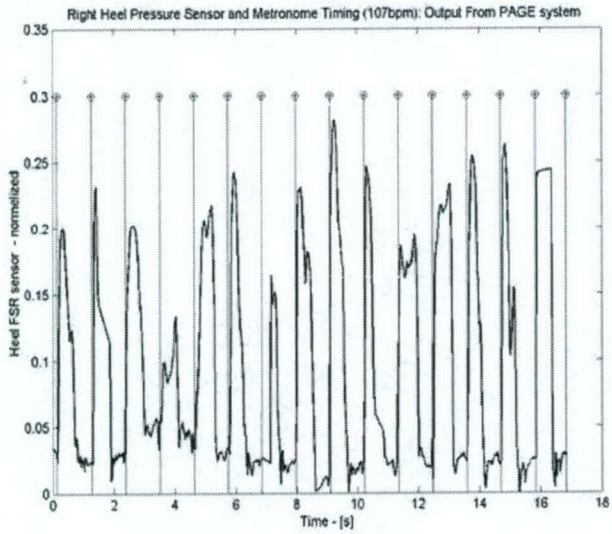

Illustration 1.

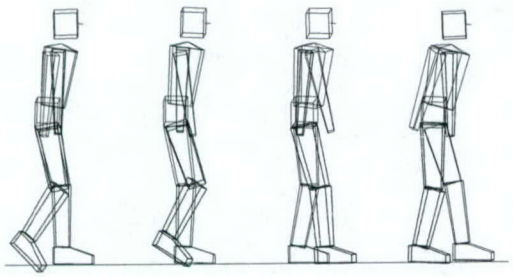

Free Gait

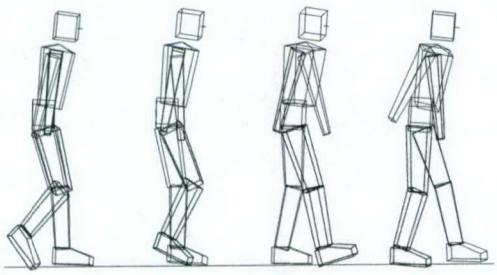

Paced Gait

Illustration 2.

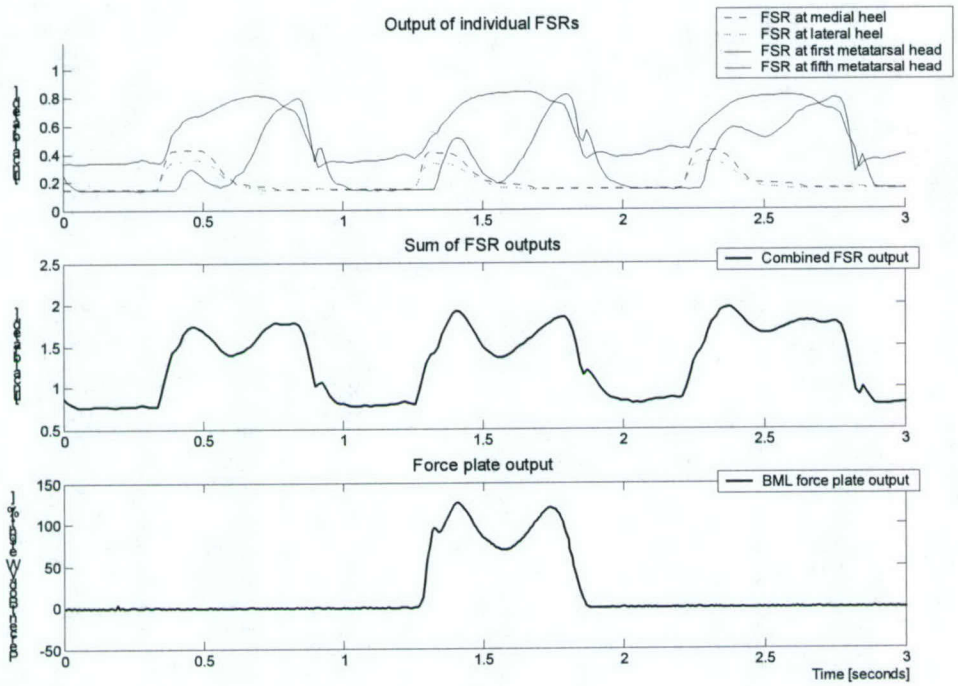

Illustration 3.

Low Coherence Interferometry System for Guidance in Lumbar Punctures

Guillermo J. Tearney, M.D. Ph.D., Donald R. Johns, M.D. Principal Investigators

Overall Objectives and Approach

In this proposal, we investigate a novel method for the improved performance of lumbar puncture (LP). LP is a frequently performed, invasive procedure for the diagnosis and therapy of a number of infectious and inflammatory neurologic diseases. Low coherence interferometry (LCI) is an optical diagnostic technique that can provide characteristic structural information of nearby tissues. LCI-guided LP (LCLIP) could provide interactive guidance of the LP needle in real-time and identify the adjacent tissue type before it is actually penetrated. The aim of this study is to develop and test criteria for LCI-based differentiation of tissues of the spine.

Progress on Specific Aims

Specific Aims

1. Construct an LCI library of different human spinal tissue types.
2. Develop model for LCI tissue classification.
3. Test the sensitivity and specificity of LCI criteria.

We developed a library for LCI-based spine tissue differentiation. We have obtained LCLIP reflectivity measurements on (n=19) sagittally sectioned spines, totaling 760 distinct samples. In order to quantitatively differentiate fat, muscle, cartilage, bone, nerve, dura, etc., two parameters were computed from the LCLIP data; the slope and standard deviation of the logarithm of the axial reflectivity profiles. The mean ± STDEV of the LCLIP slope and signal standard deviation have been computed (Table 1). Figure 1 depicts an x-y scatter plot of a portion of the training set, which demonstrates clustering of tissue types. A decision-tree classification model generated from our current data remains highly self-consistent (>90%).

Tissue type	Number	Slope ($x10^{-3}$)	Signal stdev ($x10^{-3}$)
Skin (dermis)	40	9.8 ± 1.6	111.7 ± 17.2
Adipose	40	3.3 ± 0.9	292.5 ± 34.9
Fascia	34	14.9 ± 2.2	137.5 ± 14.2
Muscle	40	20.9 ± 2.5	163.7 ± 19.9
Bone	34	32.5 ± 4.2	101.3 ± 16.8
Cartilage	34	23.3 ± 3.3	127.3 ± 15.2
Dura	34	41.7 ± 7.0	76.9 ± 10.7
Nerve	34	39.3 ± 6.6	104.8 ± 12.7

Table 1. Characteristic LCI signatures for a subset of the training set tissues.

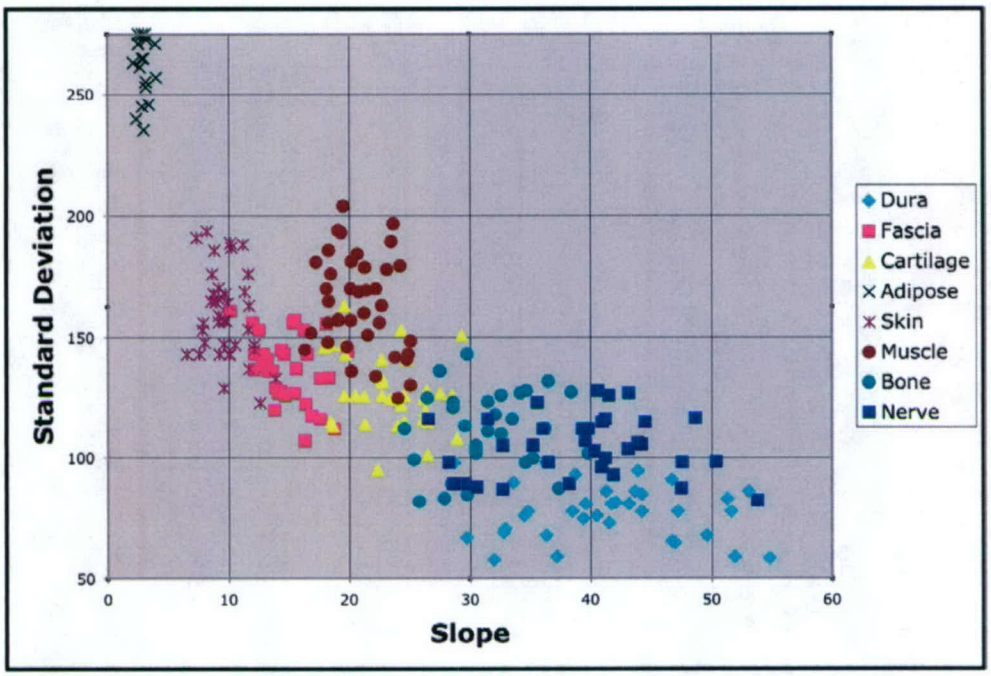

Figure 1. Scatter plot of a portion of the training set. Spine tissue types appear remain separable based on the slope and standard deviation of the LCI signal.

For the 19 spines, we have sent tissue from each of the (n=760) LCLIP data collection sites for histopathologic processing. Following receipt of the slides, we will finalize and test the classification algorithm for determining different spinal tissue types.

Changes in Protocol

Due to a change in autopsy protocol at the Massachusetts General Hospital, it has become difficult to obtain human cadaver spine segments. As a result, we have changed the protocol to conduct tissue differentiation in swine. Since the swine and human spine tissues are similar, we believe that this modification will not affect the significance of our results.

Publications and Presentations

This work was presented at SPIE Photonics West conference in January of 2004 [1]. We are also targeting manuscript submissions to *Journal of Biomedical Optics* and a clinical neurology journal in the winter of 2004.

References

1. Iftimia N, Johns D, Bouma BE, and Tearney GJ. Low coherence interferometry system for guidance in lumbar puncture procedures. SPIE Photonics West, Abstract 5318-29, 2004.

Local Incorporation of Anti-neoplastic Agents into Surgical Resection Margins Using a Minimally Invasive Delivery System

Yolonda L. Colson, MD, PhD Principal Investigator

Overall Objectives and Approach

The foundation of this proposal is the design of a minimally invasive delivery system to incorporate anti-neoplastic substances into the surgical resection margin in order to prevent local recurrence. Since endoscopic surgical stapling devices are commonly utilized for surgical resection, the goal is to evaluate the feasibility of incorporating "therapeutic" drug-eluting polymer depots, staples, or radioactive seeds within the surgical staple line as part of a convenient, and safe, minimally invasive delivery system.

Specific Aims:

1. Evaluate the risks and benefits of implanting radioactive seeds vs. chemotherapy drugs along the suture line and determine which therapy to pursue for our investigation.
2. Identify and characterize the various drug-eluting polymers in terms of their loading capacity, release profile, biocompatibility, conformability to the lung surface during ventilation, and tissue adhesion characteristics.
3. Identify the most promising chemotherapeutic agents in terms of potential local effectiveness and toxicity, realizing that future animal studies will likely be required to evaluate the kinetics of drug delivery from the various polymers as proof of concept later in the development phase

Progress on Specific Aims

The IRB proposal for this project required revision so as to be considered separate from other "discarded tissue" protocols. Therefore, a separate IRB protocol has been written, revised, and approved, so that human lung tissue can be obtained for these studies. Second, the largest expense for this project involves the purchase of stapling devises to be used in these studies. Over the past few months, a "recovery system" has been created whereby non-sterile (but biologically non-contaminated) stapler guns and insert cartridges, which have previously been discarded, can be recovered and used for the CIMIT project. This has already resulted in the estimate saving of $300 in just this past 2-3 months! This saving has now permitted me to provide salary support during the summer to a Biomedical Engineering student from Boston University (Solomon Azouz) who is leading the project for his Senior Thesis and part-time support to an engineering consultant (Ian Schwartz). The establishment of this team has dramatically facilitated the progress and development of this project.

Several potential anti-neoplastic agents for these studies were analyzed. We chose to pursue our future studies of anti-neoplastic response using paclitaxel (Taxol) chemotherapy incorporation within the resection margin for several reasons. First, we have found radiation seeds logistically difficult to work with in the operating room (OR), and significant regulatory requirements are involved in the storage and distribution of radioactive seeds or devices. This would significantly limit the rapid and immediate availability of our product in the OR and compromise our goal of personnel safety. In addition, wound/incision healing concerns are definitely a factor with local radiation at the resection margin. Second, paclitaxel has been demonstrated to be an efficacious

agent in the treatment of advanced non-small cell lung carcinoma (1-4). Third, paclitaxel can be handled using commonly available protective devices – dust respirator, lab coat, gloves, and splash goggles. We also have available a fume hood within the laboratory. Fourth, it is our understanding that paclitaxel has recently come "off patent" and is readily available for purchase through several companies including Sigma Aldrich and Calbiochem. Finally, paclitaxel has been widely studied in polymer incorporation for use in vascular stents (5-7) and into microspheres for intratumor injection (8). Demonstrating that paclitaxel possesses the chemical properties necessary for both stable incorporation within polymers and timely predictable drug release is critical for the prolonged drug delivery that is required for our planned approach. Specifically, we are focusing our investigation on drug eluting polymers, specifically microspheres embedded within/onto a tissue adhesive platform. This is proving to be an effective 'combination' therapy that will provide local drug delivery to the resection margin and overcome pliability and conformity issues that would be confronted with a larger polymer device.

After initial investigations, we determined that the incorporation of paclitaxel into bioabsorbable poly (D,L-lactide-co-glycolide) (PLGA) microspheres will permit manipulation of the kinetics of drug delivery and result in a relatively easy to use "dose delivery package". Paclitaxel has been loaded into such microspheres previously and the release kinetics have been described *in vitro* (9-11). Therefore we have begun to prepare non-drug loaded (control) microspheres in our lab (figure 1) using the water-in-oil emulsion technique described in Edlund and Albertson (12) to work out methods without any risk of chemotherapeutic agents during this learning phase. Figure 1 shows that we have prepared PLGA microspheres in our laboratory. However, our control over the process has not been perfected as seen in the inconsistency of microsphere size.

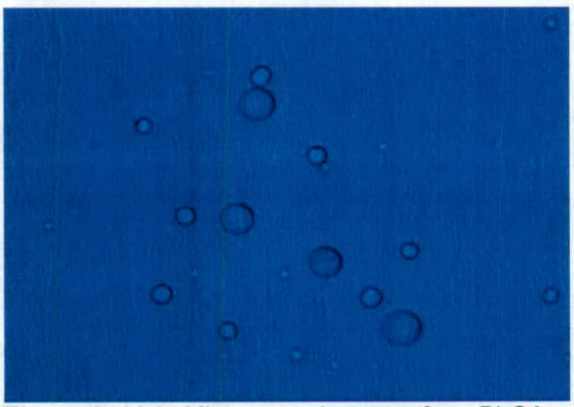

Figure 1. Light Microscope images of our PLGA microspheres. Magnification = 40x.

We also began investigations into tissue adhesive platforms that the microspheres will be embedded within. These studies have focused on amphophilic block copolymer hydrogels such as Pluronic gels. BASF corporation was kind enough to donate a stock of NF-grade Pluronic-127 and NF-68 for these studies. Such gels have altered properties at different temperatures going from liquid to gel at body temperature, and this can be utilized to our advantage. Although some tissue adhesives have been associated with problems in wound healing, pluronic gel has been shown to promote wound-closure rates in burn animal model (13) and the attachment and growth of human gingival fibroblast (14). Finally, although these experiments have yet to be performed, we expect that it will take longer for paclitaxel to diffuse to the resection margin when microspheres are embedded within Pluronic gel than microspheres alone. The likely increased time for initial drug penetration to the resection margin will be due to the increase distance that

the drug will diffuse. This could prove extremely useful because it would provide time for, and perhaps even promote wound healing before paclitaxel reaches the site.

During this last quarter, we have performed initial studies on the tissue adhesion characteristics of microspheres in association with Pluronic NF-127. For these studies, microspheres suspended in water or pluronic NF-127 gel were plated onto the surface of whole lungs harvested from murine donors. The lungs are then rocked from side to side to permit the simulation of the pleural fluid washing over the lungs as occurs during respiration in vivo. Figure 2 shows that microspheres adherence to whole mouse lung is significantly increased if embedded within Pluronic F-127 compared to microspheres alone. In addition, we have participated in the submission of an application for a Flexivent system through which we can ventilate lungs and measure murine lung mechanics and assess lung compliance after the placement of Pluronic gel + paclitaxel microspheres on the lung parenchyma. Completion of independent and amended animal care protocols in which to test the paclitaxel microspheres for tumor effectiveness and effects on wound healing have also now been approved (Protocol # 03833) in order to establish proof-of-concept for our prototype.

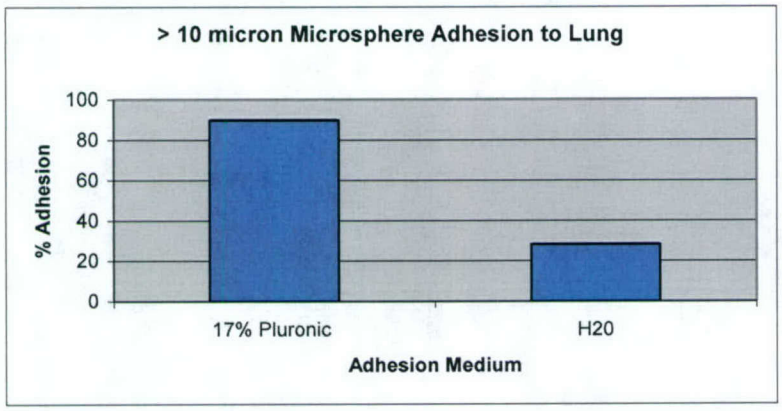

Figure 2. Adhesion to murine lungs of microspheres incubated in the presence or absence of Pluronic gel. Microspheres remaining in the supernatant were then counted on a coulter counter and the percent that adhered to the lungs was determined.

In order to assess our approach *in vitro* and *in vivo*, we have established collaboration with Dr. John V. Heymach at Dana Farber Cancer Institute to utilize his expertise in *in vitro* tumor culture and *in vivo* murine models that are important in the assessment of paclitaxel efficacy and effects on wound healing strength. As a medical oncologist, he is very interested in the potential of our model and has agreed to collaborate with us to evaluate paclitaxel dosing for loading into the microspheres and the effect of paclitaxel microspheres on wound healing. These findings can then be incorporated into the known allogeneic and xenogeneic murine models of lung cancer growth. As part of this collaboration, we have established a cell proliferation assay that permits the study of release kinetics and dosing, as well as affords us the opportunity to demonstrate that the anti-tumor effect of our microspheres are due to a dose-dependent release of paclitaxel in an *in vitro* setting. We have chosen to study four tumor cell lines, both lung cancer as well as others. We have conducted the initial experiments to determine the effective dose of paclitaxel on established cancer cell lines as a guide to choosing the loading dose within the microspheres. Figure 3 demonstrates the presence of a sharp dose response curve to paclitaxel exposure at paclitaxel concentrations >10ng/ml during in vitro culture in a melanoma cell line. We are establishing dose response curves to local paclitaxel concentrations for each of the cell lines. Our preliminary data suggests that the concentration breakpoint for preventing tumor cell proliferation is similar in

other cell lines as well. These dose/response curves give us a starting point in terms to how much drug needs to elute from our microspheres for a localized and effective therapy. Based on these studies, we anticipate that we will target a local paclitaxel delivery concentration of 50-100mg/ml from the paclitaxel-loaded microspheres. All four cancer cell lines will be tested *in vivo* with paclitaxel-loaded microspheres, and animals will be assessed for evidence of paclitaxel toxicity, wound healing, wound strength and tumor burden.

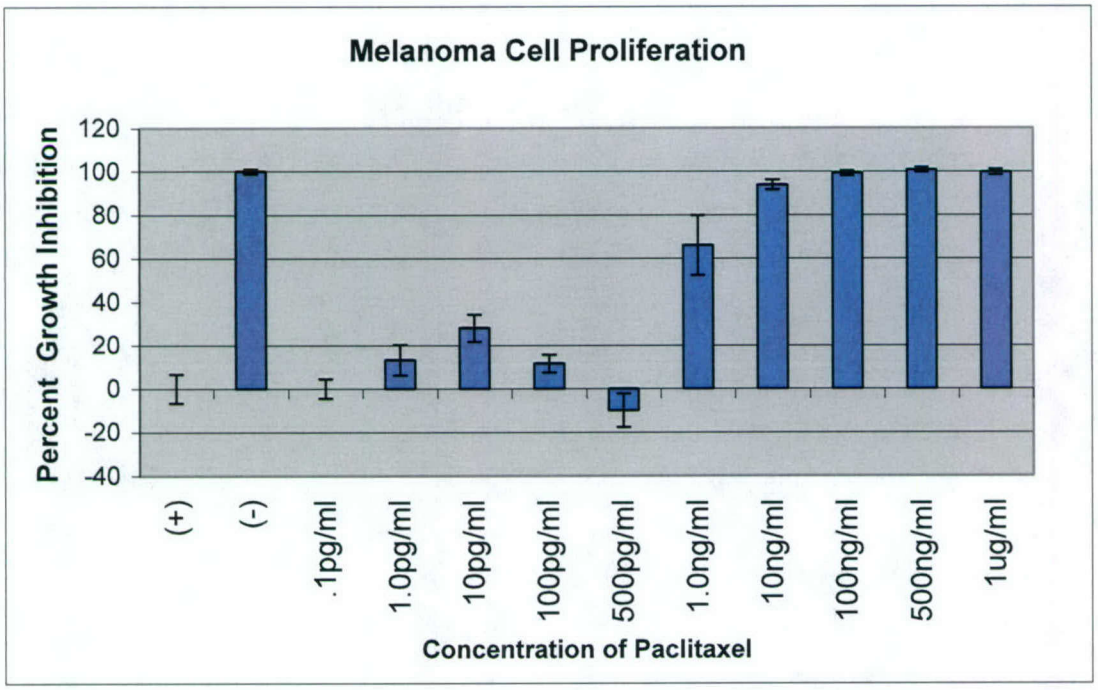

Figure 3: Dose dependent effect of paclitaxel on the proliferation of melanoma cell line.

While we have successfully produced PLGA microspheres, a major barrier still is presented in controlling their size, loading them with Paclitaxel and characterizing loading efficacy and release profiles. These barriers are primarily due to instrumentation costs and time limitations. For example, these experiments require a scanning electron microscope to address size control, and a HPLC system to address loading efficacy and release kinetics. Therefore, we have established collaboration with Boston Scientific. In the initial phase of this collaboration Boston Scientific has agreed to supply us with characterized (size and release profiles) paclitaxel-loaded poly vinyl alcohol (PVA) microspheres characterized in terms of their size, and loading efficacy (i.e. % drug weight). Although these microspheres are not biodegradable, they are biocompatible and will demonstrate a proof of concept. Further, Boston Scientific also suggested that the FDA will be more likely to approve a non-bioabsorbable device. We will repeat our proliferation assays shown in figure 3 upon receipt of our paclitaxel-PVA microspheres expected to arrive early this week. These studies will permit us to determine bead density required for our local concentration profile and we will be able to study the changes in drug delivery with Pluronic gel or other coating conditions. Upon completion of these studies we will then conduct our *in vivo* studies. This will establish our proof of concept that drug loaded microspheres can effectively deliver anti-tumor agents locally.

Publications and Presentations

On May 25, 2004 a presentation was given at the CIMIT Forum. The presentation allowed for a contact to be made with Dave Uffer, Senior Manager for new market development and strategic planning at Boston Scientific. Boston Scientific is a world-leader in paclitaxel delivery via metal stents and this is a perfect partner for our clinical interest in local drug delivery. A CDA has now been developed between Brigham Women's Hospital and Boston Scientific and two meetings have taken place between our team (myself, Solomon Azouz, and Ian Schwartz – Engineering Consultant) and representatives from Boston Scientific (Dave Uffer, Dave Sauvageau – Vice President Research and Development, and a Senior Engineer) to discuss the collaboration and we will begin testing paclitaxel-PVA microspheres in our assays over the next several months.

External Proposal Activity

Based on the proof of concept data that we will generate using paclitaxel-PVA microspheres, additional collaborative works with Boston Scientific are planned in the immediate future which will lead to funding from them or thoracic surgery foundations. In addition, these studies have led to the preparation of a second Invention Disclosure from which will further broaden clinical application and market potential.

References

1. Bunn, P. A., Jr., and K. Kelly. 1998. New chemotherapeutic agents prolong survival and improve quality of life in non-small cell lung cancer: a review of the literature and future directions. *Clin Cancer Res 4:1087.*
2. Paul, D., and D. Johnson. 1995. Chemotherapy for non-small cell lung cancer. *Johnson, BE, Johnson, DH Eds., Lung Cancer Wiley-Liss, New York:247.*
3. Smit, E., and P. Postmus. 1995. Chemotherapy of non-small cell lung cancer. *Carney, DN Eds., Lung Cancer The Bath Press, london, UK pp 156-172.*
4. Smit, E., and P. Postmus. 1995. Chemotherapy of non-small cell lung cancer. *Carney, DN Eds., Lung Cancer The Bath Press, london, UK pp 156-172.*
5. Tanabe, K., Serruys, P.W., Grube, E., Smits, P. C., Selbach, G., van der Giessen, W. J., Staberock, M., de Feyter, P., Müller, R., Regar, E. Degertekin, M., Ligthart, J. R. M., Disco, C., Backx, B., Russell, M. E. 2002. TAXUS III Trial In-Stent Restenosis Treated With Stent-Based Delivery of Paclitaxel Incorporated in a Slow-Release Polymer Formulation. Circulation. 2003;107:559-564.
6. Tanabe, K., Serruys, P.W., Degertekin, M., Guagliumi, G., Grube, E., Chan, C., Munzel, T., Belardi, J., Ruzyllo, W., Bilodeau, L., Kelbaek, H., Ormiston, J., Dawkins, K., Roy L., Strauss, B. H., Disco, C., Koglin, J., Russell, M.E., Colombo, A; for the TAXUS II Study Group. 2004. Chronic Arterial Responses to Polymer-Controlled Paclitaxel-Eluting Stents. Comparison With Bare Metal Stents by Serial Intravascular Ultrasound Analyses: Data From the Randomized TAXUS-II Trial. *Circulation 109:196-200.*
7. Stone, G.W., Ellis, S. G., Cox, D. A., Hermiller, J., O'Shaughnessy, C., Mann, J.T., Turco, M., Caputo, R., Bergin, P., Greenberg, J., Popma, J. J., Russell, M.E., for the TAXUS-IV Investigators. 2004. A Polymer-Based, Paclitaxel-Eluting Stent in Patients with Coronary Artery Disease. *NEJM 350: 221-31.*
8. Harper, E., Dang, W., Lapidus, R. G. Garver, R. I. Jr. Enhanced Efficacy of a Novel Controlled Release Paclitaxel Formulation (PACLIMER Delivery System) for Local-Regional Therapy of Lung Cancer Tumor Nodules in Mice. 1999. *Clin. Canc. Res. 5:4242-4248.*

9. Wang, Y. M., H. Sato, I. Adachi, and I. Horikoshi. 1996. Preparation and characterization of poly(lactic-co-glycolic acid) microspheres for targeted delivery of a novel anticancer agent, taxol. *Chem Pharm Bull (Tokyo) 44:1935.*
10. Sato, H., Y. M. Wang, I. Adachi, and I. Horikoshi. 1996. Pharmacokinetic study of taxol-loaded poly(lactic-co-glycolic acid) microspheres containing isopropyl myristate after targeted delivery to the lung in mice. *Biol Pharm Bull 19:1596.*
11. Mu, L., and S. S. Feng. 2001. Fabrication, characterization and *in vitro* release of paclitaxel (Taxol) loaded poly (lactic-co-glycolic acid) microspheres prepared by spray drying technique with lipid/cholesterol emulsifiers. *J Control Release 76:239.*
12. Edlund, U., and A. Albertsson. 2001. Degradable microspheres for controlled drug delivery. *Advances in Polymer Science 157:67.*
13. Paustian PW, McPherson JC 3rd, Haase RR, Runner RR, Plowman KM, Ward DF, Nguyen TH, McPherson JC Jr. 1993. Intravenous Pluronic F-127 in early burn wound treatment in rats. *Burns. 19(3):187-91*
14. Hokett SD, Cuenin MF, O'Neal RB, Brennan WA, Strong SL, Runner RR, McPherson JC, Van Dyke TE. 2000. Pluronic polyol effects on human gingival fibroblast attachment and growth. *J Periodontol. 71(5):803-9.*

Development of Ultra High Speed Optical Coherence Tomography

Johannes F. de Boer Principal Investigator

Overall Objectives and Approach

The potential applications of Optical Coherence Tomography (OCT) having the highest impact require screening or surveillance of large tissue volumes. The relatively slow image acquisition rate of current OCT technology therefore represents a significant barrier to its utility as a powerful clinical tool. The overall objective is to develop a new, parallel detection principle for OCT that is nearly a thousand-fold more efficient than current state of the art technology. This hugely improved efficiency allows for vastly improved image acquisition rate and resolution without penalty to Signal to Noise Ratio (SNR).

Progress on Specific Aims

Specific Aims

1. Development of spectral domain optical coherence tomography (SD-OCT) system.
2. Performance validation versus existing OCT technology
3. Testing in swine model

Summary of results with respect to specific aims

We have developed a high speed and high resolution clinically viable SD-OCT system that outperform current TD-OCT systems by a factor of 150. The current system produces images of equivalent quality to that of the existing OCT technology, while operating 73 times faster and with a 1.5 to 3 fold improvement in resolution. This demonstrated technological advance represents a paradigm shift from morphologic structural imaging towards high speed screening at the cellular level. For the first time, video-rate imaging of the retina was demonstrated. The project has led to NIH funded proposals and a number of patent applications (at least 7). Licensing agreements with at least 2 industrial partners are in the final stage.

Detailed description of results

The construction of a high speed spectral detection unit was completed. A detailed experimental signal to noise comparison of a time domain versus a spectral domain OCT system has been performed. The experiments verified a signal to noise improvement of 21.7 dB (a factor of 148, i.e. more than 2 orders of magnitude), exactly as predicted by theoretical calculations in the proposal. The first design iteration of the spectrometer has been interfaced to an ophthalmic slit lamp to perform in vivo measurements of the human retina. A paper has been published demonstrating the first video rate ophthalmic OCT system with high quality images. The system is a factor of 72 times faster than a current state of the art ophthalmic OCT system, with a 1.5 times better resolution. An example of a retinal image is shown in Fig 1. The phase stability of the system was investigated, and a flow analysis was performed on in vivo human retinal data. A paper describing the first in vivo retinal blood flow measurements at video rate was published.

We characterized in detail the resolution of our spectrometer. The design resolution was 0.075 nm, which would result in a depth range of 1.7 mm in tissue. We have realized a spectral resolution of 0.138 nm, resulting in a depth range of approximately 1 mm. This depth range is

sufficient for successfully continuing the project. We evaluated several designs that will give us an increased depth range. We have purchased a second camera to implement polarization diversity in the detection system.

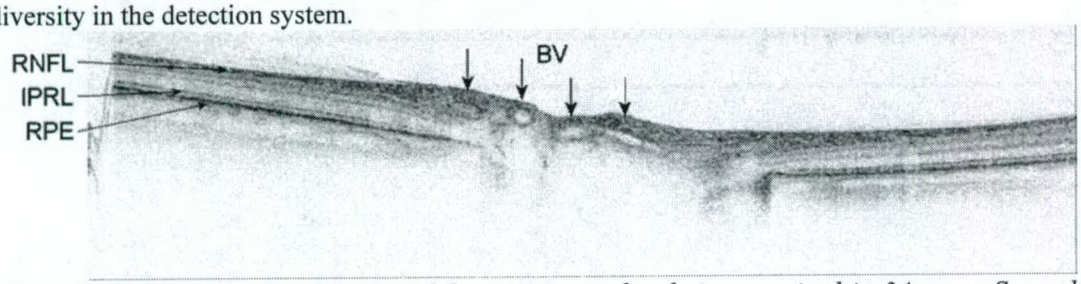

Figure 1: High speed retinal image of the optic nerve head rim, acquired in 34 msec. Several layers are marked. Arrows point to blood vessels emerging from the optic nerve.

We have developed adaptive dispersion compensation algorithms that use highly reflective structures in OCT images to address the resolution degradation in dispersive tissues. We have realized an in vivo resolution of 3.5 micron at unprecedented acquisition speed using a turn key source. As an example figure 2 shows a single frame of a movie acquired at 29 frames/sec of the retina. This demonstrates the highest confirmed resolution in tissue to date at an acquisition speed of 15,000 A-lines/sec and constitutes a speed improvement at this resolution by at least a factor of 60 over published work. In addition we have developed custom software that allows simultaneous read-out of two high speed camera's for polarization diversity and polarization sensitive detection of OCT signals. We expect to have the two camera configuration operational in the future to eliminate polarization artifacts in our OCT imaging.

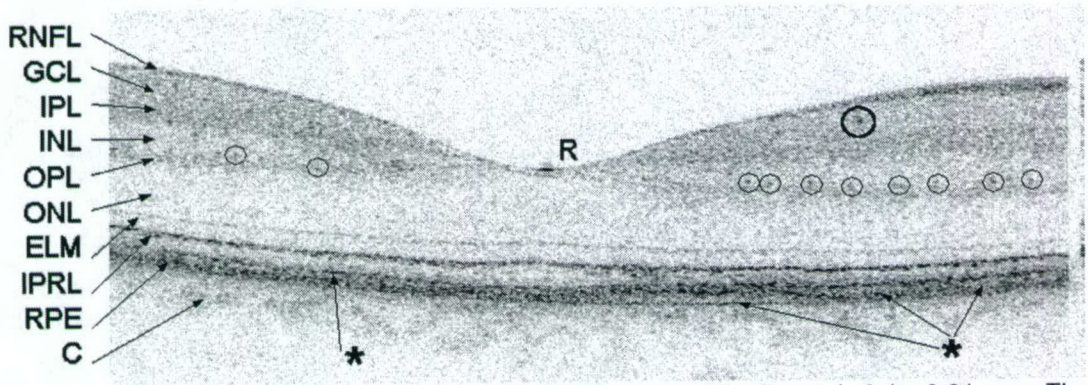

Figure 1: Structural OCT image of the fovea. The dimensions of the image is 3.1 x 0.61 mm. The image is expanded in vertical direction by a factor of 2 for clarity. Layers are labeled as follows: RNFL - retinal nerve fiber layer; GCL - ganglion cell layer; IPL - inner plexiform layer; INL - inner nuclear layer; OPL - outer plexiform layer; ONL -outer nuclear layer; ELM - external limiting membrane; IPRL - interface between the inner and outer segments of the photoreceptor layer; RPE – retinal pigmented epithelium; C - choriocapillaris and choroid. A highly reflective spot in the center of the fovea is marked with an R. A blood vessel is marked with a large circle (BV) and structures in the outer plexiform layer (believed to be capilaries) are marked with smaller circles. In the movie, these structures can also be seen in the IPL. Two layers at the location of the RPE at the left and right are marked with arrows and an asterisk (*).

Thus far all experimental results are in excellent agreement with the predictions in the proposal.

Publications

B. R. White, M. C. Pierce, N. Nassif, B. Cense, B. H. Park, G. J. Tearney, B. E. Bouma, T. C. Chen, and J. F. de Boer, "In vivo dynamic human retinal blood flow imaging using ultra-high-speed spectral domain optical coherence tomography," Opt. Express **11** (25), 3490-3497 (2003), http://www.opticsexpress.org/abstract.cfm?URI=OPEX-11-25-3490

N. Nassif, B. Cense, , B. H. Park, S. H. Yun, T. C. Chen, B. E. Bouma, G. J. Tearney, J. F. de Boer, "In-vivo Human Retinal Imaging by Ultra High-Speed Spectral Domain Optical Coherence Tomography." Optics Letters 29 (5), 480-482 (2004).

S. H. Yun, G. J. Tearney, B. E. Bouma, B. H. Park, and J. F. de Boer, "High-speed spectral-domain optical coherence tomography at 1.3 μm wavelength," Opt. Express 11, 3598-3604 (2003),
http://www.opticsexpress.org/abstract.cfm?URI=OPEX-11-26-3598

N. A. Nassif, B. Cense, B. H. Park, M. C. Pierce, S. H. Yun, B. E. Bouma, G. J. Tearney, T. C. Chen, and J. F. de Boer, "In vivo high-resolution video-rate spectral-domain optical coherence tomography of the human retina and optic nerve," Opt. Express 12, 367-376 (2004), http://www.opticsexpress.org/abstract.cfm?URI=OPEX-12-3-367

B. Cense, N. A. Nassif, T. C. Chen, M. C. Pierce, S. Yun, B. H. Park, B. E. Bouma, G. J. Tearney, and J. F. de Boer, "Ultrahigh-resolution high-speed retinal imaging using spectral-domain optical coherence tomography," Opt. Express 12, 2435-2447 (2004).

S. H. Yun, G. J. Tearney, J. F. de Boer, and B. E. Bouma, "Motion artifacts in optical coherence tomography with frequency-domain ranging," Opt. Express **12,** 2977-2998 (2004), http://www.opticsexpress.org/abstract.cfm?URI=OPEX-12-13-2977

Presentations

de Boer JF, Cense C, Nassif, NN, White B, Park BH, Pierce MC, Tearney GJ, Bouma BE, Chen TC. Ultra-high speed and ultra-high resolution optical coherence tomography and optical Doppler tomography. *ARVO Annual Meeting*, Fort Lauderdale, Florida; 2004.

de Boer JF, Cense C, Nassif, NN, Yun A, Park BH, Pierce MC, Tearney GJ, Bouma BE, Chen TC. Ultra-high resolution video rate in vivo retinal imaging with spectral domain optical coherence tomography. *OSA Biomedical Optics Topical Meeting*, Miami Beach, Florida; 2004

External Proposal Activity

Corporate sponsored research and licensing by Pentax, Terumo and Nidek is being pursued. A licensing agreement is being finalized with Terumo in the cardiovascular space. Negotiations with NIDEK in the ophthalmic space are progressing successfully.

Intellectual Property

A number of patent application were filed on the basic spectral domain OCT technology and on various improvements on the technology. The number of filed patent applications exceeds 7.

Bioadhesive PMMA Microdevices for Oral Drug Delivery

Tejal A. Desai Principal Investigator

Overall Objectives and Approach

The long-term objective of this proposal is to develop a biomedical microsystem that can be used for the delivery of pharmacologically active biopolymers such as peptides, proteins and oligonucleotides into circulation at targeted sites in the GI tract. It is expected that the proposed drug delivery system, created by microfabrication technology coupled with surface chemistry, will more closely interact with the GI system due to our ability to tailor the device in terms of size, shape, chemistry, and directional release.

The creation of oral drug delivery devices that can administer multiple drugs in a safe and effective manner has been a much sought after goal. A variety of delivery systems have been developed to improve the oral bioavailability of drugs including enterically coated tablets, capsules, particles, liposomes, and others. Microfabrication technology may offer some potential advantages over conventional drug delivery technologies. This technology, combined with appropriate surface chemistry, can permit the highly localized and unidirectional release of drugs, permeation enhancers, and/or promoters. Moreover, the use of microfabrication allows one to tailor the size, shape, reservoir volume, and surface characteristics of the drug delivery vehicle to the desired application. The overall objective of this proposal is to develop a new biocompatible and bioadhesive microsystem that can be used for drug delivery at targeted sights in the GI system. To address this, we proposed the following specific aims.

- To micromachine PMMA into reservoir-containing microdevices with tailored microscale geometries
- To chemically modify microdevices asymmetrically (on one side) with bioadhesive ligands
- To assess the bioadhesion of microfabricated devices compared to conventional microspheres in vitro

Progress on Specific Aims

Specific Aim 1. To micromachine poly(methl methacrylate) (PMMA) into reservoir containing microdevices with tailored microscale geometries.

Microdevices have been successfully constructed from PMMA by applying a series of standard microfabrication processes. Photomasks of the desired microdevice and reservoir geometries were designed in AutoCAD software and then printed on transparencies utilizing high resolution image-setting (5080 dpi). A two-step process of photolithography and reactive ion etching was used to reproduce the mask designs three-dimensionally in PMMA. Silicon <111> wafers were RCA cleaned and a thin film of PMMA was spin-coated on the surface. A layer of Shipley 1818 photoresist was spun on top of the PMMA and the photomask pattern was reproduced in the photoresist using photolithographic techniques. The patten was reactive ion etched into the PMMA with oxygen plasma. The reservoirs were carved into the devices also by applying photolithography and reactive ion etching. Though it is possible to produce a multitude of devices with various dimensions and shapes, the prototype device was maintained at 150 μm x 150 μm with 80 μm x 80 μm reservoirs centered in the particle body. *J Control Release. 2003 Mar 7;88(2):215-28.*

Specific Aim 2. To chemically modify microdevices asymmetrically with bioadhesive ligands.

The basic chemistry for incorporating bioadhesive properties was performed in three major steps: (1) amine groups were formed on the surfaces by aminolysis with N-lithioethylenediamine; (2) avidin was coupled with EDC and HOSu to form a hydroxy succinimide ester of the avidin carboxylate which in turn was reacted with the amine groups of the substrate to form an avidin conjugate; (3) biotin-labeled lectins, a class of carbohydrate binding proteins able to recognize surface structures of intestinal cells, was attached to the surface utilizing the strong interaction and affinity between avidin and biotin. Successful modification was characterized by chemical assays, fluoresence assay, atomic force microscopy (AFM), and x-ray photoelectron spectroscopy (XPS). *Journal of Biomedical Materials Research, 2003 Nov 1;67A (2): 369-375.*

Specific Aim 3. To asses the bioadhesion of microfabricated devices compared to conventional microspheres in vitro.

The targeting capabilities of the lectin-modified devices have been evaluated by examining their interactions with Caco-2 cell monolayers in vitro. The Caco-2 cell line, derived from human colorectal carcinoma cells, highly resembles the small intestinal epithelium both structurally and functionally. When grown to confluency they maintain intercellular tight junctions and expose only their apical, brush border membranes. The cells also maintain transport systems, enzymes, and ion channels similar to those of the intestinal epithelium. The glycosylation pattern of the Caco-2 cells is characterized by high amounts of N-acetylglucosamine containing oligosaccharides followed by fucosyl- and mannosyl- and minor amounts of galactosamine- and N-acetyl-galactosamine-residues. This high amount of N-acetylglucosamine oligosaccharides provides specific sites for tomato lectin to bind. Cell viability after exposure to PMMA, tomato lectin-modified PMMA and free tomato lectin was examined by MTT assay and staining of monolayers with trypan blue. No marked difference in mitochondrial dehydrogenase activity could be seen between control cells and modified/unmodified PMMA. Trypan blue staining of monolyaers after 48 hours showed no marked differences between control cells and those exposed to PMMA, and tomato lectin modified PMMA microdevices and microspheres These cells generally appeared normal with occasional single or cluster of dead cells which did not seem to be associated with the location of the particles. Cells subjected to tomato lectin appeared to have large areas of dead cells spanning the entire monolayer. This indicates that attachment of lectin to a construct may negate its damaging effects.

Bioadhesion over time was previously characterized (*Ref: J Control Release. 2003 Mar 7;88(2):215-28).* In order to simulate the gastrointestinal environment, varying concentrations of pig gastric mucin was applied to the apical cell surface. For all mucin concentrations, the percent tomato lectin-modified microdevices bound after two hour incubation was consistently twice that of the unmodified devices. The stability of bound PMMA microdevices was compared to that of PMMA microspheres under static conditions. It was found that the number of tomato-lectin modified microdevices remained consistently bound (~68%) after three consecutive washes, whereas the number of microspheres which remained bound significantly decreased. In order to assess bioadhesion under dynamic settings, future studies of this nature will be translated to a chamber apparatus subjected to constant flow. We are contiously working to set up and define a dynamic flow chamber to test the bioadhesion of our microdevices. This system will allow careful control and calibration of flow rates and particle administration, plus the ability to image dynamically particle adhesion to cells in vitro. Experiments currently in progress were developed in order to study the behavior of bioadhesive delivery devices under dynamic conditions, mimicking the in vivo environment. Adhesion under flow can encompass several adhesive states including initial attachment, firm adhesion, detachment and rolling. Micordevices and

microspheres will be tested for these adhesive behaviors in order to determine any differences in binding.

The potential of PMMA microdevices to affect Caco-2 tight junctions was assessed by observing changes in the transepitheilial electrical resistance (TEER) and flux of phenol red across a cell monolayer when grown on a collagen-coated transwell membrane. An inverse relationship between unit area resistance phenol red flux was apparent. During *days 1-4* the cells reach confluency, while during *days 4-8* complete formation of tight junction and inhibition of cell proliferation occurs. During *days 8-21* a small but marginally significant further decrease in permeability can be detected. After cell differentiation and 24 hours of equalizing in serum-free media, Caco-2 monolayers were unexposed (control) or exposed to either approximately 400 PMMA microdevices/microspheres, 400 tomato lectin-modified microdevices/microspheres, or 100 □g of free tomoato lectin in serum-free media. A significant decrease in TEER and increase in flux can be seen after equilibration. A further initial increase in permeability occurred in those monolayers exposed to the PMMA devices, and especially those modified with tomato-lectin, suggesting some effect on the epithelial integrity. Although a decrease in TEER was associated with exposure to tomato-lectin microspheres, it was not significant in comparison to the control. However, tomato lectin-modified microdevices and free tomato lectin induced a similar, significant decrease in TEER in comparison to the control over a two hour exposure period. After 4 hours, all cells, except those exposed to free tomato lectin, began to recover. After 48 hours, permeability and TEER were recovered in these cell monolayers suggesting that no irreversible damage was induced due to exposure to tomato lectin-modified PMMA. In comparision, free tomato-lectin induced a decline in TEER and increase in permeability. After 48 hours, the drastic difference suggests that these cells may have been damaged. These studies may indicate a time frame in which drugs delivered from the modified microdevice may experience enhanced permeability across the epithelial layer without permanent damage to cells (Figure 1).

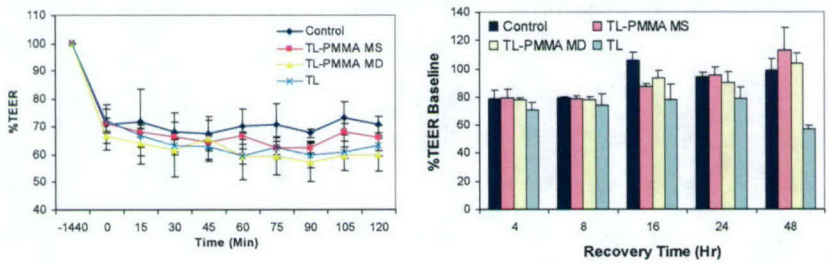

Figure 1. A) Decrease in TEER after exposure to devices. B) Recovery of TEER.

In order to observe the physical affect of the lectin and lectin-bound devices on Caco-2 tight junctions, F-actin was stained using rhodamine-phalloidin. Control cells showed a ring of F-actin around the cell body depicting the tight junctions. Similar staining was found for cells exposed to modified/unmodified microdevices and free tomato lectin. This suggests that the changes in actin composition may be to small to qualitatively assess (Figure 2A). Currently studies involving quantitatively assessing tight junction proteins such as ZO-1 and occludin are being examined. In order to examine the interactions between the microdevice and cells, Caco-2 monolayers grown on collagen-coated transwell membranes and exposed to PMMA microdevices, lectin-modified PMMA microdevices and free lectin were fixed for scanning electron microscopy (SEM). Control cells show numerous microvilli reaching 1-2 □m carpeting the surface of the polygonal cell bodies. Cells exposed to PMMA microdevices and tomato lectin-modified PMMA microdevices exhibit similar microvillar structures even at the device-cell interface (Figure 2B). However, cells exposed to free tomato lectin show a decrease in microvilli number as well as

shrunken microvilli (Figure 2C). This suggests that the free lectin exhibits some damaging effects to the cells which are not associated with bound lectin. Further studies of this nature are being conducted on microspheres as well as microparticles of various shape and size. In addition, transmission electron microscopy is being used to determine the effect of the bioadhesive device/sphere on microvillar ultrastructure.

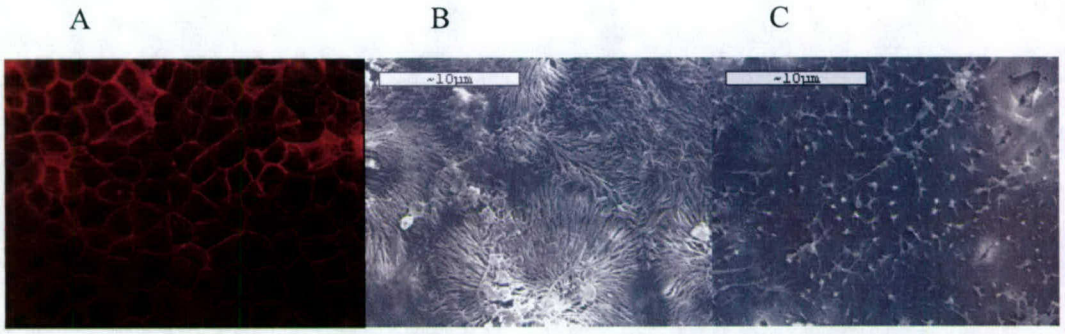

Figure 2. A) Rhodamine-phalloidin staining of F-actin. SEM of Caco-2 cells exposed to A) PMMA and B) tomato-lectin.

Future Work

In an effort to continue developing the design of the microfabricated devices, we have been working to incorporate microneedle technology. Previous studies have shown that microneedle arrays dramatically enhance transport of molecules across the skin. The needles create conduits for transport which allow compounds to rapidly diffuse through to deeper tissue to underlying capillaries. The same principle can be applied to oral drug delivery. Using microfabrication techniques, microdevice bodies can be designed to contain precisely shaped microneedles. These microneedles would allow the particle to penetrate the mucus layer as well the shedding mucosa to thereby increase the uptake of compounds into the blood vessels of the submucosa. These needles may be designed to be a simple post, to a beveled tip for increased permeation, to a rachet/hook design to act as a latch mechanism in prolonging the duration of release in the intestine. Combined with the current chemically driven targeting mechanism, these needles may provide a mechanically driven feature to provide additional support in increasing permeability and sustaining release. These microneedle-containing particles can still be fabricated to include the original flat design with reservoirs for unidirectional release. Similar chemical modifications can be made to include the chemical attachment of targeting biomolecules. These devices can be fabricated from the various materials from silicon to polymers such PMMA, SU-8, or biodegradable/erodible polymers such as PLGA and PCL (Figure 3A). We are currently exploring novel fabrication methods in order to reproduce these structures with greater efficiency. Dr. Mazur at Harvard has also developed a laser based method that allows for the fabrication of microscale spikes (Figure 3B). We plan to vary spike size (1, 5, and 10 microns) on 150 x 150 micron particles and study the effect on such geometry on bioadhesion.

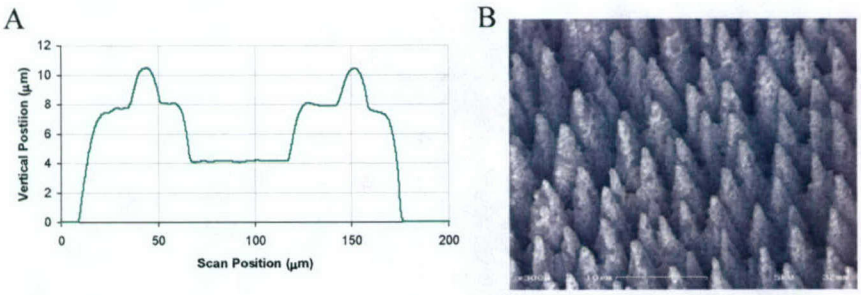

Figure 3. A) Profile scan of microdevice fabricated in SU-8 epoxy containing microneedles. B) Silicon spikes.

Publications & Presentations

Sarah Tao, Mike Lubeley, and Tejal Desai. Bioadhesive PMMA Microdevices for Oral Drug Delivery, *J. Controlled Release*, 2003 Mar 7; 88(2): 215-28.

Sarah L. Tao, Michael W. Lubeley, Tejal A. Desai. Synthesis of cytoadhesive poly(methyl methacrylate) for applications in targeted drug delivery, Invited Award Winner, *Journal of Biomedical Materials Research*, 2003 Nov 1;67A (2): 369-375.

Sarah Tao and Tejal A. Desai, Microfabricated Drug Delivery Systems: From particles to pores, Invited, *Advanced Drug Delivery Reviews,* Volume 55, Issue 3, Pages 315-328, 24 February 2003.

4. SL Tao, TA Desai. Micromachined Polymeric Devices for Applications in Targeted Drug Delivery, Invited Best Posters Special Issue, *JALA.* 2004 Jun 18;9(3):155-158.
5. T.A. Desai. "Cytoadhesive Microdevices for Oral Drug Delivery," presentation at Biomems 2004, Boston MA, March 2004
6. SL Tao, TA Desai. Micromachined Poly(methyl methacrylate) Devices: The Impact of Controlled Geometry from Cell-Targeting to Bioavailability. Controlled Release Society, June 2004. Honolulu, HI. (Capsugel Special Session)

External Proposal Activity

Pending NIH proposal (to be reviewed this July)
Pending proposal to Alza Corp.

Awards Related to this Research

2004 NASA Graduate Student Researchers Program Fellowship
Capsugel/Pfizer Innovative Aspects of Oral Drug Delivery Award (student paper competition)
2003 NASA Graduate Student Researchers Program Fellowship
EURAND Grand Prize Award for Outstanding Research in Oral Drug Delivery
2003 Best Paper Award by the Society of Biomaterials (graduate student paper competition)

Issues and Concerns

None

Liquid Repair of the Inguinal Hernia

Daniel Jones Principal Investigator

Overall Objectives and Approach

An inguinal hernia is a painful bulge in the groin caused by a defect in the abdominal muscle wall. Over 750,000 inguinal hernias are repaired in the United States every year using prosthetic mesh. Our project involves the development of liquid mesh as a substitute for currently available solid mesh. The liquid mesh is a gel or foam, which can be injected into the hernia defect. This gel or foam will solidify upon injection achieving the repair. Once available, this technology will help make the hernia operation less invasive.

Progress on Specific Aims

Specific Aims

1. Survey the literature and industry to find a product that can be used as a liquid mesh
2. If not available, develop liquid mesh using tissue engineering technology
3. Test the resultant liquid mesh product for mechanical and biological properties
4. Perform bench testing using our laparoscopic hernia repair model
5. Perform histology using animal studies.

Specific Aim 1

We have achieved our first aim of the project. We have performed a literature search and found that there is no currently available material that can be used as liquid mesh in a hernia operation. We have also contacted companies making similar products and assessed their samples for potential use in our application. Again, there is no biocompatible product in the biotech or chemical industry which can function as a liquid mesh. This search has demonstrated that our idea and research pursuit under supervision of CIMIT is novel.

Specific Aims 2 - 4

To develop a novel liquid mesh compound we have established collaboration with the laboratory of Dr. Robert Langer in the department of Chemical Engineering at M.I.T. We have established all licensing and safety approvals needed for our co-investigators to work at M.I.T. The personnel on the project include Ashish Patel (co-investigator), Dr. Molly Stevens (a post-doctoral fellow at M.I.T.), and Eric Makhni (an undergraduate student at M.I.T.)

Our initial focus has been on alginate as a potential source of liquid mesh. Alginate gel is biocompatible, biodegradable, and approved for human use by the United States Food and Drug Administration. Alginate also provides ease of use. A solution can be polymerized by simply adding a calcium solution. The disadvantages of alginate include lack of adhesiveness and mechanical strength.

Our experiments have involved making varying compositions of alginate gels. We have established that gel composition can be varied from 2% to 6 % by weight solutions. At higher concentrations, alginate forms a paste. Although not in a solution, the paste can be of equal use as a potential liquid mesh. Our experiments show that alginate gels are fragile and inadequate for use as liquid mesh in current form.

Since alginate may not be the final material of choice we have chosen collagen and hyaluronic acid as the next potential materials for development of liquid mesh. Collagen is easily available, biocompatible, biodegradable, and is already used in solid form as a mesh. Collagen solutions also polymerize when warmed to body temperature. Modification of collagen can potentially provide a material which can provide injectability, adhesiveness, and tensile strength. For this phase we have enlisted help of Dr. Xinquio Liu, a postdoctoral fellow at M.I.T. Dr. Liu has experience in synthesizing collagen modified at specific amino acid residues. Our approach to the new material has been making hyaluronic acid hydrogels and then modifying them with Poly(methyl methacrylate) PMMA and collagen. The photograph below shows hyaluronic acid gels made in our laboratory.

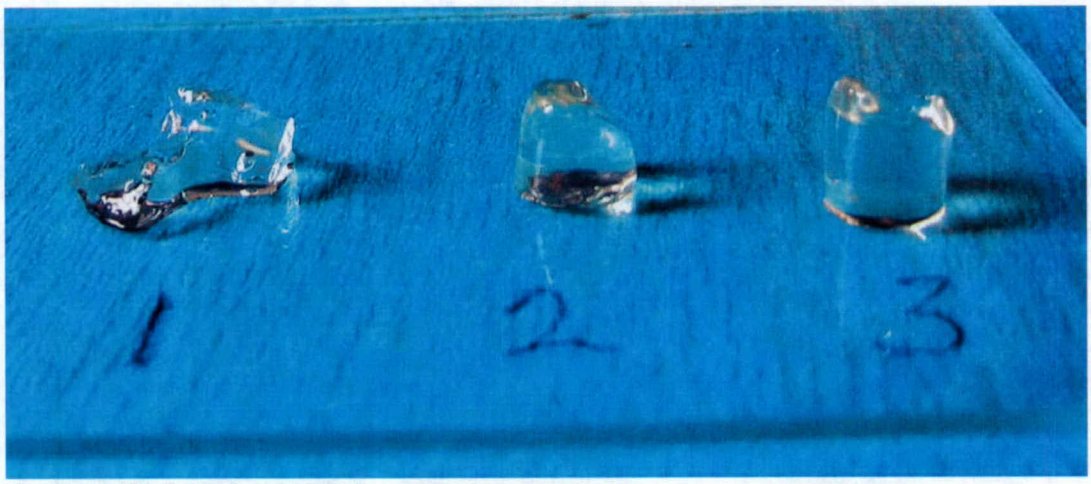

Figure 1. Hyaluronic Acid Gels

In the second half of the project period, we have established a system to achieve a minimally invasive hernia repair. This has been achieved by taking a radically new, yet simple, approach to the problem. Since the biggest obstacle with liquid mesh development has been its mechanical strength, our hernia repair will be achieved by injecting liquid mesh in expandable balloon which can be placed in a human body through surgical or radiologic guidance. We have three set of materials that can be used to fill the balloon. They include a high concentration collagen gel made of low molecular weight collagen, hyaluronic acid gels reinforced with poly(methymethacrylate) PMMA, and dimethylaminoethyl methacrylate (a material that is soluble in ethanol and solidifies in water.) The balloon itself is made currently used material polypropylene or biorubbler, a novel biodegradable material developed in our laboratory.

Specific Aim 5

The work described above is a result of efforts of several multidisciplinary investigators working together to solve a common clinical problem. This work has been made possible by the $15,000 new concept award by CIMIT. Our aim of testing our novel method of repairing inguinal hernias in animal models requires significant but fruitful additional research time. Our future work will involve testing the minimally invasive hernia repair system in animal models.

Publications and Presentations

The idea of using a liquid mesh to repair a hernia defect is novel and currently being investigated by the Technology Ventures Office at the Beth Israel Deaconess Medical Center. Regardless of this we intend to publish our work in the near future. We plan to present our work at the future meeting of the American College of Surgeons

External Proposal Activity

Development of a liquid mesh is a novel and potentially useful idea. Since we expect the pursuit to continue until success, we have submitted an additional proposal for funding the project. A grant of $15,000 has been requested to support personnel through Society of American Gastrointestinal and Endoscopic Surgeons (SAGES)

Delivery of Endogenous Adenosine Deaminase (ADA) in Experimental Models of ADA-Deficiency using Novel Genetic and Tissue Engineering Techniques

Principal Investigator: Ian C. Michelow, MBBCh DTM&H

Overall Objectives and Approach

Adenosine deaminase (ADA) deficiency is a lethal inherited genetic disorder that causes Severe Combined Immunodeficiency. The aim of this study is to design viral vectors with an ADA gene insert that can be used to infect selected target cells in vitro and in animal models using tissue engineered biodegradable constructs. The secreted enzyme ideally will serve as a sustainable and safe source of endogenous ADA, and will replenish functional enzyme. Inception of research: January, 2004.

Progress on Specific Aims

Quarter 2

1) **Construction of lentiviral and adeno-associated virus (AAV) vectors with human ADA, signal peptide and Fc gene inserts:**
   I have cloned the human ADA and signal peptide genes (derived from the NCBI database) into a self-inactivating lentiviral backbone containing an internal CMV promoter and a WPRE sequence to enhance gene transcription and expression. Two versions of the vector have been produced: with or without IRES-GFP which may be useful for monitoring transfections and transductions of target cells in vitro as well as in vivo. These plasmids have been sequenced and were confirmed to be correct. Viruses containing genes encoding human ADA, a signal peptide and IRES (internal ribosomal entry site)-GFP were packaged using 4 expression plasmids (HIV gag-pol; rev; tat; VSV-G). Subsequently virus was collected from infected FG293 cells and concentrated by ultracentrifugation to produce high titer virus. The titer was confirmed by FACS to be in the order of ~7 logs. I am in the process of designing constructs that will encode a fusion protein, specifically a synthetic IgG4 Fc fragment that will theoretically stabilize the secreted product in circulation. Further tests of secreted products will be performed by Western blot.

   In addition, I have constructed and sequenced an AAV-human ADA vector. Adeno-associated viruses with rep-cap sequences and serotype 1 capsule have been produced, purified and titered (1 μg/μL) for use in vitro and in vivo. I am currently designing additional AAV vectors with signal peptide and synthetic IgG4 Fc inserts. These viruses will be used for comparative experiments to achieve optimal expression of recombinant protein.

2) **Production of high titer lentiviral vector for target cell transduction:**
   To date the following viruses have been produced: lentivirus-huADA-IRES-GFP with or without signal peptide sequences; AAV1-huADA. Production of new lentiviral and adeno-associated viruses containing the other genes of interest are in progress.

3) **Culture of porcine MSC and murine fibroblasts for ex vivo transduction, and testing of transduction efficiency:**

A preliminary experiment revealed that porcine mesenchymal stem cells are susceptible to infection with a lentiviral vector expressing GFP. Therefore, further experiments with recombinant viruses are warranted.

4) **Establishment of ELISA test to measure human ADA concentrations.**
Initial attempts to set up an ELISA using rabbit and goat anti-human ADA polyclonal antibodies were suboptimal because of poor sensitivity and specificity. Subsequently, an accurate Western blot assay was established for this purpose (see Quarter 3).

5) **Design and testing of biodegradable polymer scaffolds for osteoblast and fibroblast implants:**
We are in the process of testing synthetic biodegradable polymers (e.g poly-lactic-co-glycolic acid, PLGA) as a vehicle for delivery of ADA-tansduced porcine bone marrow progenitor cells.

6) **Manufacture of PEG-ADA by pegylating commercially available bovine ADA:**
I have pegylated bovine ADA for use in ADA knockout mice. I confirmed the activity by means of a zymogram assay that separates enzymes electrophoretically and reveals a color change based on metabolism of substrate. The protein content of the PEG-ADA was determined to be 0.8μg/μL by a Bradford assay. I am currently setting up a spectrophotometric assay to accurately measure rate of conversion of adenosine to inosine by ADA. A functional assay of this nature will be very useful to detect active ADA production in future in vitro and in vivo experiments. The zymogram assay will also be useful to determine which murine offspring are affected and which mice will therefore need replacement therapy.

7) **Breeding of heterozygous ADA-knockout mice, diagnosis of affected offspring and treatment with PEG-ADA to ensure survival:**
Two homozygous ADA knockout male mice and their 4 female heterozygotes partners were donated by Dr Blackburn (Houston, TX). They are currently being quarantined at Charles River laboratories (Wilmington, MA). The affected males receive weekly IM injections of PEG-ADA (20μL) to remain disease free. We intend to start breeding mice for experiments within 1 month. We anticipate that 50% of offspring will be affected based on Mendelian patterns of inheritance. Zymogram assays will be performed within 5 days of birth to determine which mice need replacement therapy. A genotype will be done at 3 weeks to confirm the results.

8) **Harvesting of fibroblasts from mice for in vitro manipulation:**
We will consider this approach once we have all the recombinant vectors available.

9) **Investigation of feasability and optimal site for implantation of constructs into 3 pigs and 40 mice:**
We will consider this approach once we have all the recombinant vectors available.

10) **Study of dynamics of tissue implants: survival, durability, vascularization with or without VEGF, secretion of ADA and its physiologic impact:**
In vivo work will proceed once the mice have been removed from isolation.

Quarter 3

Detection assays: I have developed a functional spectrophotometric assay to measure the rate of conversion of substrate (adenosine) in μmol/min per mg of ADA. The advantage of this test is its ability to detect enzymatically active ADA in cell secretory products in *in vitro* and *in vivo*

systems. This assay will be used 1) to confirm and standardize PEG-ADA activity for treatment of ADA deficient mice, and 2) to quantitate ADA activity in cell supernatants and in blood of animals that have received transduced tissue-engineered constructs.

I also designed and tested a Western blot assay that accurately detects pure human ADA produced by transfected 293T cells using commercially available rabbit anti-human ADA polyclonal antibodies. Cell lysates and supernatant were tested. This test will be useful to confirm the presence of ADA in transduced animal tissues.

Once we have the appropriate vectors that express a secreted form of ADA, we will be able to test a sandwich ELISA using the commercially available rabbit anti-human ADA polyclonal antibodies and anti-human ADA monoclonal antibodies donated by Dr Hershfield (Duke University).
By combining the zymogram, the spectrophotometric assay, the Western blot, and potentially an ELISA test, we will gain a better understanding of the utility of our vectors in future experiments.

The animal models: The ADA deficient mice are currently being housed at Charles River Laboratories. The quarantine period ended recently. Cross-breeding between the homozygous male and wild-type female mice has yielded 28 offspring that we will use as future breeders. The mice will be transferred to Harvard Medical School animal facilities in the near future.

Quarter 4

Vector development: The emphasis of work during the final quarter was to complete construction and testing of lentivirus vectors that encoded:
1) recombinant human ADA fused to 2) a signal peptide to mediate protein secretion from transfected or transduced cells, and 3) reporter genes that expressed Green Fluorescent Protein (GFP) which is potentially useful for surveillance *in vitro* and *in vivo*.

We confirmed the genetic sequence of 4 constructs: lentivirus plasmids with ADA gene with/without signal peptide, and lentivirus plasmids with ADA-GFP with/without signal peptide. Then we transfected human 293T cells with each vector and prepared cell lysate material and supernatant samples for Western blot analyses. We confirmed that relatively large quantities of ADA were produced in each transfection as well as a larger product that corresponded to the signal peptide fused to ADA, as we anticipated (see Figure 1). However, contrary to our expectations, supernatant samples showed the presence of ADA associated with vectors lacking a signal peptide, whereas no secreted protein was detected when signal peptide was fused with ADA. The implications of these findings are that 1) a pathway other than the traditional secretory route of protein by the endoplasmic reticulum may exist, and we may be able to exploit that in future experiments, and that 2) the human Growth Hormone-derived signal peptide that we have used may not be well suited to our objectives.

In view of these unexpected findings, we are currently redesigning the viral vector with alternative signal peptides (e.g. signal peptide for *E. coli* β-lactamase) to achieve secretion of the protein by transduced cells. Results from these experiments will inform future direction.

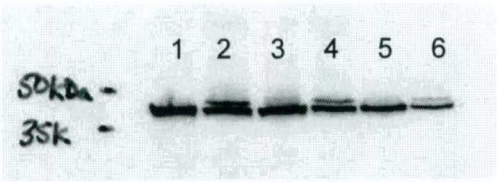

Figure 1. Western blot of human 293T cells transfected with lentivirus expression vectors. All products are ~40kDa which corresponds to the molecular weight of human ADA. Lanes 1 and 5 (1:10 dilution) are replicates and Lanes 2 and 6 (1:10 dilution) are replicates. Vectors used were identical except for the transgene they expressed as follows: Lane 1, human ADA; Lane 2, signal peptide for human Growth Hormone fused to ADA; Lane 3, human ADA with IRES-GFP; Lane 4, signal peptide for human Growth Hormone fused to ADA with IRES-GFP. The doublets noted in Lanes 2, 4 and 6 likely represent 1) cleaved human ADA and 2) uncleaved human ADA fused to its signal peptide (larger protein).

Publications and Presentations

Quarter 3
Oral presentation at CIMIT's speaker forum on 5/18/04

External Proposal Activity

We have identified the Hood Foundation as a potential additional funding agency for this project and have submitted a proposal for funding in 2005-6.

Extension Requested

An extension of the project for 1 year was approved by Dr Baum in view of our important preliminary findings and because more time to complete the project is required.

Project Summary

Title: Delivery of endogenous adenosine deaminase (ADA) in experimental models of ADA-deficiency using novel genetic and tissue engineering techniques

1) **Year end status:** Preliminary findings showed effective transfection of target cells but no protein secretion. Therefore, further investigation is required to design a new viral construct to achieve secretion of active ADA.
2) **Production of high titer lentivirus vector**: A reliable protocol to achieve this has been established. Further experiments will be performed to design new constructs with different signal peptides to express a secreted form of ADA.
3) **Ex vivo transduction of porcine MSC:** We demonstrated that high transduction efficiency of porcine primary MSCs can be achieved with a lentivirus vector. Further experiments with new constructs will be conducted.
4) **Dectection assays:** A sensitive and specific Western Blot assay has been established to detect ADA in cell lysates and supernatant. Further experiments to purify ADA for standards and to set up an ELISA are ongoing.
5) **PEG-ADA synthesis:** We have manufactured PEG-ADA for use in knock-out mice.
6) **Design and testing of biodegradable polymer scaffold:** experiments will proceed once an effective vector is available
7) ***In vivo* experiments:** isolation of murine fibroblasts and implantation of tissue scaffolds with transduced cells into pigs and mice will proceed once the optimal vectors have been constructed and tested *in vitro*.

Development of a Laparoscope for the Detection of Sub-Clinical Disease Using Near-Infrared Molecular Probes

Michael Seiden, M.D., Ph.D. Principal Investigator

Overall Objectives and Approach

Effective treatment of epithelial ovarian cancer is limited in part by the lack of adequate imaging technologies capable of detecting small residual intraperitoneal disease. An imaging platform that can reliably localize and characterize "subclinical" lesions will serve as a critical enabling technology offering several tangible benefits including the development of more rationally designed clinical trials of molecularly targeted agents. The aim of this study is to both develop a specialized laparoscopic equipment designed to function in the near infrared region of the light spectrum and initiate a pilot clinical study evaluating intraperitoneal near infrared fluoresence (NIRF) detection.

Progress on Specific Aims

1. Assembly of the optical imaging system.

Selection of the infrared camera and preliminary experiments with ICG *in vitro*

The primary goal of the CIMIT grant was the construction of a near infrared laparoscopic imaging system. The key component of this system is a near infrared camera. The relative sensitivities of several candidate cameras were tested by Lawrence Haas from MGH and David Rosen from PSI. In these analyses, the ability of each camera to detect near infrared fluorescence of the chromophore indocyanine green (ICG) was assessed. Previous analysis using a benchmark standard Roper back-thinned dewar cooled near infrared camera with a Nikkor lens at an f-stop of 4.5 has demonstrated good signal to noise performance with emission from ICG in a microcuvette containing 5% FBS at an irradiance of 1 mW/cm^2 (data not shown). In our search for a considerably faster detector, we examined a small intensified charged coupled device (ICCD) infrared camera from Stanford Photonics. This camera is capable of producing both a signal to noise ratio and resolution similar to those of the Roper camera but requires only 7% of the irradiance. Further testing demonstrated that the Stanford Photonics camera can discriminate a 2 millimeter (mm) diameter figure on a 2 mm path length microcuvette at ICG concentrations well below the 0.002 mg/ml concentration anticipated with the dosing schedule used in the pilot clinical study outlined below. This experiment supports the conclusion that imaging of tumors less then 2 mm in diameter should be very feasible in humans and provides a wide margin of engineering opportunities in the execution of our second-generation device.

Comparison and selection of a NIRF laparoscope

In additional experiments, we directly compared the infrared transmissivities of laparoscopes provided by Karl Storz and Optim. A custom built near infrared optimized 5 mm solid quartz assembly from Karl Storz was analyzed together with a 3 mm 30,000 fiber quartz scope from Optim Incorporated. The relative transmissivities under conditions of equal irradiance were determined (data not shown). The Optim "fiberscope" provided impressive transmissivity for its size. The illuminance ratio at the CCD was found to be ~ 5:3 Storz:Optim. Although the Storz system generated an image with 15x the Optim pixel intensity x size product, the Optim scope provided 3x the internal fiberguide transmission compared with the Storz scope.

Energy calculations, filters, and infrared spectral source

In Quarters 1 and 2 we defined the laser source energy parameters for optimal excitation and detection of the ICG chromophore that will be utilized in the clinical trial described in the initial

CIMIT grant. In summary, we determined that a fiber coupled diode laser emitting near 795 nanometers (nm) is the optimized method of inducing ICG fluorescence based on numerical estimation and the preliminary *in vitro* assay. This high-intensity spectral source should emit very near the ICG absorbance extinction coefficient with a full width, half maximum (FWHM) bandwidth of ~3 nm. An excitation source several nm toward the visible will facilitate spectral separation of backscattered illumination from the ICG emission maximum of 835 nm. Illumination will be transmitted via a 200 micron core multi-modal fiber. A maximum output power of 500 milliwatts (mW) together with a nominal working distance of 4 centimeters (cm) and a 70° field of view will result in a maximum irradiation density of ~20.3 mW/cm^2, well above the empirically determined irradiance requirement. Additionally, this value is well below the maximum permissible exposure limit established for human tissue and should induce less than a 0.02°C rise in tissue temperature per second of exposure. Our efforts in Quarter 3 focused on completing assembly of the laparoscopic imaging system. Toward this end, we purchased a laser source that is a fiber coupled near infrared diode laser (Model BWF2-785-500 from B&W Tek, Inc.). The laser source is rated for a maximum output of 500 milliwatts of laser optical power from the 100 micron, NA@0.22 delivery fiber. These specifications are consistent with the parameters defined in Quarters 1 and 2. We worked with engineering consultants at Optim, Inc. to design and machine an adaptor that efficiently couples the laser delivery fiber to the quartz laparoscope and allows optimal distribution of the exiting beam at the laparoscope light guide proximal end face. Additionally, we generated a second adaptor designed to securely hold a spectral filter at the interface between the near infrared camera and video coupler.

Figure 1. Detection of ICG near infrared fluorescence. *Increasing amounts of ICG were injected underneath the fascia of a chicken breast and the resulting NIRF was monitored using the complete laparoscopic imaging system. The arrow indicates the detected fluorescence from 250 picograms of injected ICG. Also shown (left to right) are the fluorescence levels detected with 2.5 nanograms, 25 nanograms, and 250 nanograms of injected ICG.*

Following assembly of the complete laparoscopic imaging system, we tested its ability to detect ICG-mediated near infrared fluorescence in an emulation model. We injected 1 and 10 microliters of increasing concentrations of ICG in 5% fetal bovine serum under the fascia of store-bought chicken breast and monitored the ability of the imaging system to detect ICG fluorescence at various laser and camera intensifier settings. All images were recorded on videotape and representative data are shown in Figure 1.

We were able to detect fluorescence from 250 picograms of injected ICG at a working distance of 9.3 centimeters indicating that the imaging system is very sensitive. The system is currently being evaluated by Luis Melendez of MGH Biomedical Engineering for final safety approval before use in the pilot clinical study.

Composite image construction and analysis

The imaging platform will consist of an optimized solid relay laparoscope whose spectral signal will permit the independent modulation and co-registration of images in the visible and near infrared spectra. Camera triggering together with signal acquisition and manipulation will be controlled by a LabVIEW (National Instruments, Inc.) software program that has been modified and tested by John Frangioni, M.D., Ph.D. Software has been developed using LabVIEW to

acquire, analyze, and combine the outputs of both cameras using NI-IMAG (National Instruments, Inc.) and IEEE (Institute of Electrical and Electronics Engineers, Inc.) drivers. Dr. Frangioni has produced a working program that will meet our requirements with few modifications. Essential properties of the software and graphical user interface (GUI) will provide camera triggering and allow for synchronization among cameras, excitation sources and camera properties such as frame rate and integration time. The GUI will also allow simultaneous co-registered live video from the color charge-coupled device (CCD) camera and monochrome ICCD and facilitate cinematic video and still image capture. Quantification of biomarker signal intensity will be measured continuously and expressed as an area or line function.

2. Pilot clinical study of ICG detection in women with ovarian cancer

Design of the ICG clinical trial

The pilot clinical study (supported by non-DoD funds) will utilize the chromophore ICG (Akorn Inc., Buffalo Grove, IL) to investigate laparoscopic-based detection of ICG–mediated near infrared fluoresence of sub-clinical disease in women with ovarian cancer. The availability of this FDA approved agent will allow both the execution of a "proof of principle" clinical trial and the iterative optimization of NIRF signal acquisition. The ICG utilized in the pilot clinical study is expected to detect early ovarian disease due to accumulation of ICG in immature and leaky vessels in the abnormal vasculature of the tumor. This aim also serves to evaluate the hypothesis that the NIRF signal obtained in the ICG studies is an accurate reflection of changes in vascular structure and defines new sites of angiogenesis. Since funding, the ICG clinical trial has been submitted to the DF/HCC Scientific Review Committee (SRC) and Institutional Review Board (IRB). This group serves as the appropriate oversight committee for all cancer-based studies at the MGH. The trial is SRC and IRB approved with activation pending review of the laparoscopic equipment by Biomedical Engineering. During Quarter 3, the pilot study proposal was submitted to the FDA for approval of the specific use of ICG in intraperitoneal imaging. We obtained FDA approval of our study following revision of the protocol to incorporate minor changes requested by the FDA. The FDA also determined that the protocol was exempt from application for an IND. The revised protocol was recently approved by the DF/HCC IRB. In quarter 3, we also focused on developing a thorough standard operating procedure for conduct of the pilot study. We worked with the MGH research pharmacy to establish a routine procedure for delivery of stable ICG to the OR at the time of the procedure. We also developed a detailed checklist of tasks involved in the use of the imaging system in the OR to insure smooth execution of the laparoscopic procedure. The pilot study will be initiated following final safety approval of the imaging system and is anticipated to begin within one month.

Validation of NIRF signal in tissue samples

Validation of the NIRF signal seen *in vivo* will be an essential component of application development and requires the utilization of available techniques that can assess various cellular or tissue specific markers that should correlate with NIRF probe activation or retention. Our initial experiments will utilize tumor tissue microarrays constructed from biopsied tissue taken from ICG-positive tumors identified in the pilot clinical study. Towards this end, using non-DoD funds, we have constructed tumor tissue microarrays using available paraffin-embedded thin sections of pathologically characterized human tissue that were arrayed on a single glass slide. The array contains both ovarian and non-ovarian tumor tissue along with normal tissue. Our preliminary experiments have focused on optimizing immunohistochemical staining methods for reproducible analysis of the tissue microarrays. A representative example is shown in Figure 2.

Figure 2. Immunohistochemical analysis of an ovarian tumor microarray. *Sections prepared from a microarray constructed with multiple samples from pathologically characterized human ovarian tumors were stained with hematoxylin and eosin (panel A) or antibodies directed against vascular endothelial growth factor (VEGF, panels B and C). Panel C is a higher magnification of the boxed sample in panel B and shows the expression pattern of VEGF in a high grade ovarian carcinoma. No staining was observed in the absence of primary antibody.*

Publications and Presentations

Ovarian Cancer and Optical Detection of Tumor, HST-MGH Biomedical Summer Optics Series, July 2004

NCI-FDA-Industry Conference-Molecular Imaging in Ovarian Cancer, Bethesda Maryland, Spring 2004

Doris Duke Conference, Clinical Interface Awardee, Molecular Imaging Platform in Ovarian Cancer, Cold Spring Harbor Institute, New York, Spring 2004

External Proposal Activity (Funded)

1. Doris Duke Foundation
   (PI: Michael Seiden)
   Title: Fluorescent Probes for the Detection and Evaluation of Ovarian Cancer
   Funding Period: 9/03-3/05
   Funding: $80,000
   Since obtaining CIMIT support we have received funding from the Doris Duke Foundation through the form of a planning grant covering September 2003 through March 2005. This was one of six planning grants awarded nationally in the field of medical science. The grant provides $80,000 that is used primarily to support a modest amount of effort from the multi-disciplinary research team at the MGH. The Doris Duke Foundation will convert two or three of these six planning grants into full clinical development grants that will provide 2.25 million dollars in funding over a five year time period. These grants will be competed in the spring of 2005.

A proposal building on the work funded by this CIMIT award has been submitted and is listed below.

External Proposal Activity (Under Review)

DF/HCC Technology Innovation Awards Application

(PI: Michael Seiden)
Construction of a Second Generation Near Infrared Fluorescence Imaging System for Laparoscopy in Humans
Funding Period 11/1/04-10/30/05
Amount $178,429
This grant looks to build a second generation imaging system and to conduct the ICG clinical trial.

BWH Operating Room of the Future
Raphael Bueno, MD Principal Investigator

Overall Objectives and Approach
Original concept funded by CIMIT: "To streamline the development of the best suited technology we propose to develop an "Operating Room of the future (ORF)" with emphasis on Thoracic and upper abdominal surgery at the BWH. This facility will encourage the development and testing of new technology in an interdisciplinary manner to define in an on-going manner the best medical innovations for the care of the surgical patients."

November-December 2003
Several meetings accomplished with the BWH leadership including Dr. Zinner and Mr. Fernandez to explain our goals and process as well as to receive guidance. A number of interested individuals recommended by the BWH and CIMIT leadership were contacted and joined (or recommended others to join) a steering committee. The members include: Drs. David Brooks (Surgery), Raphael Bueno (Surgery), Anthony Carrino (Radiology, and represents Frenc Jolez), Michael D'Ambra (Anesthesia), Hugh Flanagan (Anesthesia and OR), Michael Jaklitsch (surgery), Vania Nose (Pathology), Janice Crosby (CIMIT), Lynn Dockser (OR administration representing John Fernandez), Claire Fitzgerald-O'Shea (OR nursing), L. Michael Fraai (Biomedical Engineering), Ann Humphrey (CIMIT), Colleen Kigin (CIMIT), Charles Labins (Real Estate, Design etc.), Catherine McGoldrick (IS), Michael Roughan (Architect), Deborah Parnther (administrative assistant).

Shared drive developed to make available to all data and presentations.

February-March 2004
The steering committee met 4 times (about every other week).

Process and goals of the steering committee were defined:

1. To define a specific mission statement and objectives.
2. To explore a new "brand name" for the process at BWH.
3. To visit other sites including the MGH ORF.
4. To organize an afternoon symposium at BWH for all interested staff in order to introduce the concept and include all who would like to participate.

Approach selected to define the mission statement and objectives: Each of the committee members has or will present a 15-minute review of the current state of the OR in their specialty/field, and the possible improvements.

This process is ongoing and we hope to develop a mission statement and objectives by June-July to present to the leadership.

April-September 2004
The steering committee met for nearly every other week. We have heard from all the stakeholders as well as from a number of potential industry and hospital collaborators.

Several of us have visited other ORF and manufacturers in the US and Europe to explore options. We have developed an outline of an executive document for the plan of the ORF that was discussed and agreed upon by the stake-holders. At this time, we are in the process of preparing the final document for presentation to the hospital and department administration. The next step will be implementation. To continue this work we have applied to get a no-cost extension of the grant through this coming year.

Progress on Specific Aims

1. Visited several sites in Europe to study re: options for OR.
2. Completed hearing presentation from all stakeholders.
3. Summary document for plan for the future.
4. New concept-we will have not just one OR, but a combination of operating rooms of one service as the ORF nucleus. This will allow us to deal with the current space constraints at BWH, to eliminate the need for specialized personnel—utilize the personnel of the service—Thoracic Surgery—and allow us to leverage the ORF concept into relations with industry as soon as possible.

Operating Room of the Future Outcomes Project

G. Scott Gazelle, MD, MPH, PhD Principal Investigator

Overall Objectives and Approach

During the past year, the work of the ORF Outcomes Project team has focused on conducting a financial analysis of the current Operating Room of the Future. The analysis has made use of existing databases and of data collected during prior years.

Progress on Specific Aims

During the first quarter, the major focus of our work was on completing the data collection and analyses initiated in earlier years. At the same time, we laid out the groundwork for a financial analysis of ORF operations that was the focus of our work during the remainder of FY04. This involved collecting data on operating costs via the hospital's TSI system, and developing a plan for understanding the complexities of cost accounting that are relevant to the ORF.

During the second quarter, we completed the data collection and analyses initiated in earlier years, and continued data collection initiated during prior months. We also further developed our plan for conducting the financial analysis.

During the third quarter, we completed the detailed analytic plan and continued to work on the data collection for the financial analysis of the ORF. Meetings were held with key stakeholders, and we made an effort to clarify team member roles and expectations.

During the fourth quarter, additional meetings were held with institutional and CIMIT personnel involved in the assessment of the ORF, team member roles were further clarified, and both data collection and analysis continued.

Publications and Presentations

None

External Proposal Activity

None

CIMIT Simulation Group
Steve Dawson, M.D. Principal Investigator

Overall Objectives and Approach
Quarter 1
The Simulation Group remains busy. The highlight of our quarter, indeed the entire calendar year, was our receipt of the Army's Greatest Invention Award for the VIRGIL Chest Trauma Training System. The award was presented to only 10 inventions throughout the entire United States Army, Steven Dawson, Ryan Bardsley, Stephane Cotin were on hand to accept the award.

Our research efforts continued with a new research proposal to the NSF, continued work on the endovascular training systems, and a new effort in collaboration with the Institute for Soldier Nanotechnology at MIT. In addition, we have received a small CIMIT award to help fund more vascular research, and are currently in the process of resubmitting for an NIH grant.

Progress on Specific Aims
Smallpox-(SITU)
The SITU system progresses toward pre-production specifications, with minor design modifications of the arm form in conjunction with our partners at Sawbones in Vachon Island, WA. A Caucasian skin arm form and shoulder were developed and the previously used beta-arm forms from Camp Casey, Korea were returned for analysis. Ryan Bardsley is working with the Sawbones team to examine patterns of wear in the beta units, each of which apparently was used to train 12 medics, rather than the single use system we had anticipated. However, this "outside the design envelope" use has given us a good benchmark for materials analysis.

We have received the metrics results from 2LT Simon Strating at the 2ID training facilities at Camp Casey and have assembled those data into a paper describing the system and its field evaluations. This manuscript has been submitted to *Military Medicine* for publication.

Supplemental funds were awarded from TATRC in 2003 to complete pre-production design refinement and specifications for the SITU inoculation training system. Kaiju Studios has successfully transferred the educational CD into a universal "plug and play" format, and we are very happy with the results. A company has been secured to make product compatible molds for the containers and vaccine vial holders. A vendor has also been identified for the COTS components of the kit.

EVE
The endovascular treatment system research has focused on the integration of our 3-dimensional vascular network within the synthetic X-ray rendering system, to merge the cardiovascular system with the skeletal system. We have also modified the catheter and contrast flow algorithms in order to provide a more realistic angiogram. In this system, haptics will consist of position tracking of the catheter and guidewires used for navigation within the brain. The tracking device needs further refinement to obtain higher accuracy than we are now achieving (on the order of 2mm accuracy) and we are working with optics experts at the Wellman Laboratories at MGH to solve this problem.

Members of the EVE team have attended several interventional neuroradiology cases at MGH and begun collaborations with Dr. James Rabinov to refine anatomic detail and instrument behavior.

New Directions

Vocal cord

Dr Mark Ottensmeyer has begun instrument design for the vocal cord tissue property measurement device that will be used by Dr Stephen Zeitels during tests of vocal cord properties. We anticipate adding a second investigator to this work in the near future. This work is not funded through the TATRC/CCC research award, but is included here for a full description of our efforts during the quarter.

ISN

Through informal conversations with Dr Simona Socrate at MIT, Dr Mark Ottensmeyer has entered into a new project with the Institute of Soldier Nanotechnology at MIT. This work will initially be funded through a new CIMIT pilot project award. This work will examine tissue properties related to behind-body-armor trauma for combat injuries.

CELTS

The CELTS system continues to be upgraded with new user interface refinements and easier performance archiving. Measuring performance is the fundamental motivation behind creating CELTS, and we have identified and corrected some earlier difficulties inherent in the alpha-prototype design.

CELTS was tested in head-to-head comparisons against the commercial system known as MIST-VR (Mentice AB, Gothenburg, SWEDEN), during studies performed at the Learning Center of the 2004 Annual Meeting of the Society of American Gastrointestinal Endoscopic Surgeons (SAGES) in Denver. Preliminary results from that testing indicates that CELTS is a superior system for measuring performance and educational level when compared to MIST-VR. These results have been submitted to *Surgical Endoscopy* for publication.

VIRGIL

The VIRGIL system is partially "decommissioned," in preparation for modification for our next project in COMETS (91W). The original VIRGIL system will no longer travel to demonstrations but will begin modification for additional training modules and new interface design. While at the AMEDD training course, we were pleased to hear the reaction of MAJ Daniel St. Armand, who was unaware that VIRGIL was the result of our work, but who offered an unsolicited endorsement of the system , stating that the "VIRGIL system is the best thing out there". We anticipate that we will be able to continue that level of end-user satisfaction as VIRGIL is reborn into a new system.

At the same time that the original VIRGIL module is being redesigned, the newer "Mini-VIRGIL" system moved to the National Capitol Area Simulation Center at USUHS for validation training in head to head trials against traditional animal (pig) models of trauma training. Initial results reported to us by COL Mark Bowyer indicate that the Mini-VIRGIL system far outperformed the pig models across several rating measures. We anticipate publication of those results in the near future, in collaboration with COL Bowyer. Because of existing DOD directives, if the simulator can be shown to be equivalent or superior to existing animal models, replacement of those animal models will have to be considered.

On June 23rd, VIRGIL received one of the Army's Greatest Invention Awards, given to just 10 inventions per year. During this quarter, VIRGIL has taken a new direction: To complement the new 91W project we are refining VIRGIL into an enhanced classroom version. The next generation, VIRGIL++, will begin in parallel to our work on the 91W simulator. We have also encountered a great deal of interest in the commercialization of VIRGIL, and are working with Chris Brown of Concurrent Technologies Corporation to pursue these commercialization opportunities.

New Projects

On 14-17 March, Mark Ottensmeyer, Ryan Bardsley and Steve Dawson traveled to the AMEDD Center and School at Fort San Houston, San Antonio, Texas, to participate in and observe 91W combat medic training. Our POC at the AMEDD School is MAJ Jeff Cain, Academic Head of the 91W training program. MAJ Cain is a Special Forces doctor, trained in emergency medicine, and a veteran of two tours in Iraq and one in Afghanistan, all as a member of the Special Forces. He has begun a major restructuring of the medic training program, with the goal of assuring that all 91W are EMT-B certified, all can perform basic invasive procedures in the field and that training meets the needs of the combat medic. The School uses over 150 mannequin simulation systems from both Laerdal and METI, but none of the systems suits the training requirements faced by the combat caregiver. During the three day visit, we observed classroom exercises, special training exercises on the Schoolhouse grounds, and then traveled with MAJ Cain to Camp Bullis to experience field training exercises including multiple trauma battalion aid station triage and treatment, aircraft extrication and transport, urban combat scenarios, and Chem-Bio training. We were also able to spend two hours with nine of the 91W instructors, learning the issues they face with existing systems and gathering ideas to solve the problems they currently face.

As a result of this trip, we recognize that the issues facing 91W training are broadly based, achievable, and important. We also realize that the need for effectively trained medics will be sustained over the foreseeable future. We have presented TATRC with a white paper to address the issues brought up by the many soldiers we met at the AMEDD School. This white paper has been favorably received and we are in the process of preparing a full proposal for a completely new approach to simulator-based 91W training.

We are very grateful to MAJ Cain and also to MAJ Daniel St.Armand, US Army Nursing Corps, for the time they spent with us, helping us as civilians to understand the training needs of the combat medic program.

COMbat Medic Training System (COMETS, formerly 91W)

Our newest project is a simulator based on the Army's curriculum for training entry-level medics, called 91 Whiskys. In order to take on this large project we have added Joseph Samosky, PhD, an engineer with both engineering and medical expertise, to the team and we have a sub-contract with Rhode Island School of Design (RISD). We are working with Major Jeffrey Cain, MD, chief of the academic division of the Army's Combat Medic Training department. Major Cain has agreed to advise on the project so that it can maintain the highest degree of accuracy. COMETS was presented to MG Martinez Lopez along with TATRC and CIMIT officials at this year's ATACCC conference.

RISD Detail

Our collaboration with RISD promises to be a fruitful one. This past summer a "Design Studio" was conducted where a group of graduate students and faculty members worked on the concept of blast injury to the leg. The results were impressive, especially considering their 8-week window

of work. The demonstration was presented to Major General Martinez-Lopez who was impressed with the project and demo. This initial collaboration will continue with a 6 credit (major course offering) Fall Design Studio and a similar 6 credit Spring Digital Interface Design Studio.

Army's Greatest Invention Award
The VIRGIL Chest Trauma Training system received the Army's Greatest Invention Award for 2003. This award is chosen by representatives from Army Operations and is presented to just ten Army research programs per year. VIRGIL represents the first medical project to be recognized for this honor. COL Dean Calcagni, Deputy Director of TATRC, Harvey Magee, Dr Gerry Moses, Dr Steve Dawson, Ryan Bardsley and Dr Stephane Cotin shared the award presented to them by GEN Paul J. Kern, Commanding General, Army Materiel Command.

OpenMedSim Project (CAML)
After meetings with Dr Ken Curley, from TATRC, at the ATACCC meeting in August, we have reconvened an international consortium to once again investigate the enabling technology of a Common Anatomic Modeling Language, or CAML. This project has been renamed OpenMedSim and will comprise investigators from The Simulation Group at CIMIT, University of California-Berkeley, ETH-Zurich, and the ALCOVE Group at the Technical University of Lille (France). This team will present an initial demonstration at the 2005 MMVR meeting.

MEDCEUR 2004 - Lithuania
This July The Simulation Group participated in the 2004 MEDical exercises Central EURope (MEDCEUR). Group members Steven Dawson, MD, Stephane Cotin, PhD, Mark Ottensmeyer, PhD, Paul Neumann, PhD, and Ryan Bardsley visited the host country of Lithuania to use the VIRGIL the chest trauma training system to teach medics from the Baltic States.

MEDCEUR is a joint NATO/US Air Force Europe/USAREUR led "In the Spirit of Partnership for Peace" (ISO PfP) exercise designed to train US, NATO, and Partner nations, to respond to a disaster relief/mass casualty situation. This exercise marks the first major military training event for Latvia, Estonia and Lithuania since becoming part of NATO in March, 2004.

MEDCEUR 2004 saw soldiers from 14 nations come together in the Baltic States for exercises designed to provide medical training and assess participating nation's ability in anti-terrorism, search and rescue, and disaster relief scenarios. Roughly 2,000 troops took part in the 15-day RESCUER/Medical Exercise Central Europe (MEDCEUR) 2004, in Lithuania, Latvia, Estonia and Bulgaria. Soldiers from the United States, Germany, Poland, Romania, Moldova, Ukraine, Georgia, Armenia and Azerbaijan took part with the host nation's troops.

Participation was a good opportunity to see medical facilities in a military setting overseas, and to act as ambassador to the American medical community. We are grateful to CIMIT for supporting this important diplomatic and medical opportunity.

2004 International Symposium on Medical Simulation
ISMS 2004 was a great success. Co-hosted by Stephane Cotin of The Simulation Group and Professor Dimitris Metaxas of Rutgers University, the symposium brought together leading researchers from all over the globe present their latest work in the field of medical simulation. The highlight of the second day was a very high profile panel of speakers including Ajit Sachdeva, MD, Director of Education for the American College of Surgeons, Richard Satava, MD, of DARPA, COL Mark Bowyer, MD, Director of the National Capital Area Simulation Center, Mandayam Srinivasan, PhD, Director of the Touch Lab at MIT, and David Rattner, MD, head of general surgery at MGH to discuss the future of medical simulation. We are grateful for

the conference support that TATRC provided for this international meeting of leading scholars. The proceedings from the Symposium, and a follow-up web page is available as a resource for those who attended and as summary for those who did not
www.medicalsim.org/symposium2004/followup.html

Advanced Initiatives in Medical Simulation (AIMS)
The first annual AIMS meeting was held in a two-day session on May 10-11, 2004. Steve Dawson, MD, co-hosted the meeting along with COL Mark Bowyer, and Jackie Eder-Van Hook and Bob Waters of the Center for Telemedicine Law. The first day was held at the Walter Reed Army Institute of Research, consisting of a planning session where participants discussed the general field of medical simulation and initiated plans for a national coordinated program in medical simulation. The second day was held in the Dirksen Senate Building where companies and labs from around the world demonstrated their work for members of Congress and their staffers.

Publications and Presentations

Medical Simulation: International Symposium, ISMS 2004, LNCS 3078
Stephane Cotin, Dimitris Metaxas

S. Cotin, P. Neumann, X. Wu, V. Pegoraro, R. Bradsley, and S. Dawson, Interventional Neuroradiology Training through Simulation, Innovation and Research in Interventional Radiology (IR2) Research Conference: Stroke Interventions, January, 2004.

X. Wu, *V. Pegoraro, , P. Neumann, R. Bradsley, and S. Dawson, and S. Cotin, New Approaches to Computer-based Interventional Neuroradiology Training, Proceedings of 13^th MMVR, January, 2005.**

X. Wu,* T. Goktekin, and F. Tendick "An Interactive Parallel Multigrid FEM Simulator", Proceeding of International Symposium on Medical Simulation 2004, LNCS vol. 3078, pp 124-33, June 2004.

X. Wu* and F. Tendick "Multigrid Integration for Interactive Deformable Body Simulation", Proceeding of International Symposium on Medical Simulation 2004, LNCS vol. 3078, pp 92-104, June 2004.**

S. Cotin, P. Neumann, *X. Wu, *V. Pegoraro, R. Bradsley, and S. Dawson, Interventional Neuroradiology Training through Simulation,* *Innovation and Research in Interventional Radiology (IR^2) Research Conference: Stroke Interventions, January, 2004.**

Konofagou, Elisa E., Ottensmeyer, Mark P., Agabian, Sue, Dawson, Steven L., Hynynen, Kullervo. Estimating localized oscillatory tissue motion for the assessment of the underlying mechanical modulus. Ultrasonics, vol. 42, 951-6, 2004.

Ottensmeyer, Mark P., Kerdok, Amy E., Howe, Robert D., Dawson, Steven L. The Effects of Testing Environment on the Viscoelastic Properties of Soft Tissues. In S. Cotin and D. Metaxas (Eds.): ISMS 2003, LNCS 3078, pp. 9-18, 2004. Springer-Verlag Berlin Heidelberg 2004

Proceedings of the International Symposium on Medical Simulation,
Cambridge, MA, USA, June 17-18, 2004.

External Proposal Activity
During the past quarter, team members wrote and submitted two major research proposals, which, if funded, would extend our enabling technologies efforts into new methods of learning. The first submission, "Cluster-based Neuroradiological Training and Planning Framework" went to the National Science Foundation, with Paul Neumann, PhD as principal investigator. The second proposal, to develop and validate core components for endovascular therapy simulation, went to the National Institute of Biomedical Imaging and Bioengineering, with Stephane Cotin, PhD as PI

Femur Fracture SBIR
In July, we were awarded a Phase 1 SBIR grant in collaboration with Sawbones to develop a plan and prototype for a femur fracture simulator that can be used to train combat medics. This work is underway and we anticipate filing a Phase 2 application in November, 2004.

CiMeRC Collaboration
We have begun a new Collaboration with CiMerRC (The National Bioterrorism Civilian Medical Response Center) to develop a desktop simulation for Mass Casualty Incident responses. The collaboration is in its early stages of both funding and development. We hope that this project will be able to increase the breadth of the group's work, and will help to work with more TATRC funded organizations.

Patent Activity
On March 2nd, 2004, we filed European and Canadian patents on our "Medical Procedure Training System", the official designation of VIRGIL.

On March 10th, 2004, we filed conversions of the provisional patent on our "Surgical Training System for Laparoscopic Procedures", the official name of CELTS, with the United States Patent Office.

On August 10th, 2004, we filed a United States Provisional Patent application for our "Interventional Radiology Training System", with Stephane Cotin as principal author.

During the year, we received notification that international patents had been filed on the VIRGIL training system, CELTS, and SITU, the smallpox training system.

Development of an Injectable, Self-Assembling Engineered Myocardium

Richard T. Lee, M.D. Principal Investigator

Overall Objectives and Approach

Cardiac regeneration is a promising approach to cardiac injury and heart failure. We are developing injectable peptide scaffolds that can potentially promote recruitment of progenitor cells. This project aims to establish that injectable microenvironments are feasible in the myocardium.

Progress on Specific Aims

Aim 1. To establish the importance of endothelial cell – cardiac myocyte interactions for myocyte survival and structural organization into myocardium-like tissue in vivo.

This Aim will test the hypothesis that the inclusion of endothelial cells will promote myocyte survival, organization, connexin 43 expression and formation of functional gap junctions within the self-assembling peptide gel in vivo.

We completed this study and published it in Circulation this year (Narmoneva 2004). We are currently exploring which proteins may mediate the specific effects of endothelial cells on cardiac myocytes. If we can further define this interaction, we will develop strategies that promote cardiomyocyte-endothelial adhesion in vivo by delivery of that factor. The abstract of this manuscript follows:

> Background: Endothelial-cardiac myocyte interactions play a key role in regulating cardiac function, but the role of these interactions in cardiomyocyte survival is unknown. This study tested the hypothesis that endothelial cells (EC) promote cardiac myocyte (CM) survival and enhance spatial organization in a three-dimensional configuration. Methods and Results: Microvascular EC and neonatal CM were seeded on peptide hydrogels in one of three experimental configurations: CM alone, mixed with EC (coculture), or seeded on pre-formed EC networks (prevascularized). Capillary-like networks formed by EC promoted marked CM reorganization along the EC structures, in contrast to limited organization of cardiomyocytes cultured alone. The presence of EC markedly inhibited CM apoptosis and necrosis at all time points. In addition, CM on pre-formed EC networks resulted in significantly less CM apoptosis and necrosis as compared with simultaneous EC-CM seeding ($p<0.05$, ANOVA). Furthermore, endothelial cells promoted synchronized contraction of cardiomyocytes as well as connexin 43 expression. Conclusions: These results provide direct evidence for a novel role of endothelium in survival and organization of nearby cardiomyocytes. Successful strategies for cardiac regeneration may therefore depend on establishing functional cardiomyocyte-endothelial interactions.

Aim 2. To optimize the peptide gel for studies of angiogenesis and cardiac tissue engineering.

We have made substantial progress, summarized in a manuscript currently submitted. The abstract of this manuscript:

Congestive heart failure is increasing throughout the world and most therapies slow progression but do not treat the underlying process. The dominant cause of heart failure is loss of myocardium due to infarction and the limited regeneration potential of cardiomyocytes in mammals. Regeneration of myocardial tissue is an actively developing area of research aiming to restore cardiac function. We hypothesized that a novel approach to cardiac tissue engineering could create microenvironments within the myocardium that promote cell survival. These microenvironments could be provided through an injectable tissue engineering scaffold. Here we demonstrate that self-assembling peptides can be injected into the myocardium, and the resulting peptide scaffold microenvironment recruits progenitor cells that express endothelial markers initially, followed later by cells that express cardiomyocyte markers. Furthermore, our results show that injection of donor cells with the self-assembling peptides results in survival of transplanted cells in the peptide scaffold microenvironment as well as an increase in endogenous progenitor cell recruitment. These experiments suggest that injectable myocardial tissue engineering may be feasible though self-assembling peptide microenvironments.

We have also developed conditions for creating microenvironments in vivo in mice, and we are characterizing progenitor cells in this environment. There are both neomyocytes as well as endothelial progenitors in the microenvironments. The abstract of this manuscript follows. We will continue exploring the role of this new technology in vivo.

Background: Promoting survival of transplanted cells or endogenous precursors is an important goal. We hypothesized that a novel approach to promote vascularization would be to create injectable microenvironments within the myocardium that recruit and promote the survival and organization of endothelial cells. Methods and Results: Here we demonstrate that self-assembling peptides can be injected and the resulting nanofiber microenvironments are readily detectable within the myocardium. Furthermore, the self-assembling peptide nanofibers microenvironments recruit progenitor cells that express endothelial markers, as determined by staining with isolectin and for the endothelial-specific protein PECAM-1. Vascular smooth muscle cells are recruited to the microenvironment and appear to form functional vascular structures. Following endothelial cell population, cells that express alpha-sarcomeric actin and the transcription factor Nkx2.5 infiltrate the peptide microenvironment. When exogenous donor GFP-positive neonatal cardiomyocytes were injected with the self-assembling peptides, transplanted cardiomyocytes in the peptide microenvironment survived and also augmented endogenous progenitor cell recruitment. Conclusions: These experiments demonstrate that self-assembling peptides can create nanofiber microenvironments in the myocardium and that these microenvironments promote vascular cell recruitment. Because these peptide nanofibers may be modified in a variety of ways, this approach may enable injectable tissue regeneration strategies.

An example of in vivo application of this technology is shown below, where we injected mouse hearts with the self-assembling peptides approach.

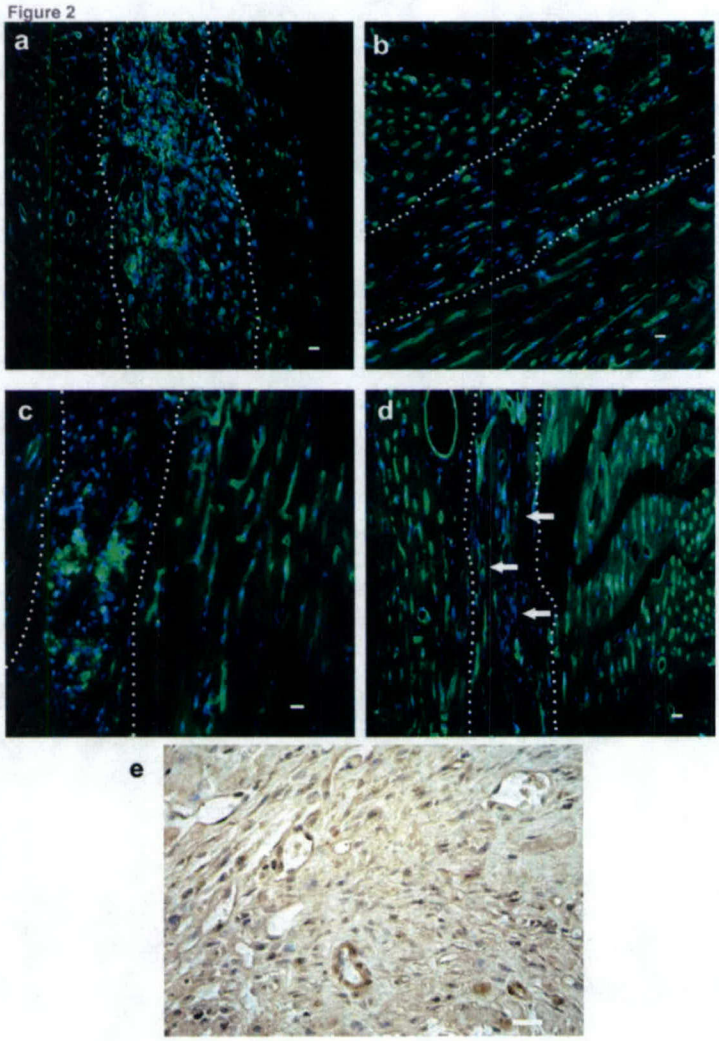

Figure. Endothelial cells spontaneously populate cell-free peptide microenvironment after 7 days and organize at later time points. a, Many cells (nuclei=blue, DAPI) within the peptide microenvironment (dotted lines as determined by light microscopy) stained positively with the endothelial cell marker isolectin-FITC (green) 7 days post-injection. b, Endothelial cells were still present within the microenvironment 14 days following injection and appeared to be elongated in shape. c, Following 21 days after injection, the endothelial cells appeared to be clustered within sections of the peptide microenvironment. d, Distinct capillary-like structures (arrows) were seen within the microenvironment 28 days post-injection. e, Endothelial cell phenotype confirmed by immunohistochemical staining for PECAM-1 (CD31, brown staining) within the peptide microenvironment at 28 days. Note the vessels within the gel highlighted by arrows that contain red blood cells. Scale bars represent 20 um.

Publications and Presentations

Narmoneva DA, Vukmirovic R, Davis ME, Kamm RD, Lee RT. Endothelial Cells Promote Cardiac Myocyte Survival and Spatial Reorganization: Implications for Cardiac Regeneration. Circulation 2004;in press.

Under review: Narmoneva DA, Oni O, Zhang S, Gertler JP, Kamm RD, Lee RT. Self-Assembling Peptides As A Novel Biomaterial For Promoting Angiogenesis

Under review: Injectable Self-Assembling Peptide Microenvironments for Cardiac Tissue Engineering. Michael E. Davis, J.P. Michael Motion, Daria Narmoneva, Tomosaburo Takahashi, Roger D. Kamm, Shuguang Zhang & Richard T. Lee

External Proposal Activity

We have submitted a Bioengineering Research Partnership NIH proposal, including multiple other investigators at MIT, to further develop Smart Scaffolds for tissue regeneration.

Application of Micro-Mechanical Forces to Accelerate Wound Healing

Dennis P. Orgill, M.D., Ph.D. Principal Investigator

Overall Objectives and Approach

Micro-Mechanical Forces (MMFs) are a potent force in stimulating cellular proliferation and angiogenesis *in vitro*. We seek to demonstrate in our rat ear model of angiogenesis that MMFs are equally effective *in vitro*. Cyclical and static MMFs of different magnitudes, frequencies and waveforms will be compared in our rat ear model of angiogenesis to determine the optimal parameters for use in stimulating wound healing.

Progress on Specific Aims

We have successfully completed our static tension studies on angiogenesis. Using 55g of static tension applied over a period of 4 days, we were able to demonstrate an approximately 114% difference between tension and tension free ears (Fig.1). Immunochemistry and Evan's Blue

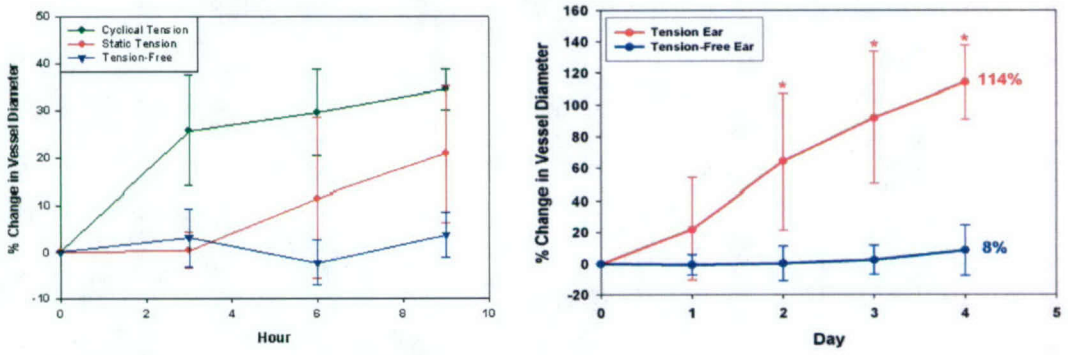

Figure 1: Tension vs. Tension-free Ear Vessel Diameter a) cyclical tension (green) results in larger vessel diameters than static tension (blue) Significant differences between cyclical tension and tension-free ear vessel diameters. b) No significant differences were noticed during day 1 of static stretch.

extraction study results corroborate the observed changes in the ear vasculature (Fig.2a & 2b). Vessels of the tensioned ear stained for VEGF showed a marked difference compared with that of the tension free ears. Similarly, significant differences in the quantity of Evan's Blue dye extracted from tension ears compared to that of tension free ears were observed, corresponding to the expected volume differences observed with larger vessel size and greater blood flow into tension ears. Mercox corrosion casting studies were also performed to demonstrate these vascular changes three-dimensionally (Fig.3). Analysis of these studies has been complicated by incomplete filling of the vasculature. It is currently unclear whether this is due to a flaw in our casting technique or whether it is due to the vascular changes being observed. With the collaboration of Dr. Moritz Konerding, a professor of Pathology at the University of Mainz in Germany and the world expert in corrosion casting, we have been able to refine our corrosion casting technique and hopefully resolve our problems. Multiple new casts from both statically and cyclically stimulated ears are currently being processed. These casts will be examined by Dr. Konerding using an electron

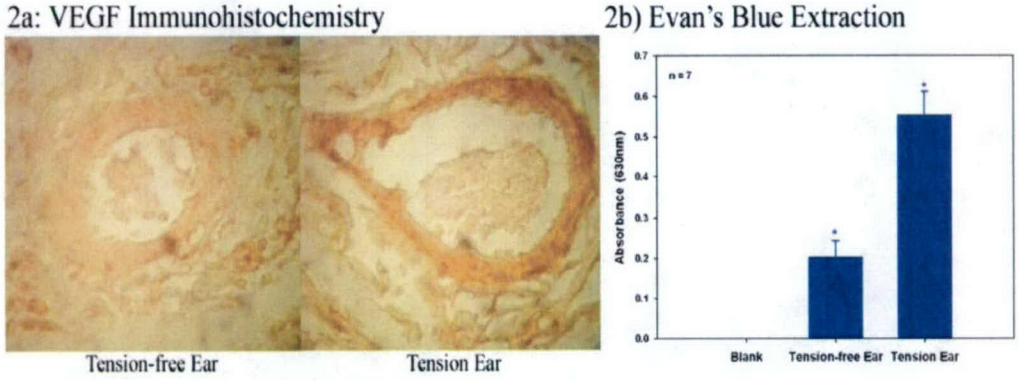

Figure 2: a) Immuno-histochemistry of Tension and Tension-free ears b) Evan's Blue Extraction for ear fluid volume determination

microscope, allowing us to look at vascular changes on the capillary level, something we are unable to do using intra-vital microscopy.

Figure 3: Corrosion Casting Images of a Normal Rat Ear at 92 x magnifications. Arterioles branching into smaller superficial capillaries can be seen here.

With the completion of the first phase of our project, we are currently working on the application of varying amounts of force to the rat ear, both statically and cyclically. We have designed and assembled a custom-built prototype device for this purpose (Fig.4 & 5). Our ear-stretching device will be computer controlled allowing us to actively measure and control the amount of force being applied to the ear. In addition, it will allow us to vary the manner in which the force is applied by changing frequencies and waveforms. In order to optimize our device's capabilities, we have begun collaborating with Draper labs. This partnership will hopefully result in a user-friendly device with a high degree of controllability. Initial data indicate that cyclical tension is more effective than static tension for inducing changes in rat ear vessel vascular morphology. After cycling tension every 2 hours, more significant changes were observed than when tension was applied statically over the same period of time (Fig.1a). This data also corresponds with our earlier static stretch data where there were no significant differences in vessel diameter during the first 24 hours (Fig.1b).

We have submitted an amendment to our current protocol to include the study of cyclical tension on the dorsal skin as well as on the vessels of the ear. With our custom built device, it should be easy to test the effects of cyclical tension on epithelial cells in vivo. This will permit us to demonstrate that cyclical tension stimulates both angiogenesis and cellular proliferation in the rat

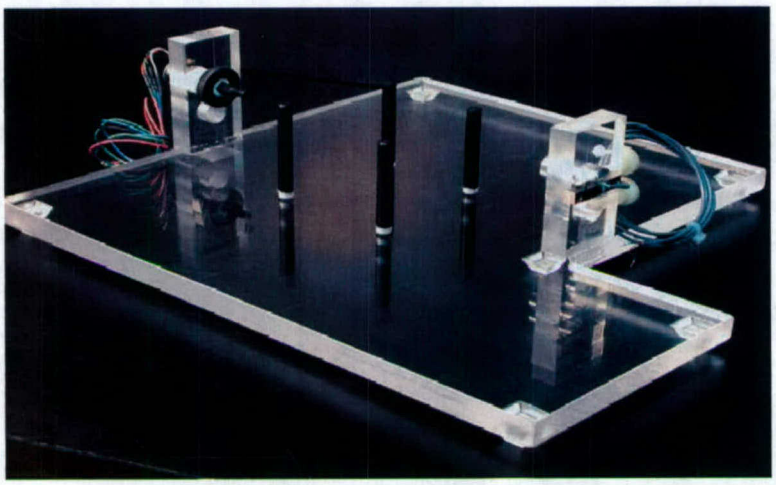

Figure 4: Picture of tissue stretching device

model. Both of these factors are essential for wound healing. Results from both types of studies will also contribute to the development of a wound healing device that utilizes optimized micro-mechanical forces to accelerate wound healing.

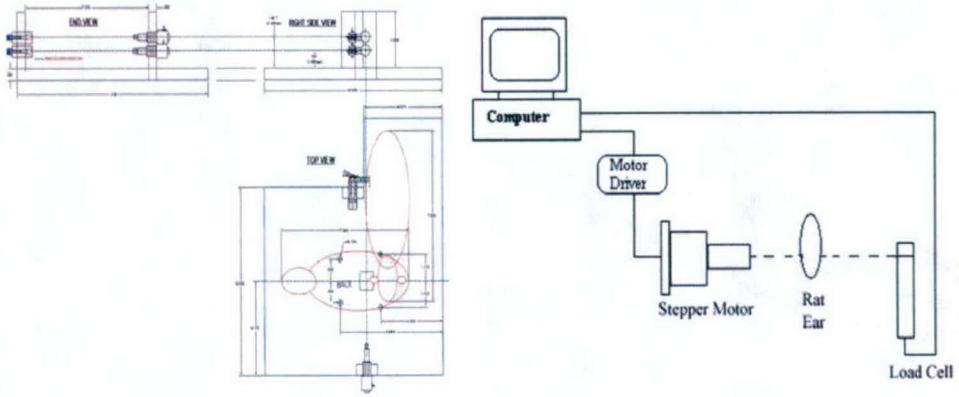

Figure 5: Schematics of tissue stretching device (left) and diagram of entire tissue stretching setup (right). This device contains adjustable heights for motor and load cell.

As our project progresses, we are undergoing discussions with Kinetic Concepts, Inc. (KCI) regarding the development of an advanced wound-healing device based on the application of cyclic tension to a wound. We have an excellent relationship with KCI and are involved in three clinical trials of the current VAC device. We have also had discussions with RTI, as there may be synergistic opportunities to use their expertise. Because of the impressive growth in the use of VAC sponge technologies, several other companies are now becoming very interested in pursuing

this technology. We hope that are article to be published in October of 2004 in Plastic and Reconstructive Surgery will be stimulus to further the interest in this field. We are beginning to make progress in applying cyclical tension of varying frequencies and hope that this will be an even more effective method to stimulate cell growth and division. In addition Vishal Saxena is doing his doctoral thesis at MIT using gene chip analysis to look at changes induced by our ear stretch model.

Publications and Presentations

Presentations

Micro-mechanical Force Stimulation of Angiogenesis , American Burn Association Annual Conference in Vancouver, BC March 23-26, 2004

Micro-mechanical Force Stimulation of Angiogenesis, BWH Research Day Poster Session and won "Poster of Distinction"

Micromechanical Forces in the Healing of Burns. North American Burn Society, January 24-29, 2004, Squaw Valley, California.

Vacuum Assisted Closure Device: Clinical Applications of Micromechanical Forces in a Surgical Practice. International Confederation for Plastic Reconstructive and Aesthetic Surgery, Sydney, Australia, August 2003.

Micromechanical Forces in Wound Healing, Boswick Burn and Wound Healing Symposium, Maui, Hawaii, February 25, 2004.

American College of Surgeons 90th Annual Clinical Congress – October 10-14, 2004 *Micro-Mechanical Forces as a Potent Stimulator of Wound Healing*

Publications

Saxena V, Hwang, CW, Huang S, Eichbaum Q, Ingber D, Orgill DP. Vacuum Assisted Closure: Micro-Deformations of Wounds and Cell Proliferation. *Plastic and Reconstructive Surgery*, accepted for publication 11/2003, MS#03-ma0951

Abstract: Liu P, Lew D, Chan R; Mayer H, Ingber D; Mentzer SJ; Orgill DP. Micro-mechanical Force Stimulation of Angiogenesis, *Supplement to Journal of Burn Care & Rehabilitation* March/April 2004, Vol. 25, No.2

Submitted Manuscripts

"Micro-Mechanical Forces as a Potent Stimulator of Wound Healing" abstract has been accepted for publication in the supplemental to the Journal of the American College of Surgeons
Manuscript entitled "Micro-Mechanical Force Stimulation of Angiogensis" is currently being prepared for submission to the Journal of the American Burn Association

External Proposal Activity

NIH R21 Grant application 6/1/04 – Accelerated Wound Healing using Micromechanical Forces

DARPA Battlefield MMF Based Wound Healing Device

Micro-vascular Hemofiltration: Precursor to a Totally Implantable Tissue Engineered Renal Replacement System

Joseph P. Vacanti, M.D. Principal Investigator
Engineering Team Leader: Jeffrey T. Borenstein, Ph.D. (Draper Laboratory)
Program Coordinator: Mohammad Kaazempur-Mofrad, Ph.D. (MIT)

Investigators:
Nicholas Krebs (MGH)
Eli Weinberg (Draper/MIT)
Brian Orrick (Draper)
Theo Marentis (Draper/MIT)
Eleanor Pritchard (Draper)
Edward Barnard (Draper)
Cathryn Sundback, Ph.D. (MGH)

Overall Objectives and Approach

Renal failure is a significant cause of morbidity and mortality in the U.S., with over 200,000 patients on hemodialysis. Current treatment for acute and chronic renal failure is focused on waste removal and uses dialysis and/or hemofiltration to replace the waste removal and fluid balance functions of the kidney. A small, portable, and possibly wearable renal replacement therapy unit can be built using microfabrication technologies and fractal microvascular network designs. This microscale hemofiltration device will offer a distinct improvement in clearance performance compared to the current hemofiltration/dialysis technologies. Further, the microvascular networks embody a fractal system that allows for streamlined flow of blood through the device and can be optimized toward minimizing thrombosis within microchannels, and hence require less anticoagulation. The low resistance of the devices will allow for ultrafiltration of blood without the need for a pump, i.e. the arterio-venous pressure difference is sufficient to drive the blood. The device consisting of stacks of bilayers allowing for ultrafiltration of blood will be built using microfabricated designs of microvascular networks.

Progress on Specific Aims

Aim 1: Design and fabrication of an engineered renal ultrafiltration device.

Fractal microvascular designs based on computational fluid dynamic models developed in this work were applied to the design of a renal ultrafiltration device. The basic design component is a bilayer device consisting of a microvascular compartment separated from a parenchymal compartment by an ultrafiltration membrane (see Fig. 1).

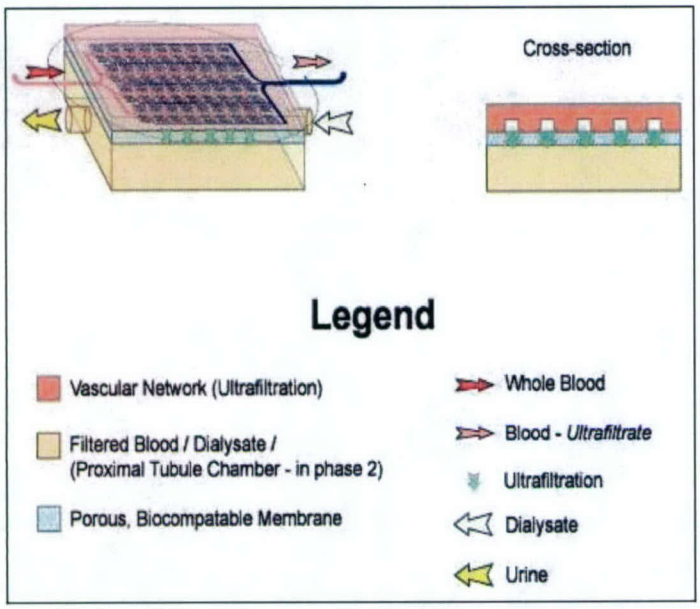

Figure 1. Schematic for MEMS-based ultrafiltration unit

We completed the design of a "Constant Shear" device, the first microvascular design which produces flow patterns in which the wall shear stress is uniform everywhere in the network. This will be important for future devices because of the critical role shear stress plays in mechanotransduction phenomena in cell-based systems. A diagram of the Constant Shear device is shown in Fig. 2, below.

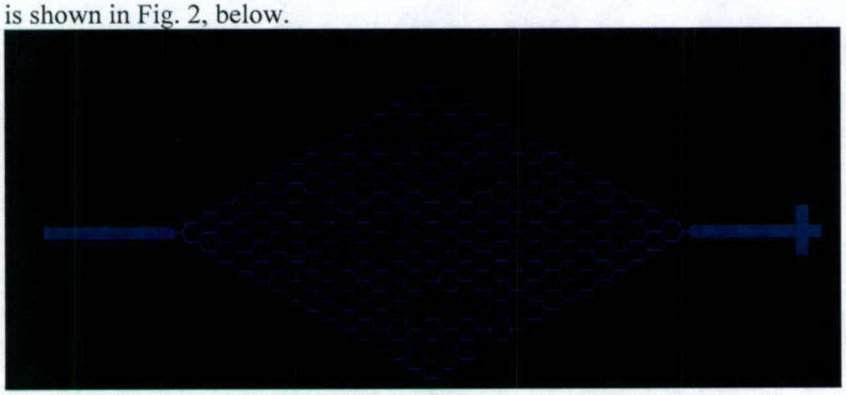

Figure 2. Layout of Constant Shear device.

A new model for the diffusion and convection processes in the microfabricated construct, which will be used to generate higher-efficiency and more compact devices for wearable dialysis, has been developed. A schematic time-sequence of the ultrafiltration process as predicted by this model is shown in Fig. 3, below.

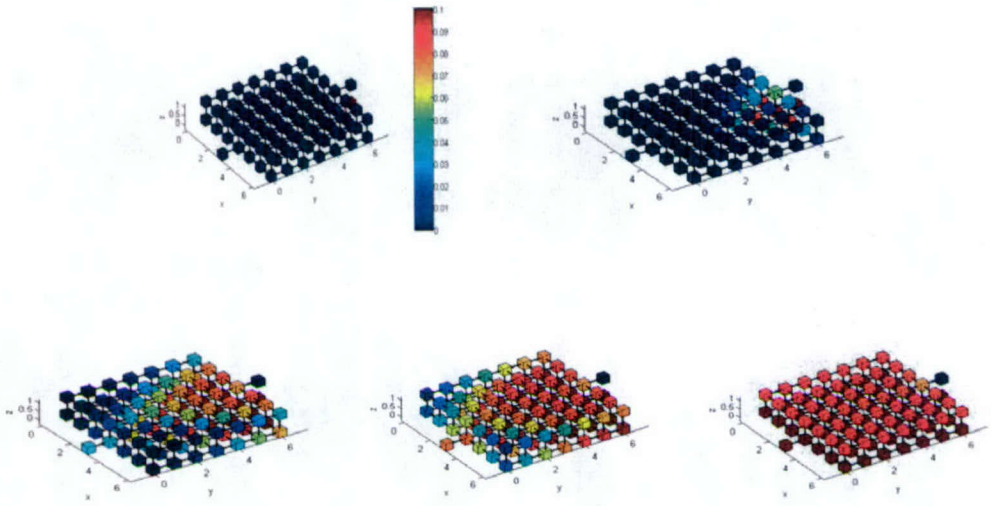

Figure 3. Time-sequenced model of solute diffusion from lower vascular network into upper dialysate network

Aim 2: Microfabricate an engineered renal ultrafiltration device

Replica molding techniques developed under this CIMIT program were used to construct thin PDMS films for the microvascular and parenchymal layers of each bilayer device. After casting each layer, a biocompatible, polyethersulfone membrane is cut to the proper dimensions and adhered to the layer with the microvascular network using a silanizing technique. Finally, the two layers are chemically bonded together using an oxygen-plasma technique and the inlet and outlet tubing connections for each network were installed.

Replica molding has been utilized to construct bilayer devices using synthetic membranes selected because of their hemofiltration properties. Early designs, reported in the previous quarterly report, utilized a polycarbonate membrane. This choice was made because of well-established techniques for integration of polycarbonate into micromolded systems. Most recently, we have produced a bilayer device with a polyethersulfone (PES) membrane, a major milestone in the project. Polyethersulfone, unlike polycarbonate, is a well-established material for hemofiltration systems, based on excellent filtration properties and hemocompatibility.

A new process, which uses oxygen plasma bonding in a multi-step process, has been developed for the rapid construction of bilayer ultrafiltration devices with PolyEtherSulfone membranes. This new process dramatically reduces the amount of manual processing and intervention previously required to build bilayer devices. We have demonstrated the viability of this process using thin PDMS films with a PES membrane sandwiched between a vascular and a parenchymal layer. Moreover, a new parenchymal layer design has been generated which has larger, more robust structures, and this new design has been used to build multiple PES bilayer devices for testing.

Recently, we have developed a new, patentable process for assembling the bilayer devices that comprise multilayer renal replacement prototypes. This new process, as well as an alternative assembly process developed at Draper Laboratory are in the process of being patented by the

MGH CSRL, and will be described in more detail in a future report. The new process development work has led to the construction of devices with as many as 20 - 35 layers.

Aim 3: Assess the ultrafiltration properties of the device

To study the ultrafiltration capabilities of these devices, the clearances of urea and creatinine from the vascular/"blood" stream into the parenchymal/"dialysate" stream were examined at varying flow rates under single-pass countercurrent conditions. The vascular fluid consisted of ultra-pure water containing dissolved urea and creatinine at concentrations of 400 and 200 mg/dl respectively, while the parenchymal fluid consisted of only ultra-pure water. The urea and creatinine solutions were pumped through the vascular layer containing the microvasculature and the ultra-pure water/"dialysate" was pumped through the open parenchymal chamber. The flow-rate ratios of vascular flow (Q_B) : parenchymal flow (Q_D) and individual flow rates used for each solute were ≈2:1 (Q_B:Q_D) at 0.9 and 2.0 ml/hr respectively, 1:1 (Q_B:Q_D) at 1.0 ml/hr, and 1:1 (Q_B:Q_D) at 2.0 ml/hr. In an incubator at 37°C, a syringe pump was used to administer each fluid into its respective layer, under conditions of countercurrent, single-pass flow. As the fluids moved through their respective layers, samples from each flow stream were taken at various time points, up to five hours, and analyzed for final concentration levels. These concentration values were first plotted versus time and then used to calculate the individual solute clearances of urea and creatinine from the vascular fluid. Finally, the calculated clearance values for urea and creatinine obtained here were normalized with respect to current hemodialysis parameters, including overall surface area and flow rate, and compared with published clearance values for overall efficiency.

The results of the initial ultrafiltration experiments reported here are very promising with respect to the clearance of uremic solutes – urea and creatinine – from a vascular stream into a dialysate stream in these micro-fabricated devices, especially when compared to conventional hemodialysis clearances. When the data is normalized and compared to conventional hemodialysis parameters, including total surface area for filtration, total internal volume, and total flow rate through the system, these bilayer devices show a two-to-three fold improvement over current published urea and creatinine clearance data that is representative of the efficiency of current hemodialysis therapies (see Fig. 4). The concentration versus time data for urea and creatinine show slightly different trends with respect to the dialysate-side clearances. However, both sets of data, suggest that an approximate 2:1 vascular : parenchymal flow rate ratio, where QB = 0.9 ml/hr and QD = 2.0 ml/hr, is the optimal ratio for the clearance of both solutes, which is the ratio used in conventional hemodialysis. This can be attributed to the establishment of a higher concentration gradient of solute between the vascular and parenchymal networks when the vascular fluid is allowed to remain in the device longer, relative to the parenchymal fluid. The normalized data for both urea and creatinine clearance show that these bilayer devices are significantly to moderately more efficient at clearing uremic solutes from an incoming vascular stream than conventional hemodialysis membranes, with urea clearance at a 2:1 flow rate ratio showing the most drastic improvement. Consequently what makes these micro-fabricated devices so attractive is their ability to be miniature, wearable, and continuous. Therefore, from these initial ultrafiltration experiments, this work has shown that these MEMS devices have the potential to make a significant improvement the current hemodialysis technology as their ultrafiltration capacities are superior to those of current therapies. Finally, these ultrafiltration units, when coupled with proximal tubule reabsorptive units, will offer the most effective means of delivering efficient hemodialysis to patients needing these therapies.

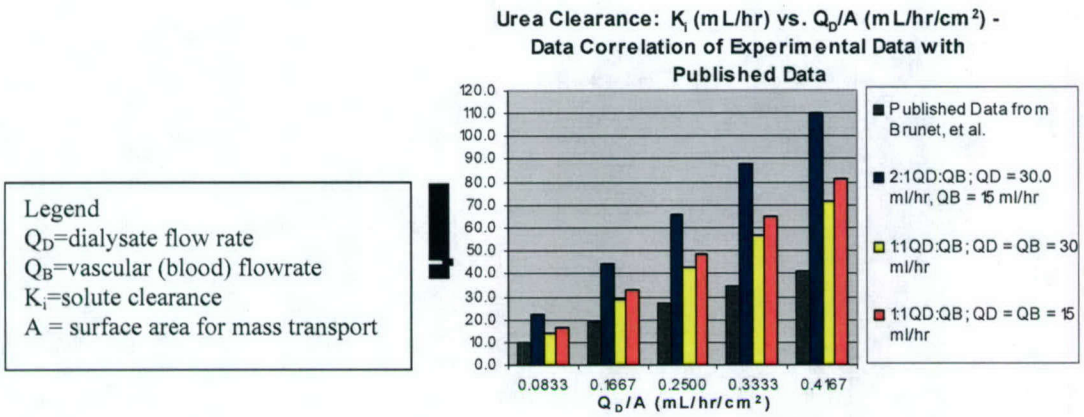

Figure 4. Normalized experimental urea clearance— comparison with published data

Extensive data on urea and creatinine filtration obtained on a polycarbonate-based bilayer device was reported. Diffusion experiments using PES membranes have been completed, and are reported in Figure 5, below. Note that surface treatment of the PES (using oxygen plasma) does not appear to affect the filtration rate for urea, a very important result. *Plan:* The current plan is to thoroughly evaluate the ultrafiltration properties of the polyethersulfone-based system; these results will be reported in the next quarterly.

Preliminary ultrafiltration data has been obtained on PES bilayer devices; these results are currently being evaluated and tests are being conducted on multiple devices constructed using the new process sequence.

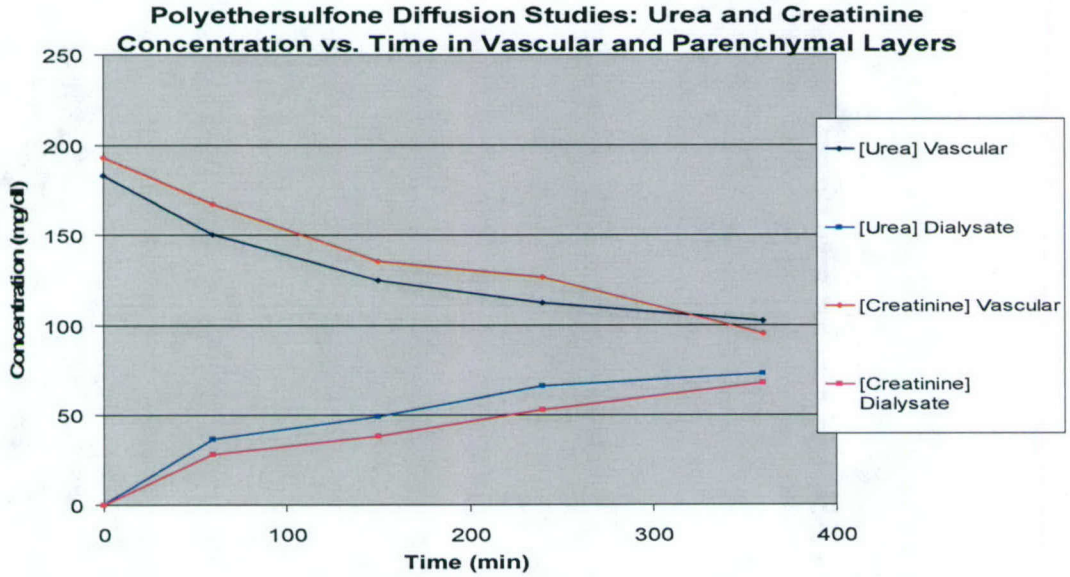

Figure 5. Urea and creatinine concentration vs. time in dual-chamber diffusion cells

Aim 4: Integration of dialysis clinical and engineering objectives.
Extensive systems-level analysis of the engineered construct has begun, including estimates of the surface area and filtration capacity as a function of device volume and processing recipe. These analyses are aimed at developing a template for a wearable, continuous, pump-free dialysis system based on microfabrication technology.

Publications and Presentations

J.T Borenstein, W. Cheung, L. Hartman, M.R. Kaazempur-Mofrad, K.R. King, A. Sevy, M. Shin, E.J. Weinberg, and J.P. Vacanti, Technical Digest for the Transducers 2003 Conference, 2003.

M.R. Kaazempur-Mofrad, E.J. Weinberg, J.T. Borenstein and J.P. Vacanti. "Tissue Engineering: Multi-Scaled Representation of Tissue Architecture and Function", to appear in Complex Systems Science in Biomedicine (Eds.: T.S. Deisboeck, J.Y. Kresh and K.B. Kepler), Kluwer Academic - Plenum Publishers, NY, 2004.

E.S. Kim, M.R. Kaazempur-Mofrad, J.T. Borenstein, J.P. Vacanti, and R.D. Kamm, "A Single Capillary-Parenchymal Co-culture Bioreactor using Self-Assembling Peptides", Computational Fluid and Solid Mechanics 2003 Ed. KJ Bathe), Vol. 2: 1738-1741, Oxford: Elsevier Science Ltd, 2003.

E.J. Weinberg, M.R. Kaazempur-Mofrad, and J.T. Borenstein. "Numerical Model of Flow in Distensible Microfluidic Network", Computational Fluid and Solid Mechanics 2003 (Ed. KJ Bathe), Vol. 2: 1569-1572, Oxford: Elsevier Science Ltd, 2003.

M.R. Kaazempur-Mofrad, J.T. Borenstein, L. Hartman, A. Sevy, M. Shin, E.J. Weinberg, and J.P. Vacanti. "A Novel Microfabricated Device for Microvascular Hemofiltration: Toward a Tissue Engineered Renal Replacement System", Proc. 6th Annual Meeting of the Tissue Engineering Society International, Orlando, FL, December 10-13, 2003.

K.R. King, C.J. Wang, M.R. Kaazempur-Mofrad, J. P. Vacanti, and J.T. Borenstein, "Biodegradable Microfluidics," *Advanced Materials, In Press.*

M.R. Kaazempur-Mofrad, N.J. Krebs, J.P. Vacanti and J.T. Borenstein, "A MEMS-Based Renal Replacement System," Proc. 2004 Sensors and Actuators Conf., 67-70.

M.R. Kaazempur-Mofrad, J.T. Borenstein, N. Krebs, E.J. Weinberg, B. Orrick, C.A. Sundback, J. P. Vacanti, "A Novel MEMS-Based Ultrafiltration Unit for Continuous Wearable Renal Replacement", Proc. TESi 2004.

J.T. Borenstein, E.J. Weinberg, M.R. Kaazempur-Mofrad and J.P. Vacanti, "Tissue Engineering of Microvascular Networks," in Encyclopedia of Biomaterials and Biomedical Engineering, eds. G. Wnek and G. Bowlin, (Marcel Dekker, New York), In Press.

Fidkowski C, Kaazempur-Mofrad MR, Borenstein JT, Vacanti JP, Langer R, Wang Y. "Endothelialized Microvasculature Based on a Biodegradable Elastomer ", Tissue Engineering, In Press.

External Proposal Activity

NIH Interdisciplinary Research Teams of the Future Planning Grant for Regenerative Medicine, submitted to NIH Roadmap Initiative, February 24, 2004, David T. Scadden, PI. Joseph P. Vacanti and Jeffrey T. Borenstein, co-investigators.

"Nanoscale platforms for the design and integration of three-dimensional vascular networks," proposal in progress, to be submitted to the NIH NHLBI Programs of Excellence in Nanotechnology RFA, due 7/21/04, PI Angela Belcher (MIT); co-investigators Joseph Vacanti and Jeffrey Borenstein.

An Experimental Approach to Bioengineer Mature Tooth and Jaw Segments

Conan S. Young Principal Investigator

Overall Objectives and Approach

We have demonstrated that small tooth crowns containing enamel, dentin and pulp tissues can be grown on biodegradable polymer scaffolds seeded with pig or rat tooth bud cells[1,2]. Using a similar approach, Milestone #1 was to bioengineer dentin and enamel layers that conform to the size and shape of the scaffold. Milestone #2 of this study was to bioengineer tooth and bone in a coordinated manner to generate biological tooth structures, anchored by roots, to bioengineered bone.

Progress on Specific Aims

Bioengineering dentin and enamel layers that conform to the size and shape of the scaffold. Our method, as schematized in Figure 1, was as follows. Spherical scaffolds (3 mm in diameter) were fabricated from polyglycolide bonded with poly-L-lactide (PGA/PLLA). The PGA/PLLA scaffolds were seeded with pulp organ mesenchymal cells obtained from six-month old Yucatan mini-pig third molars. Gelfoam, an absorbable gelatin sponge material (Pharmacia&Upjohn) was cut into 10 x 7 x 2 mm^3 strips and seeded with enamel organ epithelial cells obtained from the same molar teeth. Varying ratios of dental epithelial and mesenchymal cells were seeded onto either the Gelfoam, or the PGA/PLLA scaffolds, respectively, at a density of 10 x 10^6 cells per seeded scaffold. The dental epithelial:mesenchymal cell-seeding ratios examined were 9:1, 4:1, 2:1, and 1:1. The two cell-seeded scaffolds were joined together with opposing 7-0 Prolene sutures, and implanted in the omenta of athymic rat hosts to provide a blood supply to the implant. The hybrid implants were removed after 20 weeks, fixed in 10% formalin, embedded in paraffin and sectioned for histological analysis.

The total diameter of the hybrid constructs before implantation was approximately 5 mm – 2 mm Gelfoam strip and 3 mm PGA/PLLA sphere. After growth in the omentum for 20 weeks, we obtained tooth structures that approximated this size (Figure 2). The diameters of the bioengineered tooth structures ranged from 3-5 mm, and approximated the size and shape of the original Gelfoam/PGA/PLLA hybrid scaffolds.

The bioengineered mineralized tooth tissue appeared to consist primarily of dentin (Figure 2). The greatest amount of dentin formed when a seeding ratio of 2:1, dental epithelial to mesenchymal cells, was used. Notably, mineralized tissues formed in the 1:1, 2:1 and 4:1 cell seeding ratios, while no mineralized tissue formed in the 9:1 dental epithlelial:mesenchymal cell ratio (Fig. 2).

The bioengineered dentin roughly conformed to the outer curvature of the scaffold sphere. These results demonstrate that dental tissues can be bioengineered to conform to a predetermined size and shape, as defined by the scaffold. Small amounts of dental epithelia were identified at the periphery of the tooth implants, corresponding to the location of the dental epithelial cell seeded Gelfoam strip. The formation of relatively large amounts of dentin by the dental pulp mesenchymal cells and reduced amounts of enamel suggests that these processes are not well coordinated in the hybrid tooth constructs. This differs from natural tooth development where the dentin forms first, and is followed by the formation of enamel.

Bioengineered tooth/bone constructs (TBCs) demonstrate the integrated formation of bone, tooth and tooth roots.
Cup-shaped, polylactide-co-glycolide (PLGA) fused wafer bone scaffolds were fabricated and designed to accommodate one or two spherical tooth implants. PLGA scaffolds were seeded with differentiated osteoblast cells generated from porcine bone marrow mesenchymal progenitor cells (BMPCs).

Dental cells were isolated from third molar tooth buds of the same pig from which the BMPCs were harvested, either as a mixed dental epithelial and mesenchymal cell population, or as isolated enamel organ and pulp organ cell populations. The mixed cells were seeded onto spherical PGA/PLLA scaffolds (3 mm in diameter), while the isolated dental epithelial and mesenchymal cell populations were seeded onto hybrid Gelfoam/PGA/PLLA scaffolds at a ration of 2:1. Dental cell seeded scaffolds were joined to osteoblast seeded bone constructs (Fig. 3), and surgically implanted in the omenta of athymic rats. After 8 weeks, the tooth-bone implants were removed, fixed in 10% formalin and photographed. The tooth constructs were clearly distinguishable from the bone constructs.

Analysis of tooth tissues. (Fig. 4A). Small quantities of enamel were observed at the periphery of the tooth implants. Columnar ameloblasts were always found adjacent to enamel matrix. The enamel matrix appeared to form in the dental epithelial cell seeded Gelfoam strip, as indicated by the location of the sutures. In approximately 40% of the tooth/bone constructs (4 out of 10 TBCs that formed both dental and bone tissues), immature root-like structures were identified at the tooth bone interface. An example of a bioengineered root structure is shown (Fig. 4B, 1), which consists of a long extension of dentin lined with columnar odontoblasts. A rudimentary root structure resembling the Hertwig's epithelial root sheath (HERS), is present at the apical tip of the root. In naturally formed teeth, HERS consists of epithelial cells that induce adjacent dental mesenchymal cells to differentiate into dentin-producing odontoblasts, which extend the developing root. Immunohistochemical analysis of bioengineered root structures revealed localized bone sialoprotein (BSP) expression along the tooth root surface facing the bone construct (Fig. 4B, 2), similar to BSP expression in natural tooth roots [3], and indicate the presence of cementum in bioengineered tooth roots.

Our results demonstrate that certain bioengineered tooth/bone constructs formed tooth roots, localized to the tooth/bone tissue interface. In addition, connective tissue characteristic of periodontal ligament was also present at the tooth/bone interface, connecting the two tissues (Fig. 4C, 1, 2). In some instances, mature bone was identified within the bone implant, while the majority of bioengineered bone appeared to consist of immature osteoid tissue (Fig. 4D).

Summary
In this study, we demonstrate the generation of bioengineered tooth structures composed of dentin and small amounts of enamel, which roughly conform to the size and shape of the scaffold. Enamel formed on the dental epithelial cell seeded Gelfoam strip portion of the hybrid scaffold, although enamel production was not as robust as that of dentin. About 40% (4 out of 10 TBCs that formed both dental and bone tissues) of the constructs examined to date exhibited immature root structures, characteristic of Hertwig's epithelial root sheaths, which formed at the interface between the tooth and bone constructs. We identified small amounts of mature bone in some of the implants (10 out of 15 TBCs) while most bioengineered bone tissue consisted of immature osteoid tissue. Connective tissue characteristic of periodontal ligament was observed between the bioengineered tooth and bone tissue. Also, tooth and bone tissues integrated by connective tissues resembling periodontal ligament were successfully bioengineered. Together, these results

suggest that a hybrid bioengineered tooth/bone approach may eventually provide a clinically relevant treatment for tooth loss with associated alveolar bone resorption.

Data Acquisition and Processing

We bioengineered a total of 15 tooth/bone and 20 hybrid tooth constructs. After growth in the omentum (8 weeks for tooth/bone constructs and 20 weeks for hybrid tooth implants), implants were excised, and processed for histological analysis. Analyses of all of the bioengineered tooth/bone constructs have been completed and the results have been submitted for publication in the journal, *Tissue Engineering*. Histological and immunohistochemical analyses of hybrid tooth tissues, using antibodies specific for amelogenin, dentin sialoprotein, bone sialoprotein, osteocalcin, and collagen type I, will soon be completed. Quantitative histomorphometric measurements of dentin and enamel produced on hybrid tooth constructs are being performed, for correlation with dental epithelial and mesenchymal cells seeding ratios. These analyses will be completed by the end of October 2004, and will be submitted for publication.

Illustrations

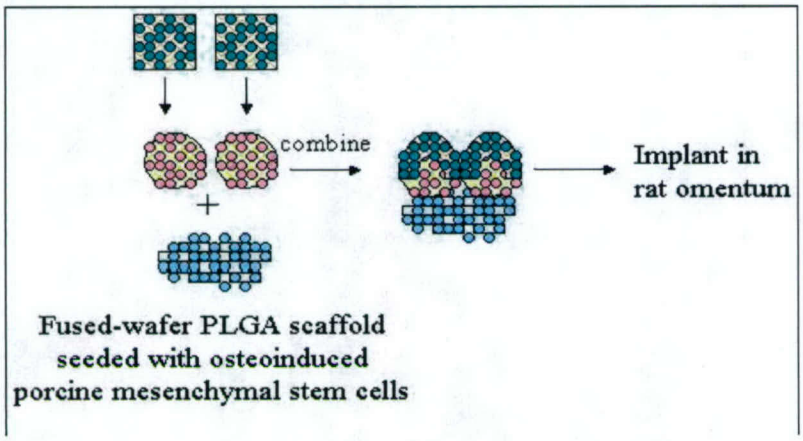

Figure 1. Hybrid tooth scaffolds composed of polyglycolide/poly-L-lactide (PGA/PLLA) spheres and Gelfoam strips. Dental mesenchymal cells (red circles) were seeded onto PGA/PLLA spheres and dental epithelial cells (green circles) were seeded onto Gelfoam strips. The two cell-seeded scaffolds were joined with sutures. In some cases, hybrid Gelfoam/PGA/PLLA tooth constructs were combined with PLGA scaffolds seeded with osteoblast cells (blue circles) to generate tooth/bone constructs.

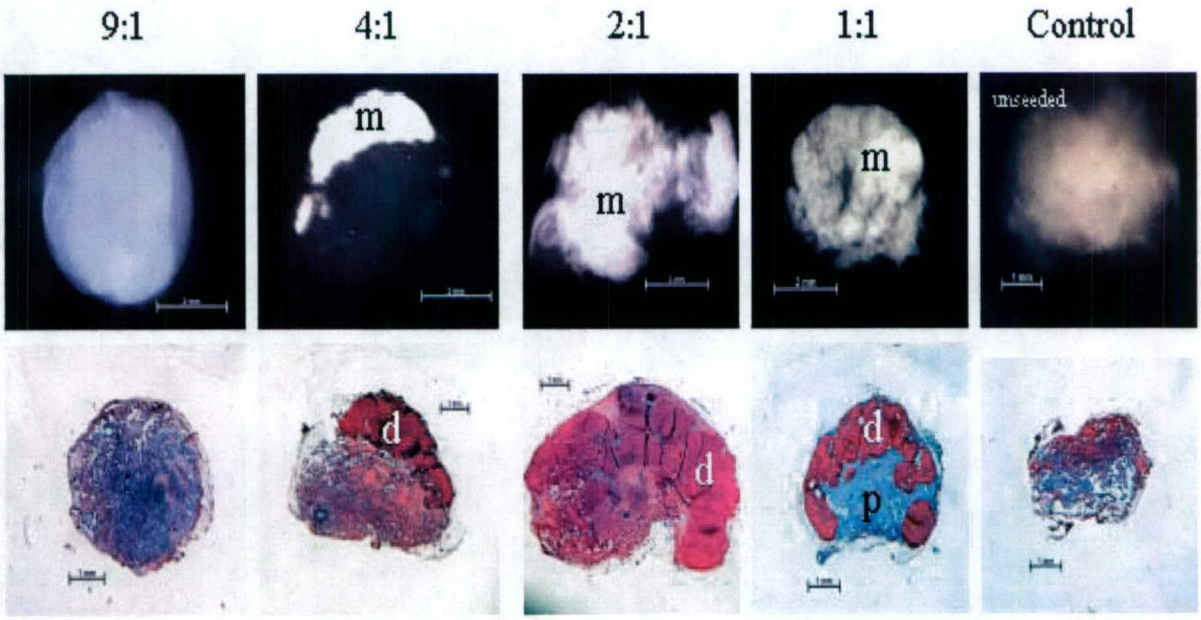

Figure 2. Radiographic and histological analysis of bioengineered teeth. Porcine dental epithelial:mesenchymal cell seeding ratios are as indicated. Top row, radiographs demonstrate radio-opaque mineralized tissues in bioengineered tooth implants. Bottom row, representative H&E stained tooth implant sections. Mineralized tissues roughly conformed to the contour of the spherically shaped scaffold. Abbreviations: d, dentin; m, mineralized tissue; p, pulp tissue.

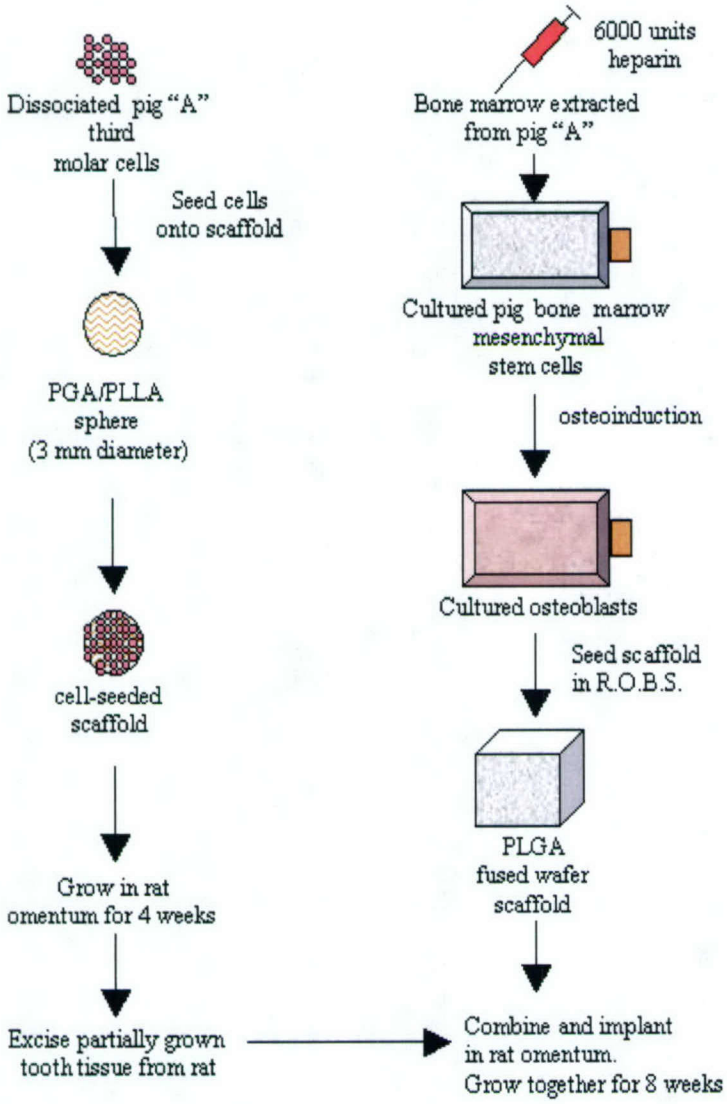

Figure 3. Schematized method for bioengineering tooth and bone constructs.

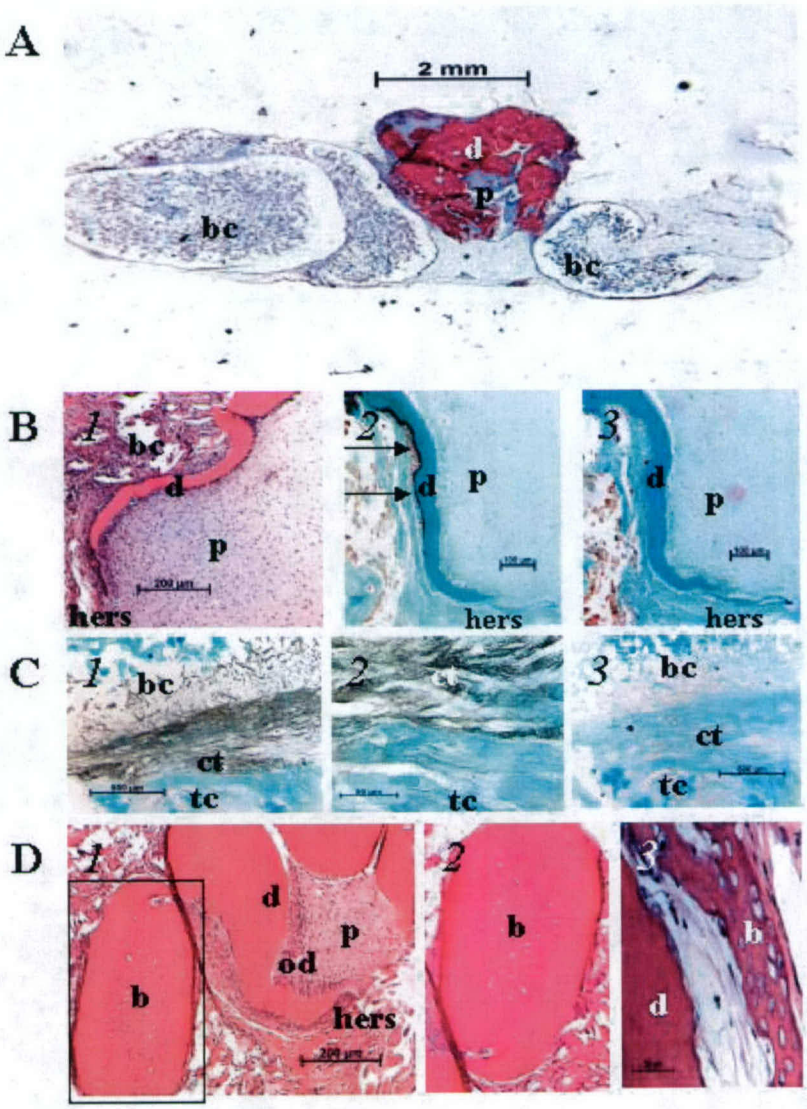

Figure 4. Histological and immunohistochemical anlayses of tooth/bone constructs and bioengineered tooth roots. (A) Histological analysis of sectioned, H&E stained tooth/bone implant. (B) *1*. Bioengineered tooth root formed at the tooth/bone interface. *2*. Immunohistochemical analysis of BSP along tooth root surface (black arrows). *3*. Pre-immune serum negative control. (C) *1*. Immunohistochemical detection of collagen type III in connective tissue forming between a tooth and bone construct (brown stain). *2*, High magnification image of collagen type III-positive connective tissue. *3*, Mouse IgG isotype matched negative control. (D) *1*, Bioengineered tooth root adjacent to bioengineered bone. *2*, Bioengineered compact bone. *3*, Bioengineered alveolar bone at tooth/bone interface. Abbreviations: b, bone; bc, bone construct; ct, connective tissue; d, dentin; hers, Hertwig's epithelial root sheath; od, odontoblast; p, pulp tissue; tc, tooth construct.

Publications and Presentations

Duailibi, M. T., Duailibi, S. E., Young, C. S., Bartlett, J. D., Vacanti, J. P., and Yelick, P. C. Bioengineered teeth from cultured rat tooth bud cells. J Dent Res **83**, 523, 2004.

Abukawa, H., Shin, M., Williams, W.B., Vacanti, J.P., Kaban, L.B., and Troulis, M.J.. Reconstruction of mandibular defects with autologous tissue-engineered bone. J. Oral Maxillofac. Surg. **62**, 601, 2004.

Young, C.S., Kim, S.-W., Qin, C., Baba, O., Butler, W. T., Taylor, R.R., Vacanti, J.P., Bartlett, J.D., and Yelick, P.C.. 2004. Developmental analysis and three-dimensional computer modeling of bioengineered teeth. Submitted to J. Dent. Res..

Young, C.S., Abukawa, H., Troulis, M.J., Kaban, L.B., Vacanti, J.P., Bartlett, J.D., and P.C. Yelick. 2004. Coordinated bioengineering of teeth and bone segments. IADR/AADR/CADR 82nd General Session (March 10-13, 2004), Honolulu, HI.

Young, C.S., Abukawa, H., Troulis, M.J., Kaban, L.B., Vacanti, J.P., Bartlett, J.D. and P.C. Yelick. 2004. An approach for bioengineering tooth and alveolar bone segments. Patent prepared for submission.

Young, C.S., Asrican, R., Preffer, F., Scadden, D., Vacanti, J.P., and P.C. Yelick. 2004. Identification and characterization of post-natal dental stem cells for applications in tooth tissue engineering. 2nd Annual Meeting of the International Society for Stem Cell Research, Boston, Massachusetts.

Young, C.S., Abukawa, H., Troulis, M.J., Kaban, L.B., Vacanti, J.P., Bartlett, J.D., and P.C. Yelick. NIH R21 grant application submitted 2/1/2004. Coordinated Bioengineering of Tooth and Bone in the Jaw. Specific Aims: #1- To bioengineer tooth and alveolar bone segments in the jaw demonstrating the coordinated formation of tooth crowns, roots and bone. #2- To bioengineer enamel and dentin layers proportionate to that of natural teeth. (PROPOSAL FUNDED, 9/29/04)

Young, C.S., Abukawa, H., Asrican, R., Ravens, M., Troulis, M.J., Kaban, L.B., Vacanti, J.P., and P.C. Yelick. 2004. Tissue engineered hybrid tooth and bone. Submitted to *Tissue Engineering*.

A manuscript on bioengineering dental tissues on hybrid scaffolds is in preparation and will be submitted for publication in October 2004 to *Tissue Engineering*.

External Proposal Activity

Drs. Young, Abukawa and Yelick have recently been funded for an R21 grant, NIH/NIDCR.

References

1. Duailibi, M. T., Duailibi, S. E., Young, C. S., Bartlett, J. D., Vacanti, J. P., and Yelick, P. C. Bioengineered teeth from cultured rat tooth bud cells. J Dent Res 83, 523, 2004.

2. Young, C. S., Terada, S., Vacanti, J. P., Honda, M., Bartlett, J. D., and Yelick, P. C. Tissue engineering of complex tooth structures on biodegradable polymer scaffolds. J Dent Res 81, 695, 2002.

3. Macneil, R. L., Sheng, N., Strayhorn, C., Fisher, L. W., and Somerman, M. J. Bone sialoprotein is localized to the root surface during cementogenesis. J.Bone Miner.Res. 9, 1597, 1994.

Continuous Cardiac Output Monitoring for Combat Casualty Care

Richard J. Cohen, MD, Ph.D. Principal Investigator
Whitaker Professor in Biomedical Engineering
Harvard-MIT Division of Health Sciences and Technology
Massachusetts Institute of Technology

Overall Objectives and Approach

One of the key problems involved in managing combat casualties is determining whether a soldier is going into shock due to internal bleeding. Peripheral arterial blood pressure (ABP) can be monitored noninvasively and continuously, but because of the body's multiple feedback and control systems, ABP is maintained even while cardiac output (CO) is falling. Thus, the development of hypotension is a late and often precipitous event. It would be extremely desirable to monitor CO noninvasively and continuously, but reliable techniques for doing so have not been available.

We have developed a technique for continuous monitoring of CO by analysis of the ABP signal. While there have been many attempts to do this in the past, they have not been based on an accurate, quantitative analysis of the physiology and thus have not proven successful. Our technique measures CO to within a proportionality constant and can be used to measure quantitatively changes in CO. We tested this technique in animal experiments, and our results to date have provided excellent agreement with measurements made with an aortic flow probe.

Progress on Specific Aims

1) **Animal Studies** We have conducted experiments, under a protocol approved by the MIT animal care committee, in six pigs so as to be able to compare cardiac output measured directly from an implanted aortic flow probe with cardiac output derived from the analysis of a peripheral arterial blood pressure signal. During these experiments cardiac output was varied by means of hemmorhage and volume infusion, administration of vasodilators and vasoconstrictors, and manipulation of heart rate.

2) **Algorithm Development** We have developed the initial version of an algorithm to compute cardiac output, within a proportionality constant, from a continuous arterial blood pressure signal according to the method described in our proposal.

3) **Comparison of Derived and Actual Cardiac Output Measures.** We have compared the actual and derived cardiac output measures obtained during the many hours of data from our animal studies. Currently the two sets of measures agree within a standard deviation of 15%. This is excellent agreement and compares favorably, for example, with the accuracy of invasive thermodilution measures.

Illustration

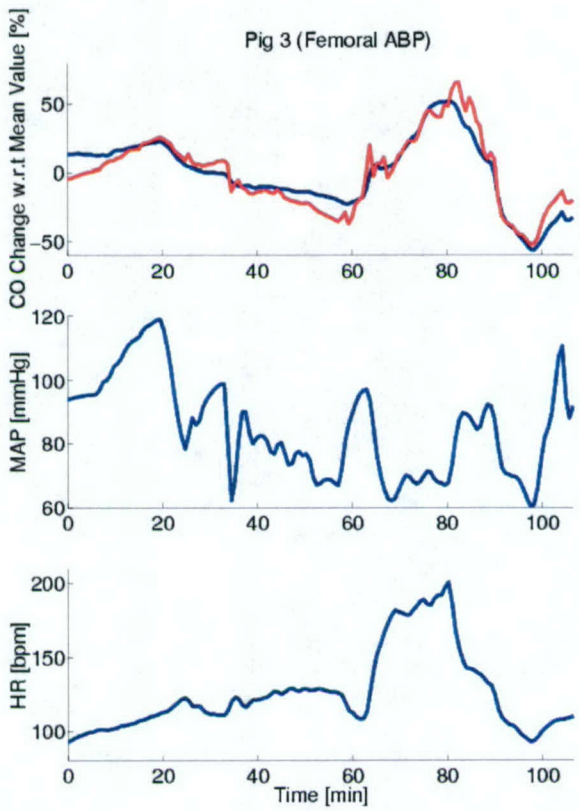

Comparison of cardiac output measured from aortic flow probe (blue) and cardiac output derived from peripheral arterial pressure (red).

Summary of Animal Studies

Summary of "Radial" ABP Results

ANIMAL	CO RANGE [L/MIN]	MAP RANGE [MMHG]	HR RANGE [BPM]	CO ERROR SD [%]
1	1.6 – 5.2	29 – 100	96 – 180	19.1
2	2.3 – 4.2	54 – 127	101 – 204	16.0
3	1.9 – 5.8	70 – 120	96 – 186	16.7
4	1.3 – 4.3	27 – 106	103 – 198	12.3
5	2.4 – 5.0	65 – 118	91 – 198	8.0
6	2.3 – 5.6	52 – 108	109 – 177	14.7
Total	**1.3 – 5.8**	**27 – 127**	**91 – 204**	**15.0**

Correlation coefficient between CO Errors and CO (0.11), MAP (0.47), and HR (-0.08)

Publications and Patents

1) R Mukkamala, AT Reisner, HM Hojman, RG Mark, RJ Cohen. Continuous Cardiac Output Monitoring by Peripheral Blood Pressure Waveform Analysis. Computers in Cardiology, accepted for publication.

2) R Mukkamala, RJ Cohen. Methods and Apparatus for Determining Cardiac Output. US Patent Application filed.

Field Cooling and Heating of Injured Soldiers

Massimo Ferrigno, M.D., F.C.C.M. Principal Investigator

Overall Objectives and Approach

Induced hypothermia protects vital organs during ischemia. Presently, there are no fast and practical noninvasive methods to induce deliberate core hypothermia or to warm patients from accidental hypothermia. Our approach relies on heat exchange in the respiratory system, bypassing the periphery of the body. Main goal of this study is measurement of rates of cooling and warming using hyperventilation with a pre-cooled or pre-warmed dense saline mist in a porcine model system. Cardiovascular, respiratory and histopathological effects of this new method are also studied.

Progress on Specific Aims

1. Develop and demonstrate a nebulizer-based system for hyper and hypothermia.

Work on this proposal was started in summer 2003. After first prototype of appropriate nebulizer was designed, built and tested during first quarter of Grant period, a second and final prototype has been designed and built by Sonaer, Inc, using data collected during test of first prototype. At the present time, Sonaer is conducting a series of tests with this new prototype to measure mist density under different air-flow speeds. Delivery of this prototype is schedule before end of January 2004. Once received, we will start using it in animal experiments.

This new nebulizer prototype (see enclosed pictures) was built according to our specifications: in particular, it incorporates fifty-two elements with a liquid saline film (covering the elements) 1.5 cm deep to maximize amount of saline mist produced (mist output) and to minimize energy lost in the liquid saline. Its elements operate at a frequency of 2.4 MHz to produce mist particles with mean diameter of 4.7 microns.

During these three months, we have also prepared the cooling and warming components of the breathing circuits to be used with saline mist. The nebulizer prototype will be inserted on the inhalation side of a standard breathing circuit, attached to an anesthesia ventilator. In case of cooling, saline at near freezing temperature will be fed into the nebulizer chamber using a feed-back system which provides a constant depth of saline film covering the nebulizer elements; in case of rewarming, saline (to be fed into the nebulizer chamber) will be warmed so as to maintain mist temperature at 45°C. During mechanical ventilation, gas will be pushed by the ventilator bellow through the nebulizer, where either pre-cooled or pre-warmed mist is added, and then into the endotracheal tube.

2. Evaluate the performance of the system in a porcine model.

The final nebulizer prototype was delivered by Sonaer, Inc in February 2004. In March 2004, we set up the animal operating room with equipment necessary to monitor physiological parameters. We have conducted the initial animal experiments.

Because of the theoretical concern that cold or warm mist particles may deposit in the respiratory system during cooling/warming, we added new equipment to measure possible changes in both

pulmonary compliance and respiratory are fed into a computerized system called Pulmodyne developed by Harvard Apparatus and modified by us for use with larger animals in our experiments. Post-mortem examination of the lungs and trachea has been conducted by Dr. John Godleski, a lung pathologist at Brigham and Women's Hospital and Harvard School of Public Health. In particular, the airways are dissected and examined for evidence of injury such as areas of hyperemia, erosions, or other pathologic change; any areas with changes will be sampled for histology. Then, the lung parenchyma is systematically sliced for gross examination by Dr. Godleski; areas of atelectasis, hyperemia, consolidation, or other pathological changes are sampled and examined histologically for presence of hemorrhage, inflammation, necrosis, or other pathologic changes.

These new physiological measurements and histopathological examinations allow assessment of possible effects of deposition of cold or warm mist particles on functional and structural properties of the lungs and airways. This information is essential to determine safety of this new method for cooling and warming.

Following the initial studies, we performed seven data-producing experiments in 55-70 Kg pigs: four experiments using a commercially-available intravascular heat-exchange catheter placed in the inferior vena cava; two using a surface cooling/warming blanket and one evaluating spontaneous cooling rate.

Preliminary results of cooling and warming rates in the pulmonary artery (PA) and brain (example of temperature changes in body core) are summarized in attached figure (where different colors indicate different experiments with method specified under horizontal axis): cooling rates achieved with the intravascular catheter ranged between 0.87 and 3.11 'C/hour in the brain and between 0.92 and 3.67 'C/hour in the pulmonary artery; with surface blanket, cooling rates of 1.32 and 2.35 'C/hour in the brain and of 1.29 and 2.62 'C/hour in the pulmonary artery were observed; finally, spontaneous cooling rates of 0.36 'C/hour in the brain and 0.46 'C/hour in the pulmonary artery were also measured.

Cardiovascular and physiological parameters, including heart rate, arterial blood pressure, cardiac output, pulmonary compliance and respiratory resistance were also measured throughout these experiments. These data are being reduced and tabulated. Finally, lungs and tracheas from these animals were harvested and stored in formaline to be analyzed by pathologist for possible changes induced by these cooling/warming methods. Experiments conducted so far will be used for comparisons to our new inhalation method.

Status

Technical problems with the nebulizer system (spurious mist deposition) have been identified and, through joint efforts with the vendor, resolved. The unfortunate effect of this is to delay the program by an additional quarter so that the final report will be similarly delayed.

Evaluation of Transport Ventilators for Forward Military Use

Robert M. Kacmarek, , Principal Investigator

Overall Objectives and Approach

To determine the most suitable currently available transport ventilator for use by the military in forward positions. The evaluation is being performed at the bench and in the animal laboratory. All ventilators will be evaluated on healthy and lung injured animals.

Progress on Specific Aims

We have experienced considerable frustration in attempting to complete the animal laboratory portion of the evaluation. Since we began this portion of the evaluation, we have only successfully evaluated one group of 5 ventilators on 2 healthy animals. The reason for this is problems with the procurement of healthy animals. We have had to send back to the farm 1 to 2 animals per week most weeks since the beginning of May because they have arrived with severe pneumonia. Other weeks no animals have been sent because the farm could not find healthy sheep. This inability to complete the animal evaluation has prevented us from completing the bench evaluation on the last five ventilators since we do not want to bring them to the MGH until we are sure we will be able to study them on animals. We are currently assured by the veterinarians that healthy animals should be now available because it is summer. As I write this we are in the laboratory with what appears to be a healthy sheep. We still expect to complete the evaluation by October 1, 2005.

We have completed all aspects of the protocol except the evaluation of 5 ventilators on a second lung-injured sheep. We attempted to complete this last experiment on October 4th but the animal was initially too sick to study, and the protocol could not be completed. However, based on all other aspects of the study protocol we are able to rank the ventilators studied on their suitability for transport of critically injured in forward military positions.

In general all of the ventilators tested performed at or close to specification under test conditions. However, many did not meet some of the established criteria which make them unsuitable for military use in forward positions (see attached table).

The following ventilators are pneumatically powered and cannot be used without external compressed gas: Bird Avian, Biomed Devices MRI, Biomed Devices Crossvent, Magellan, Parapac Transport 200D, Parapac Medic, Carevent ATV +, Autovent 2000, Percussionaire TXP, and Respirtec Pro. Furthermore, the Autovent 2000, Magellan, Percussionaire TXP, and Respirtec Pro do not have alarms to indicate either a disconnect or high pressure situation.

The five remaining ventilators all contain an internal battery and are capable of functioning without external compressed gas: Univent Eagle 754, Versamed I-vent, Newport HT50, Pulmonetic LTV1000, and the Pneupac Compac. All have the ability to have oxygen added thus increasing the delivered FIO2, are all fairly simple to operate, and are capable of ventilating both healthy and injured lungs. The advantages and disadvantages of these five ventilators are summarized below.

Univent Eagle 754
Advantages: This ventilator has a relatively long battery life, up to four hours at 21% oxygen. The battery life is extended when oxygen is added. It is simple to operate, relatively lightweight and portable, and contains alarms to alert the user to a disconnect and/or high pressure event.

Disadvantages: The maximum flow is 60 liters/minute. The ventilator shuts down if the patient's inspiratory demand exceeds this level. The oxygen consumption is approximately double the minute ventilation at a FIO2 of 1.0.

Versamed I-vent
Advantages: This ventilator has good flow delivery that is capable of ventilating a wide range of patients. Flow may be set by the user or self regulated based upon patient demand. The controls are clearly identified and easy to adjust. The ventilator incorporates an extensive alarm system alerting the user to a variety of situations including disconnect and high pressure. The oxygen consumption is approximately equal to the minute ventilation at a FIO2 of 1.0

Disadvantages: This is the heaviest of all the ventilators weighing 10 kilograms. It has a short battery life and requires a proprietary patient circuit for operation.

Newport HT50
Advantages: This ventilator is capable of ventilating a wide range of patients and has an extended battery life of over 8 hours on 21% oxygen. The controls are clearly identified and easy to operate and the alarm system identifies disconnect and high pressure situations.

Disadvantages: The ventilator was tested was a non-disposable proprietary circuit that offered considerable expiratory resistance. Auto-PEEP developed at high respiratory rates. One could most likely substitute a generic, disposable circuit, although this was not tested.

Pulmonetic LTV1000
Advantages:This ventilator has good flow delivery and can ventilate a wide range of patients. The extensive alarm and monitoring system alerts the user to a variety of situations including disconnect and high pressure. The controls are clearly identified and easy to use.

Disadvantages: The ventilator has a short battery life and the oxygen consumption is approximately double the tidal volume at a FIO2 of 1.0. This ventilator requires a proprietary patient circuit for operation.

Pneupac Compac
Advantages: This ventilator has a relatively long battery life. The controls are clearly identified and easy to use. The alarm system alerts the user to disconnect and high pressure situations.

Disadvantages: This is the largest and second heaviest of all the ventilators tested. It has a limited range of respiratory rate with the maximum being 27 breaths per minute (although the control indicates a maximum of 30).

Conclusions:
Both the Univent Eagle 754 and the Newport HT50 are acceptable for use by the military in forward positions. The Univent is the lighter of the two, however the Newport has a longer battery life and consumes less oxygen. The Newport offers the user additional modes of ventilation, including pressure support and pressure controlled ventilation. Although these may be

desirable in a more controlled ICU type environment, they may be a source of confusion in the unstable, combat setting.

Publications and Presentations
None

External Proposal Activity
None

Issues and Concerns
Inability to procure healthy animals.

Table – Comparison of Tested Ventilators

Ventilator		Size		Weight	Battery	Battery	External Gas
	Height	Width	Depth		Powered	Life*	Required
Univent Eagle 754	29cm	23cm	11cm	4.5kg	yes	4 hours	no
Bird Avian	25cm	30cm	12.7cm	4.5kg	yes	N/A***	yes
Versamed I-vent	33cm	24cm	26cm	10kg	yes	90 min	no
Newport HT50	26cm	27cm	20cm	6.8kg	yes	8 hours, 10 min	no
Biomed Devices MRI	26cm	16cm	9cm	4.1kg	no	N/A	yes
Biomed devices Crossvent 3	22.9cm	28cm	12.7cm	4.32kg	yes	N/A***	yes
Magellan	12.7cm	17.8cm	10.2cm	2.1kg	no	N/A	yes
Parapac Transport 200D	9.2cm	22cm	16.2cm	3.1kg	no	N/A	yes
Parapac Medic	9.2cm	22cm	16.2cm	2.4kg	no	N/A	yes
Carevent ATV +	23.5cm	11.1cm	16.2cm	4.1kg	no	N/A	yes
Autovent 2000	15cm	4.5cm	9cm	0.68kg	no	N/A	yes
Percussionaire TXP****	10.6cm	10.6cm	16.5 cm	0.68kg	no	N/A	yes
Pulmonetic LTV 1000	8cm	25cm	30cm	6.1kg	yes	75 min	no
Respirtec Pro****	16.76cm	6.35cm	8.38cm	0.165kg	no	N/A	yes
Compac	36cm	21cm	21cm	8.5kg	yes	4 hours	no
Ventilator		Size		Weight	Battery	Battery	External Gas

* Battery life is based upon tidal volume of 1,000 ml, resp rate of 10 and 21% oxygen.

** These are pneumatically powered, electronically controlled ventilators. Battery and/or AC power required for electronic controls, monitoring, etc.

*** Target tidal volumes were small and therefore the desired paCO2 was difficult to achieve due to the small size of the animal model relative to an adult human.

**** These are true pressure limited ventilators. Changes in resistance or compliance significantly alter the delivered tidal volume. Both are difficult to set at desired parameters.

Continuation of Table – Comparison of Tested Ventilators

Ventilator	Extrernal Gas	Oxygen	Disconnect	High Press	Able to Ventilate	Able to Ventilate
	Optional	Consumption**	Alarm	Alarm	Normal Lungs	Injured Lungs
Univent Eagle 754	yes	35 min	yes	yes	yes	yes***
Bird Avian	no	30 min	yes	yes	yes	yes***
Versamed I-vent	yes	52 min	yes	yes	yes	yes
Newport HT50	yes	72 min	yes	yes	yes	yes
Biomed Devices MRI	no	30 min	no	no	yes	yes
Biomed devices Crossvent 3	no	53 min	no	no	yes	yes
Magellan	no	60 min	yes	yes	yes	yes
Parapac Transport 200D	no	62 min	yes	yes	yes	yes
Parapac Medic	no	68 min	yes	yes	yes	yes
Carevent ATV +	no	65 min	yes	yes	yes	yes
Autovent 2000	no	60 min	no	no	yes	no
Percussionaire TXP****	no	77 min	no	no	yes	yes
Pulmonetic LTV 1000	yes	32 min	yes	yes	yes	yes
Respirtec Pro****	no	variable	no	no	yes	yes
Compac	yes	65 min	yes	yes	yes	yes
Ventilator	Extrernal Gas	Oxygen	Disconnect	High Press	Able to Ventilate	Able to Ventilate

* Battery life is based upon tidal volume of 1,000 ml, resp rate of 10 and 21% oxygen.

** These are pneumatically powered, electronically controlled ventilators. Battery and/or AC power required for electronic controls, monitoring, etc.

*** Target tidal volumes were small and therefore the desired paCO2 was difficult to achieve due to the small size of the animal model relative to an adult human.

**** These are true pressure limited ventilators. Changes in resistance or compliance significantly alter the delivered tidal volume. Both are difficult to set at desired parameters.

Intravascular MRI Coil Development

Jerome L. Ackerman Principal Investigator

Overall Objectives and Approach

The majority of all deaths in the United States result from cardiovascular disease. The rupture of an atherosclerotic plaque is often suspected to be the event precipitating a heart attack or stroke. MRI and MR spectroscopy (MRS) are playing an increasing role in the identification and characterization of potentially vulnerable plaque, but often exhibit marginal spatial resolution and signal to noise ratio (SNR) in this role. Intravascular MR coils, which can be inserted into blood vessels and placed in close proximity to vessel walls, offer the promise of greatly improved SNR, but have not attained the desired performance characteristics to be clinically useful.

The goal of this project is to refine the design of cylindrical meanderline intravascular (IV) magnetic resonance imaging (MRI) coils which were initially developed during a first year of CIMIT funding, and to move the research to the next phase: testing the coils in an animal model and with human arterial specimens. These coils are intended for high performance scanning of arterial walls, in particular for characterizing atherosclerotic plaque. Shielded cylindrical meanderlines, multinuclear coil designs, RF preamplifiers incorporated into the catheter, and continuously optimized remote electronic tuning methods will be developed. Coils will be tested in a rabbit model for atherosclerosis and with human surgical or autopsy specimens.

Progress on Specific Aims

The specific aims in this project were to simulate, design and construct a series of intravascular coils including a number of variations on the basic design, develop a means of remote automated tuning by means of varactor diodes, develop an intracatheter preamplifier, and test coils in human artery specimens and rabbits.

Simulations and Testing in Phantoms and Artery Specimens

Two computer programs for simulating the RF field and electrical properties respectively were developed. In conjunction with the use of the commercial software package XFDTD BioPro 5.2 (Remcom, Inc.), these programs permit exploring certain features of the coils and finding solutions to problems without actually building the coils. A typical coil is pictured in Figure 1 on the left. On the right side of Figure 1 is the image of a 3 mm coil immersed in water. The coil is used for reception, so that the bright area represents the sensitivity profile of the coil (water is excluded from the interior of the coil). Ideally, the sensitivity profile should be a circular ring. However, the profile is significantly distorted from circular symmetry. It was found from simulations that the ideal circular symmetry of the receptive volume is lost when the coil is immersed in a high dielectric medium such as water (which has a dielectric constant of about 78), and that the addition of distributed tuning capacitance at the coil restores the symmetry. The image in Figure 2 is obtained with a coil that contains a tuning capacitor to approximate the distributed capacitance. The symmetry has been restored to essentially circular.

Figure 3 compares the shapes of the sensitivity profiles of two common intravascular coils (the loopless antenna and the single loop) with the cylindrical meanderline. The significant feature of the cylindrical meanderline (rightmost images) is that its peak sensitivity occurs in a ring at its periphery, whereas the other two coils show peak sensitivities at smaller radii. The cylindrical

meanderline is thus best suited to imaging vessel walls, while exhibiting reduced sensitivity to the blood.

A prototype balloon-expandable coil was developed to permit adjusting the coil diameter to the vessel diameter in situ while maintaining blood flow through the coil.

Scans of human arterial specimens using the intravascular coil as a receiver provided highly improved signal to noise and spatial resolution compared to the use of a volume coil as a receiver. The volume coil was used as the transmit coil in both cases. In the intravascular coil images, features as small as 100 microns were resolved. As expected, the high sensitivity of the intravascular coil occurs close to the coil structure, and drops off dramatically with distance from the coil.

Animal Studies

The rabbit studies were begun, but exhibited problems due to the difficulty of making very small diameter (2 mm) coils which are smooth enough to be inserted into the rabbit aorta. The prime difficulty was producing a compact and externally smooth electrical connection between the coil and the cable. The solder joint causes a lumpiness in the catheter cross section, resulting in a tendency for the vessel to rupture. For the purposes of completing the animal studies, new coils without the local tuning capacitor will be constructed and used in this application. A short run of fine parallel wires will be used between the coil and the coaxial cable to enable a reduction in the diameter at the junction. A no-cost extension to the project was requested to permit the completion of these experiments.

Preamplifier and Automated Tuning

In a collaborative project with the Biomedical Engineering Center in the Charles Stark Draper Laboratory (partially supported by Draper and CIMIT), we have developed a prototype preamplifier for intravascular coils. The preamplifier contains a one-stage low noise transistor amplifier; a PIN diode for protection of the amplifier from the transmitter pulse and for detuning the coil; and a pair of varactor diodes for tuning the coil remotely. The preamplifier was tested in the scanner, and worked well. It will serve as a prototype for future amplifiers that can be built small enough to be incorporated into the catheter near the coil to obtain the maximum possible signal-to-noise ratio.

Because of the substantial fluctuations in intravascular coil tuning experienced as the catheter is inserted, and because the coil is subjected to continual physiological motion and blood flow, it is difficult or impossible to maintain optimal tuning in use. The automated tuning system will continuously sense the state of tuning, and update the tuning adjustments with electronically variable capacitors, thereby maintaining optimal tuning and good reproducibility while the coil is in use, and eliminating the time spent in manual adjustment of tuning. An inexpensive and compact data acquisition system, the CyberResearch UDAQ 1600, was set up for use in automatic continuously optimized tuning. The data acquisition system has two analog output voltages for adjusting the bias voltages which control the capacitance of the tuning diodes, and a multichannel analog to digital converter for measuring the tuning condition of the coil circuit. A computer closes the loop by adjusting the tuning diodes to optimize the tuning.

The electronic circuitry needed for detecting the tuning condition was not completed during the project, and will be completed during the extension.

Personnel

Jerome L. Ackerman, Ph.D. (PI) and Christian T. Farrar, Ph.D. (postdoctoral fellow) were supported on this project.

Patents

A U.S. patent application based in part on the subject matter of this project, "Radio Frequency Coil and Catheter for Surface NMR Imaging and Spectroscopy," was filed October 21, 2003.

Publications and Proposals Submitted

An NIH Bioengineering Research Partnership proposal (four years, $4,620,564 total costs), with MGH and Draper Laboratory as partners, was submitted in August. The specific aims of this work include development of the technology of intravascular MR coils and associated integrated electronics, development of an integrated circuit version of the electronics, packaging of the coils and catheter systems, and testing of these devices in live pigs.

Manuscripts

A manuscript, "The Cylindrical Meanderline Radio Frequency Coil for Intravascular Magnetic Resonance Studies of Atherosclerotic Plaque," by Christian T. Farrar, Van J. Wedeen and Jerome L. Ackerman, was accepted for publication in *Magnetic Resonance in Medicine.*

Presentations

Farrar CT, Wedeen VJ, Ackerman JL. Use of cylindrical meanderline catheter coils for intravascular imaging. Eleventh Scientific Meeting, International Society of Magnetic Resonance for Medicine, Toronto, Canada, July 10–16, 2003.

Farrar CT, Wedeen VJ, Ackerman JL. The cylindrical meanderline radiofrequency coil for intravascular magnetic resonance studies of atherosclerotic plaque. Forty-fifth Experimental NMR Conference, Asilomar, CA, April 18–23, 2004.

Farrar CT, Wedeen VJ, Ackerman JL. The cylindrical meanderline radiofrequency coil for intravascular magnetic resonance studies of atherosclerotic plaque. Fifth Interventional MRI Symposium, Boston, MA, October 15–16, 2004.

Grant Applications

Three National Institutes of Health grant applications relevant to this project were submitted:

"MRI-Enhanced Endoscopy with Tracking-Imaging Probes" (SBIR Phase II)

Participating institutions	Robin Medical, Inc., MGH, Johns Hopkins University
Principal investigator	Erez Nevo, M.D., Ph.D. (Robin Medical, Inc.)
Submitted	11/19/03
Period	4/1/04 – 3/31/07
Annual direct costs	$386,400; $40,000 to MGH
Specific aims:	To evaluate the use of intracoil motion tracking devices to reduce motion artifacts in endoscopic MRI exams; MGH will design and construct RF coils to be incorporated into endoscopes containing Robin

	Medical's magnetic tracking technology, permitting optical and MR endoscopy with continuous device position and orientation tracking
Status:	Funded; industrial research agreement with Robin Medical in negotiation

"Intravascular MR Coil Development for Atherosclerosis"

Principal investigator	Jerome L. Ackerman
Proposed period	12/1/04 – 11/31/08
Submitted	3/1/04
Annual direct costs	$225,000
Specific aims:	to develop, construct and evaluate in phantoms, human surgical specimens and rabbits the performance of novel cylindrical meanderline intravascular RF coils; to develop automated continuously optimized coil tuning methods and intracatheter electronics for highest signal to noise ratio
Status:	Not funded; will be revised and resubmitted

"Advanced Technology for Intravascular MR Coils"

Principal investigator	Jerome L. Ackerman
Proposed period	7/1/05 – 6/30/09
Submitted	8/19/04
Annual direct costs	$582,136; $287,878 to MGH
Specific aims:	To develop and extend cylindrical meanderline MR coil technology; to evaluate coils in phantoms, tissue specimens and live pig coronary arteries; to develop intracatheter integrated circuits for local preamplification and active continuously optimized tuning; to develop vascular-compatible packaging for coils and intracatheter electronics; to optimize methods for reduction of motion and flow artifacts associated with intravascular coils; to develop methods for continuously optimized tuning
Status:	In review

Issues and Concerns

The automatic tuning system and animal studies have not been completed. A no-cost extension of the project has been requested in order to complete these tasks.

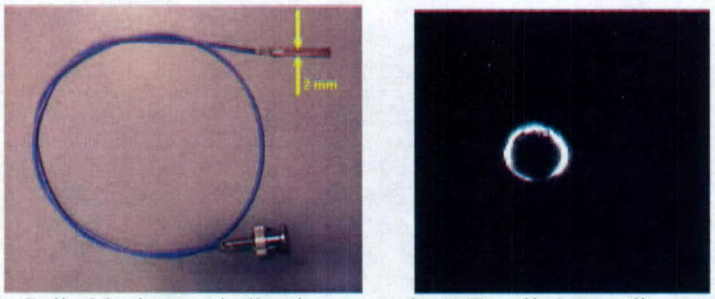

Figure 1. Left: Cylindrical meanderline intravascular MR coil, 2 mm diameter, containing a fixed tuning capacitor at the coil. Right: Sensitivity profile of an early stage design 3 mm intravascular coil (without local tuning capacitance), showing poor circular symmetry (compare this image with the improved profile in Figure 2 below).

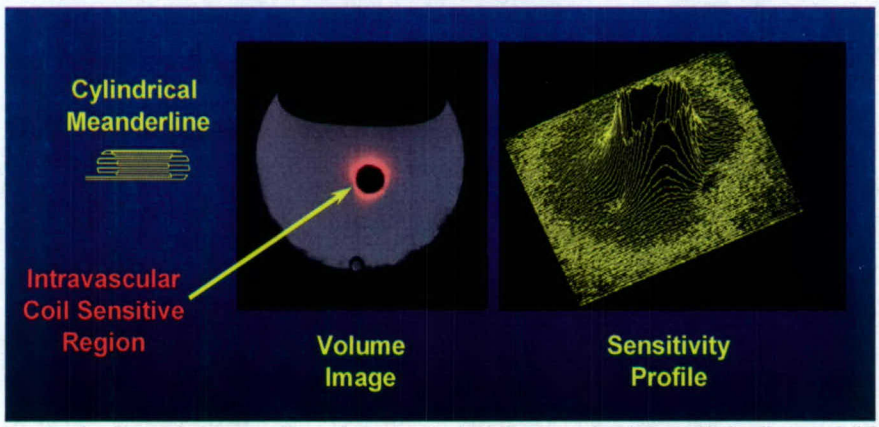

Figure 2. Left: Sensitivity profile of the cylindrical meanderline coil (red) overlaid on the image (gray) obtained with a volume coil. Right: Graphical representation of the coil sensitivity profile of the coil. At its surface the cylindrical meanderline shows an intrinsic sensitivity of two orders of magnitude greater than that of the volume coil.

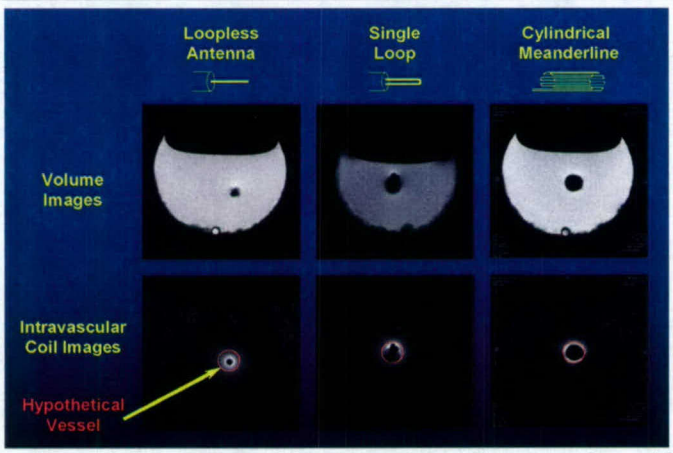

Figure 3. Comparison of three types of intravascular coil geometries. All three coils are immersed in water. In the top row, a volume coil is used for a receiver, and the surrounding water (bright area) is fully visible. In the bottom row, the intravascular coil is used as a receiver, and the restricted reception volume (bright area) is demonstrated, along with a ring representing a typical blood vessel wall. The cylindrical meanderline geometry is best suited to imaging vessel walls because of the extended radius of its sensitive volume.

MEMS-Based Intravascular Devices for Enhanced Diagnosis Of Cardiovascular Disease with Magnetic Resonance Imaging

Jerome L. Ackerman, Massachusetts General Hospital, PI
Mathew Varghese, Charles Stark Draper Laboratory, Co-PI

Overall Objectives and Approach

The majority of all deaths in the United States result from cardiovascular disease. The rupture of an atherosclerotic plaque is often suspected to be the event precipitating a heart attack or stroke. MRI and MR spectroscopy (MRS) are playing an increasing role in the identification and characterization of potentially vulnerable plaque, but often exhibit marginal spatial resolution and signal to noise ratio (SNR) in this role. Intravascular MR coils, which can be inserted into blood vessels and placed in close proximity to vessel walls, offer the promise of greatly improved SNR, but have not attained the desired performance characteristics to be clinically useful.

In a novel approach to improving the SNR of intravascular coils, the aims of this project encompass the design and testing of a prototype electronics package that can (in a future miniaturized version) be incorporated into a catheter containing an intravascular MR coil with enhanced performance. Specifically, a technical assessment of circuit designs for intravascular MR coils with miniaturized integral electronics will be performed by the Draper team. The MGH team will then implement and test these designs on a 4.7 T MR scanner. The work will serve as a prototyping step and test bed enabling the further development of integrated coil/electronics systems with vastly improved performance.

Progress on Specific Aims

The Draper team considered the following features (developed by the MGH team) required of an MR coil system incorporating an active electronics package:

1. A pair of varactor diodes for remote electronic tuning and impedance matching of the meanderline or other intravascular RF coil
2. A low noise transistor preamplifier stage
3. A means to detune the RF coil and protect the preamplifier from high power RF pulses during transmit
4. A means to turn the preamplifier on during signal reception and off during transmit
5. Implementation of the above functions with a minimum of components to make the entire electronics package as compact as possible
6. The elimination of all magnetic materials such as ferrite cores

Various options for the low noise transistor and varactor diodes were considered, and a detailed set of electronic design specifications (jointly developed by both teams) were finalized. The Draper team simulated the circuit for an MR scanner operating at 200 MHz (4.7 T magnetic field strength), using several options for the low noise transistor. Following final selection of the transistor based on performance, the Draper team then created a detailed schematic and board design and fabricated two copies of the circuit on FR4 circuit board at 30 x 35 mm scale for preliminary testing. The circuit incorporates a pair of varactor diodes to enable electronic tuning of the RF coil, a PIN diode for detuning and preamplifier protection during the high power

transmit RF pulse, and an Agilent (Hewlett Packard) surface mount ATF531P8 low noise pseudomorphic high electron mobility transistor (PHEMT) to serve as the preamplifier stage. This transistor was among a set of four chips that were evaluated, and was selected on the basis of its low noise performance. The circuit was simulated to select optimized bias conditions and impedance matching networks for the transistor. In the process, several problems in the circuit simulation models that Agilent provided for their amplifier chip were identified and corrected. Bench testing indicated a preamp gain of 22 dB, bandwidth of 20 MHz, and RF transmitter pulse rejection of 20 dB, all within design spec. Preliminary testing within the magnet on the scanner showed that the preamplifier contained no ferromagnetic material, functioned well within the magnet, and yielded a signal to noise ratio superior to that achievable with the scanner's normal preamplifier. Figure 1 shows the schematic diagram of the circuit used for the simulations, and Figure 2 shows the board layout and a photograph.

In this preamplifier design, separate DC bias lines are provided to operate the preamplifier stage, bias (tune) the varactor diodes, and switch the PIN diode to detune the RF coil and protects the input of the preamplifier stage from high power RF pulses. Appropriate decoupling of RF and DC is provided throughout the circuit as necessary with blocking capacitors and RF chokes.

Personnel

This was a joint project between The Charles Stark Draper Laboratory Biomedical Engineering Program and the Massachusetts General Hospital Martinos Center for Biomedical Imaging. Draper personnel included Mathew Varghese, Ph.D. (Draper Co-PI), Jeffrey T. Borenstein, Ph.D. (technical consultant; technical and administrative liaison) and A. Jay Bruso, M.S. (RF engineer). MGH personnel included Jerome L. Ackerman, Ph.D. (MGH Co-PI) and Christian T. Farrar, Ph.D. (postdoctoral fellow).

Patents

A U.S. patent application based in part on the subject matter of this project, "Radio Frequency Coil and Catheter for Surface NMR Imaging and Spectroscopy," was filed October 21, 2003.

External Funding and Industrial Partnerships

In a joint project with Robin Medical, Inc., an Israeli medical device company with offices in Baltimore, we will be constructing active MR coils to be incorporated in endoscopes. The endoscopes will additionally incorporate Robin's active magnetic tracking technology. An NIH Phase II SBIR grant entitled "MRI-Enhanced Endoscopy with Tracking-Imaging Probes" ($1,457,650 total costs, $70,000 to MGH), with participation from Johns Hopkins Medical Center and Siemens Medical Systems, has been awarded to Robin Medical to support the work.

An NIH Bioengineering Research Partnership proposal (four years, $4,620,564 total costs), with MGH and Draper Laboratory as partners, was submitted in August. The specific aims of this work include development of the technology of intravascular MR coils and associated integrated electronics, development of an integrated circuit version of the electronics, packaging of the coils and catheter systems, and testing of these devices in live pigs.

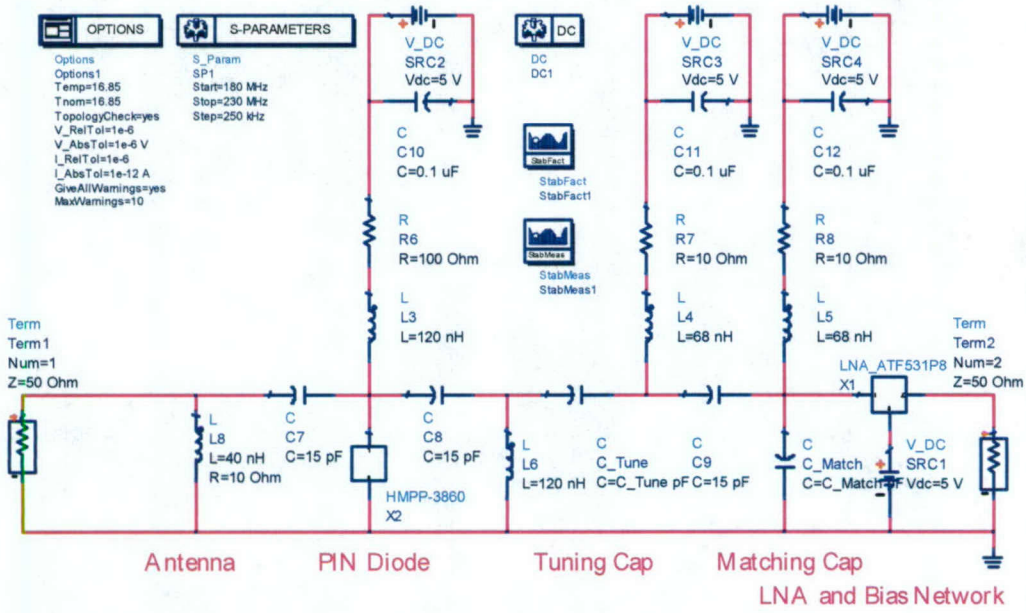

Figure 1. Complete schematic of prototype low noise preamplifier with PIN diode protection and tuning and impedance matching varactor diodes showing the simulation setup.

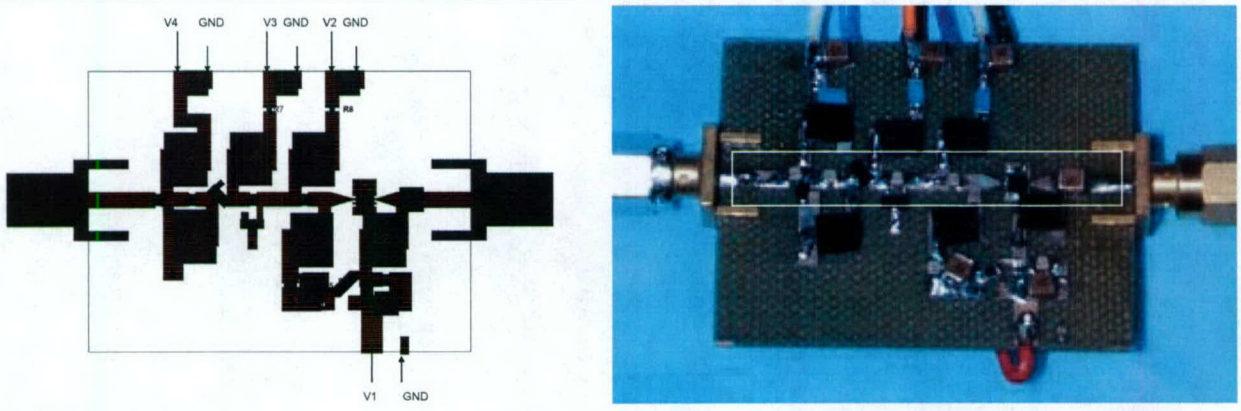

Figure 2. *Left:* Board layout, intended as a prototype for future electronics module that can be incorporated directly into the catheter. *Right:* Board photograph. The RF coil is connector via the SMA connector to the left, and the scanner is connected at the right. The board operated within the scanner magnet at full magnetic field strength. The active components (marked by the white rectangle) occupy a thin strip about 2 mm in width, and with some modification of this circuit could be placed within a 7F catheter. Use of an integrated circuit for the electronic functions would result in a further dramatic reduction in size, and is expected to be used in a clinical version of the device.

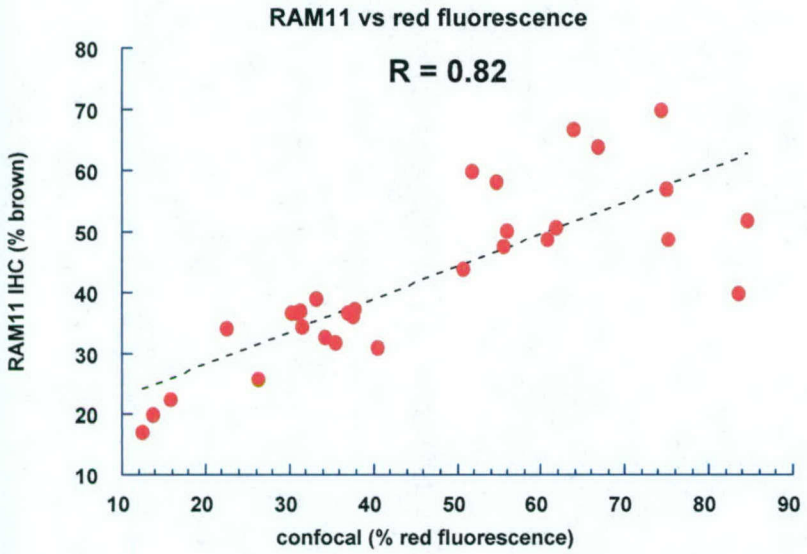

Figure 1. Correlation of quantitative immunohistochemistry with red fluorescence measured in the plaques present in aortic segments of rabbits injected with macrophage-targeted BSA-ce6-mal.

Progress on Specific Aims

Specific Aim 1

Optimize the combination of macrophage-targeted dye conjugate, intravascular excitation and emission fiber optic(s) and measurement optoelectronics for detection of fluorescence in plaques through flowing blood.

We have in the course of this project conducted much work on attempting to optimize the ideal conjugate for both fluorescence diagnosis and PDT of macrophage-rich plaques. We synthesized, purified and characterized the macrophage-targeted near-infrared fluorescent probe – BSA-Cy5.5-mal. This dye absorbs at 670-nm and emits fluorescence centered at 695-nm and should be incomparably better for fluorescence detection of vulnerable plaque through flowing blood. Maleylated albumin was conjugated to the tricarbocyanine dye Cy5.5. This was accomplished by reacting the N-hydroxysuccinimide ester of Cy5.5 with BSA in bicarbonate buffer pH 9.3 (molar ratio of 2.5 dye to 1 protein). The protein dye conjugate was then treated with solid maleic anhydride (equal weight ratio to protein) in 1M bicarbonate buffer. Purification was carried out by repetitive ultrafiltration using an Amicon 30 and washing with PBS. Five successive ultrafiltration steps were necessary to completely separate conjugate from free dye. Characterization was carried out by spectrophotometry. [Cy5.5 dye]=(A678)/250000; $\varepsilon_{678}^{cy5.5}$ = 170,000 $M^{-1}cm^{-1}$; $A_{250} = 0.12 \cdot A_{678}$; $A_{280} = 0.18 \cdot A_{678}$; [BSA]=[A280 - (0.18•A678)]/44300; $\varepsilon_{280}^{BSA} = 44300 M^{-1}cm^{-1}$; $A_{250}^{BSA} = 0.597 \cdot A_{280}$ $\varepsilon_{250}^{\varepsilon\text{-maleyllysine}} = 3{,}360\ M^{-1}cm^{-1}$; $\varepsilon_{280}^{\varepsilon\text{-maleyllysine}} = 308\ M^{-1}cm^{-1}$

We studied the relative macrophage-targeting abilities of the two conjugates i.e. mal-BSA-ce6 and mal-BSA-Cy5.5. Although mal-BSA-Cy5.5 is recognized and taken up by macrophage cell lines to a greater degree than non-macrophage control cell lines, the difference is not as large as that found with the mal-BSA-ce6 conjugate. The reason for this difference in specificity is not immediately clear. It is possible that the molecular characteristics of the dye molecule are involved in recognition of the conjugate by the macrophage scavenger receptor as well as the

maleylated albumin moiety that was the original rationale for the cell-type specific targeting. Further work will be necessary to confirm this possibility.

Specific Aim 2

Test the hypothesis that vulnerable plaque (VP) can be effectively treated using PDT.

We have carried out intravascular PDT experiments with atherosclerotic rabbits using Antrin as photosensitizer. We injected Antrin into the lateral ear vein at a dose of 10 mg/kg. Twenty-four hours later we anesthetized the rabbits with ketamine/xylazine and obtained vascular access via a femoral cutdown. A 200-micron OD 3-cm long diffusing tipped fiber was inserted into the femoral artery and maneuvered through the iliac artery to the mid-abdominal aorta. We have delivered several total fluences in an empirical dose escalation study. The 730-nm diode laser runs at a total power of 5.5 W equivalent to 1.7 W/cm diffuser. Therefore a ten minute illumination will deliver 1000 J/cm. While this may seem a high dose of light it must be remembered that this light is being delivered through flowing blood. Rabbits were sacrificed at various time points after illumination and arteries removed for histological and immunohistochemical examination. Frozen sections were stained with the DNA binding dye DAPI allowing cell nuclei to be counted, and Masson trichrome allowed quantitation of collagen with the arterial wall. Preliminary data shows a very significant reduction in cells in the plaque of illuminated segments of artery not seen in arterial segments that received no light. There are hints that the total plaque burden may be reduced and the collagen content of the residual plaque increased thus adding to its stability.

We then proceeded to carry out intravascular PDT with the macrophage-targeted conjugate mal-BSA-ce6. We used a dose 5 times lower (2mg/kg of BSA-ce6) compared to the dose we previously employed with Antrin. For rabbits injected with conjugate we delivered 665-nm light from a 1W diode laser at a total power of 900 mW equivalent to 300 mW/cm diffuser length. Since the rate at which light was delivered varied by a factor of five between the two lasers and the time during which the light could be conveniently and safely delivered should not vary much between rabbits, this meant that Antrin rabbits received 5 times as much light as conjugate rabbits. Therefore the total PDT dose (drug time light) was 25 times higher for rabbits that received Antrin compared to those that received conjugate.

Intra-arterial PDT using both regimens (Antrin and BSA-ce6-mal) was safe and non-toxic. Decisions had to be made at what time to sacrifice rabbits in order to determine the effects of the treatment on the aorta by histological and immunohistochemical techniques. In these first experiments we used a relatively early time-point after PDT of 3 days.

Aortas and iliac arteries were removed for histological and immunohistochemical examination. Frozen sections were stained with the DNA binding dye DAPI allowing cell nuclei to be counted, and Masson trichrome allowed quantitation of collagen with the arterial wall. The data shows a very significant reduction in cells in the plaque of illuminated segments of artery not seen in arterial segments that received no light.

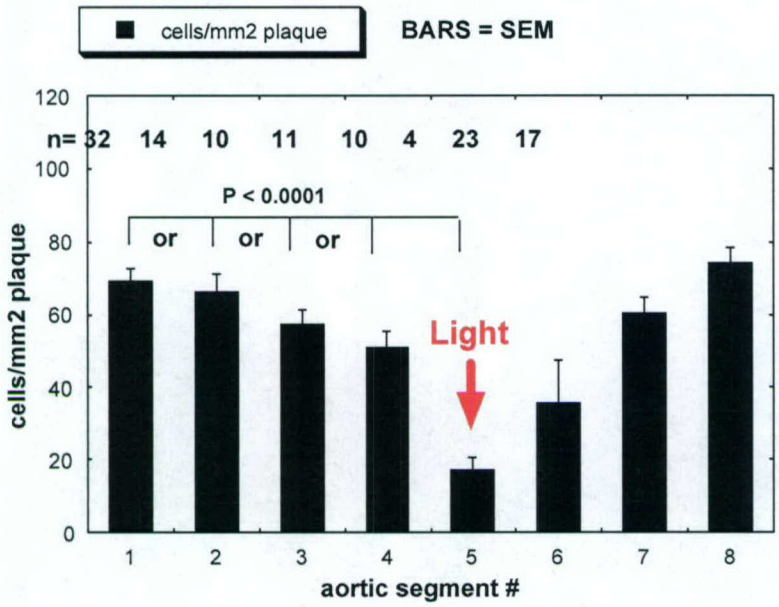

Figure 2. Plot showing the number of cell nuclei per square mm of tissue section from arteries removed from PDT treated rabbits at 8 days post Antrin-PDT. Section 5 received the largest dose of light, while sections 4 and 6 by virtue of being near the diffuser ends received a smaller dose of light.

Similarly in aortas of rabbits that had been treated with conjugate mediated PDT there was a significan t positive effct. In this case wer did quantitative immunohistochemsitry for RAM11 (stains for macrophages)

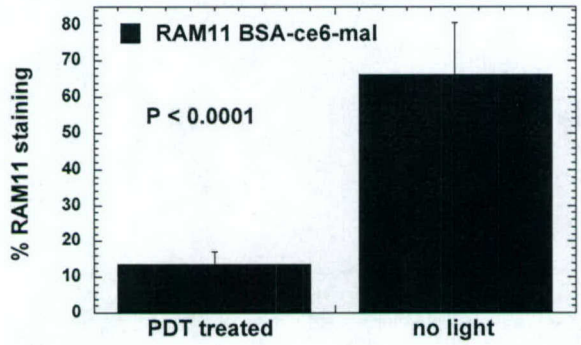

Figure 3. Plot showing the quantative immunohistochemistry for the RAM11 macrophage marker inm control (no light) and PDT treated aortic segments in rabbits that had been injected with 2 mg/kg BSA-ce6-mal.

Publications and Presentations

Publications

Hamblin MR, Tawakol A. Castano AP, Gad F, Zahra T, Ahmadi A, Stern J, Ortel B Chirico S, Shirazi A, Syed S Muller JE. Macrophage-targeted photodynamic detection of vulnerable atherosclerotic plaque. In: Gregory KW, Whittaker P, Woodburn KW Editors, Lasers in Surgery: Advanced Characterization, Therapeutics, and Systems, Jan 25-31

2003, Bellingham, WA, The International Society for Optical Engineering, Proceedings of SPIE; 2003, Vol 4949: p 466-476.

Demidova TN and Hamblin MR, Macrophage targeted photodynamic therapy. Int J Immunopathol Pharmacol. 2004 17(2):117-126

Presentations

Hamblin MR, Tawakol A. Migrino RQ, Chirico S, Castano AP, Gad F, Ahmadi A, Zahra T, Shirazi A, Stern J, and Muller JE. Macrophage-targeted photoactive molecules localize in vulnerable atherosclerotic plaques in vivo. 31st Annual Meeting of American Society for Photobiology, Baltimore, MD, 2003.

Tawakol A, Fischman A, Gewirtz H, Muller JE, Brady T, Hamblin MR, Intravascular detection of inflamed atherosclerotic plaques with a novel macrophage-targeted fluorescent photodynamic compound. ACC-03, Chicago, IL, 2003.

External Proposal Activity

A R01 application entitled "Targeted photodynamic therapy for detection and therapy of vulnerable plaque" was submitted to NIH-NHLBI for Feb 1st, 2004 deadline. It requested five years of funding at $250,000 per year. It was not rated highly enough for funding and will be revised for resubmission in 2005.

A phase I SBIR proposal "Fluorescence Detection of Vulnerable Plaques in Vivo" in conjunction with Aurora Optics Inc of Dartmouth, NH was submitted Aug 1st 2004. Grant 1R43 HL080841-10 is presently under review.

Immune Modulation to Enhance Detection and Therapy of Vulnerable Plaques

Ahmed Tawakol Principal Investigator

Overall Objectives and Approach

The over-all goal of this study is to test the hypothesis that adjunctive administration of immune modulators, selectively enhances the uptake of macrophage-targeted ligands, resulting in enhanced imaging of, and drug delivery to VP. Specifically, we will test the hypothesis that the cytokines GM-CSF, (granulocyte macrophage colony stimulating factor) and IFNγinterferon gamma), selectively enhance uptake of both metabolic tracers as well as macrophage surface receptor-targeted ligands in: 1) macrophage cell cultures, and 2) an animal model of macrophage-rich atherosclerotic plaque.

Progress on Specific Aims

The specific aims of this protocol are to test the hypothesis that the cytokines GM-CSF, (granulocyte macrophage colony stimulating factor) and IFNγinterferon gamma), selectively enhance uptake of both metabolic tracers as well as macrophage surface receptor-targeted ligands in: 1) macrophage cell cultures, and 2) an animal model of macrophage-rich atherosclerotic plaque.

The initial investment of effort in this protocol has been to develop the balloon injury model of atherosclerosis. To that end, we have surgically balloon injured the rabbits needed for the protocol and are awaiting their atherosclerotic plaques to mature during exposure to a high cholesterol diet.

Further, we have thus far examined the effect of GMCSF treatment on six atherosclerotic animals. In each case, the animals were studied twice (after saline injections vs after GMCSF injections). Animals were subsequently imaged using FDG PET. Our preliminary results revealed a **4X** increase in target to background signal after GMCSF compared with placebo.

Publications and Presentations

None

Patent Application Status

A patent application has been prepared by MGH's chosen law firm of Frommer Lawrence & Haug LLP.

External Proposal Activity

None

Polarization Sensitive OCT (PS-OCT) Assessment of Collagen in Atherosclerotic Plaques

Guillermo J. Tearney, M.D. Ph.D. Principal Investigator

Overview

The stability of atherosclerotic plaque is related to the collagen content of the fibrous cap and necrotic core. Hence the determination of collagen density may likely provide an index of plaque vulnerability to rupture. The aim of this study is to quantify collagen content in atherosclerotic plaques by the measurement of collagen birefringence using polarization sensitive optical coherence tomography (PS-OCT).

Progress on Specific Aims

Specific Aims

1. Develop gold standards for collagen quantification
2. Determine the relationship between PS-OCT measurements of birefringence and collagen content in aortic plaques ex vivo

Specific Aim 1

Picrosirius Red Standardization

In order to validate the capability of PS-OCT to quantify collagen content in situ, we needed to develop a reliable gold standard for collagen content. Our current gold standard for collagen content is quantitative Picrosirius Red (PSR) analysis of histologic slides. In our preliminary study, we utilized a conventional brightfield microscope with off-the-shelf polarizers to obtain digital images of PSR-stained slides. However, these images were not rotationally independent, due to the poor quality of the polarizers and birefringence within other optical components of the brightfield microscope. Without correction, this rotational dependence would significantly impair the reliability of our gold standard. We therefore purchased a specialized polarizing microscope, which utilizes high-quality, customized polarizers and strain-free microscope objectives. This microscope now produces rotationally independent images of PSR, enabling robust quantification of collagen content for comparison with PS-OCT.

PolScope quantitative birefringence system

Our customized LC-PolScope™ (Cambridge Research Instrumentation, Woburn, MA) system combines a unique liquid crystal based polarized light universal compensator with our current polarization microscope. The compensator is computer-controlled, enabling accurate measurement of birefringence and optical axis. The system will be configured to acquire birefringence measurements on unstained slides, which will be utilized as an additional gold standard for PS-OCT. Our work in this area has initiated the development of a multi-institutional consortium for collagen content measurement standardization, which includes investigators from Cambridge Research Instrumentation, Partners, University of Massachusetts and Albany Medical College.

Specific Aim 2

Data Acquisition and Processing

PSOCT imaging: We have imaged 178 randomly selected aortic plaques obtained from 23 human cadavers. All specimens were imaged within 48 hours postmortem. Polarization sensitive

images of the aortic plaques were obtained using the fiber-based PSOCT system developed in our lab. The centre wavelength of the optical source used in the system was 1310 nm with a 70 nm bandwidth and the image resolution was approximately 10 μm in the axial direction. The lesion site was marked with India ink and images were acquired at 1 frame per second by scanning a 5 mm x 5 mm region across the lesion. All the aortic specimens were imaged in a PBS bath maintained at 37°C, with the luminal side of the aortic tissue exposed just above the surface of PBS. Histology sections were obtained at the lesion site and stained with Trichrome and Picrosirius Red stains.

PS-OCT image processing: PS-OCT images were selected for processing and compared with their corresponding histology sections. Plaque collagen content in selected regions of interest (ROI) was determined using polarized light microscopy images of PSR stained sections and compared with the depth dependent slope of the phase retardation images. In the PS-OCT image shown in Figure 1, the depth-dependent intensity banding representing phase retardation from 0-180 degrees (Fig. 1B) provides evidence of a collagen-rich plaque, which is corroborated in the corresponding PSR image. The slope of the phase retardation plot and collagen content were measured for two regions of interest (Fig.1C). As seen in Fig.1D, PSR measurements of collagen content correlated with PS-OCT measurements of tissue birefringence in each ROI.

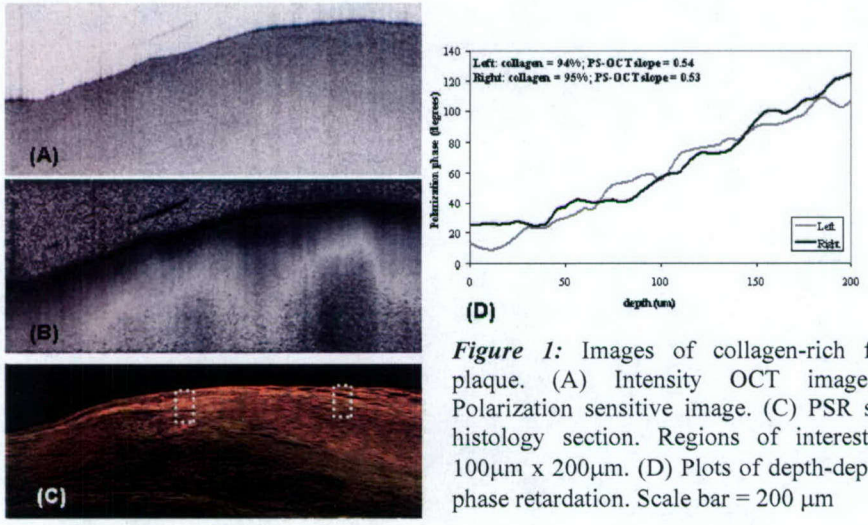

Figure 1: Images of collagen-rich fibrous plaque. (A) Intensity OCT image. (B) Polarization sensitive image. (C) PSR stained histology section. Regions of interest were 100μm x 200μm. (D) Plots of depth-dependent phase retardation. Scale bar = 200 μm

In Figure 2, analysis of three regions of interests in the PS-OCT images demonstrated good correlation between phase retardation and collagen content for the left and mid- ROI. However, the phase retardation slope underestimated collagen content in the right ROI. We expect that this result may arise due to the random orientation of collagen fibers within the focal volume resulting in reduced birefringence. Our current analysis technique can detect and quantify changes in the polarization state of backscattered light due to the presence of regularly oriented structures, therefore, randomly arranged collagen may remain under-represented in the phase retardation images.

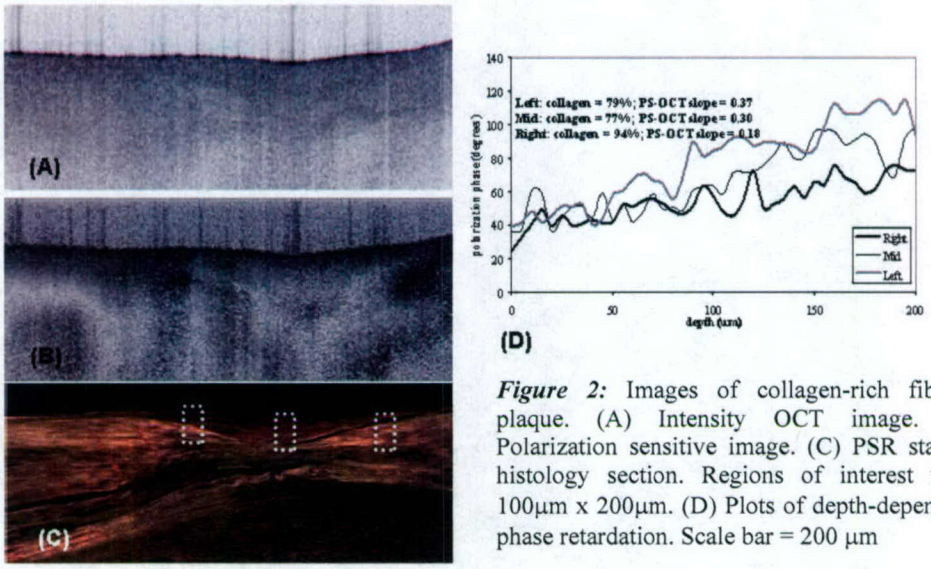

Figure 2: Images of collagen-rich fibrous plaque. (A) Intensity OCT image. (B) Polarization sensitive image. (C) PSR stained histology section. Regions of interest were 100μm x 200μm. (D) Plots of depth-dependent phase retardation. Scale bar = 200 μm

Summary

Our work to date suggests that when collagen is oriented perpendicularly to the optical beam, PS-OCT provides a measurement of collagen content that is highly related to collagen content determined by histopathological techniques. Since this comprises the majority of cases in atherosclerotic plaques, we expect that PS-OCT will be a useful technique for assessing coronary collagen content in patients. In cases where collagen is randomly oriented, additional processing may be required to better estimate collagen content. Future work will address this issue by combining polarization sensitive image data with intensity data to correct for collagen orientation.

Publications and Presentations

We are targeting a manuscript submission to *Circulation* by Jan. 2005.